



Terms and Conditions of Use of Digitised Theses from Trinity College Library Dublin

Copyright statement

All material supplied by Trinity College Library is protected by copyright (under the Copyright and Related Rights Act, 2000 as amended) and other relevant Intellectual Property Rights. By accessing and using a Digitised Thesis from Trinity College Library you acknowledge that all Intellectual Property Rights in any Works supplied are the sole and exclusive property of the copyright and/or other IPR holder. Specific copyright holders may not be explicitly identified. Use of materials from other sources within a thesis should not be construed as a claim over them.

A non-exclusive, non-transferable licence is hereby granted to those using or reproducing, in whole or in part, the material for valid purposes, providing the copyright owners are acknowledged using the normal conventions. Where specific permission to use material is required, this is identified and such permission must be sought from the copyright holder or agency cited.

Liability statement

By using a Digitised Thesis, I accept that Trinity College Dublin bears no legal responsibility for the accuracy, legality or comprehensiveness of materials contained within the thesis, and that Trinity College Dublin accepts no liability for indirect, consequential, or incidental, damages or losses arising from use of the thesis for whatever reason. Information located in a thesis may be subject to specific use constraints, details of which may not be explicitly described. It is the responsibility of potential and actual users to be aware of such constraints and to abide by them. By making use of material from a digitised thesis, you accept these copyright and disclaimer provisions. Where it is brought to the attention of Trinity College Library that there may be a breach of copyright or other restraint, it is the policy to withdraw or take down access to a thesis while the issue is being resolved.

Access Agreement

By using a Digitised Thesis from Trinity College Library you are bound by the following Terms & Conditions. Please read them carefully.

I have read and I understand the following statement: All material supplied via a Digitised Thesis from Trinity College Library is protected by copyright and other intellectual property rights, and duplication or sale of all or part of any of a thesis is not permitted, except that material may be duplicated by you for your research use or for educational purposes in electronic or print form providing the copyright owners are acknowledged using the normal conventions. You must obtain permission for any other use. Electronic or print copies may not be offered, whether for sale or otherwise to anyone. This copy has been supplied on the understanding that it is copyright material and that no quotation from the thesis may be published without proper acknowledgement.

Simulation of Bone Fracture and Cutting Using the Theory of Critical Distances

Saeid Kasiri Ghahi

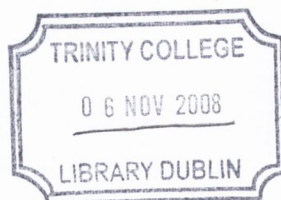
A thesis submitted to the University of Dublin for the degree of

Doctor in Philosophy

April 2008

Supervisor

Prof. David Taylor



External Examiner
Prof. Deepak Vashishth
Rensselaer Polytechnic Institute

Internal Examiner
Prof. John Monaghan
Trinity College Dublin

**Department of Mechanical and Manufacturing Engineering
Trinity College Dublin**

Thesis
8612

Dedication

For

my mother

and

my father

who knew the value of
education and gave me
the opportunity they did
not have.

تقدیم به

مهربان مادرم

و

زنده یاد پدرم

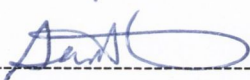
تقدیمشان باد

که ارزش علم و دانش را دانستند
و آنچه را برای خودشان میسر نشد
برای فرزندان خود مهیا کردند.

Declaration

I declare that the present work has not previously submitted as an exercise for a degree at any other university. It consists entirely for my own work, except where references indicate otherwise.

Library of Trinity College Dublin may lend or copy this thesis on request



Saeid Kasiri
April 2008

Acknowledgement

I have been so lucky to work with Prof. David Taylor as my supervisor. I would like to thank Prof. David Taylor who always offered me help and advice in a patient, encouraging and constructive way. It was a great pleasure for me to carry out this research with such supervision.

I would like to thank Mr. Ger Reilly who did the experimental part of the project. Also, he was a good project manager and I would like to thank him for sorting out what we needed to make this work possible.

I would like to thank my colleagues at Trinity College and Institute of Technology Sligo and especially Dr Brendan McCormack. It has been a great pleasure to work with you all. Also I would like to thank my friends, who helped me over the years Shawn McCourt, Reza Moqadasi and Michaela Briand and a special thanks to Angelina Marie Cox who was a great support.

I would like to thank various other members of staff in the Mechanical Engineering Department at Trinity College Dublin particularly Prof. John Monaghan, Joan Gillen and Sheena Brown who have helped me out with so many problems so many times. Also, thanks to all the postgraduate students and postdoctoral at TCD that I have worked with over the years, it has always been a pleasure.

I would like to thank my family especially my mom and my sisters, Somaye, Zahra and Zohre who have been so supportive of me, in every way, they are really the ones that made this possible. I could not have done this without their help and encouragement.

I gratefully acknowledge the funding provided for this research from the Council of Directors Strand III Research Program.

Abstract

This work was concerned with the prediction of bone fracture in situations where fracture was initiated in areas of stress concentration. Two conditions were studied: (i) fracture in bones and bone samples weakened by the introduction of holes, notches and cracks; (ii) fracture during indentation with a sharp metal blade as occurs during cutting of bone with an osteotome.

Computer simulations (finite element models) were created to model these two processes, using a new approach known as the theory of critical distances (TCD). This approach has been used previously to study fatigue and brittle failure of engineering materials. For the first time, the TCD was applied to study fracture of bone. It was shown that the TCD is applicable to predict the effect of stress concentrations like holes and notches.

Firstly, four different critical distance methods were studied. It was shown that the methods predict almost the same results but they have different advantages and areas of application. For example in the case of indentation, methods based on introducing cracks into the model (Finite Fracture Mechanics and the Imaginary Crack Method) were found not to be applicable, whilst stress-based methods (known as the Point Method and Line Method) were found to be appropriate and so were used in further work. The necessary material parameters (critical distance and critical stress) of bone were found using data from the literature on bending, tension and torsion of bones containing various features. For example, it was shown that the TCD is capable of predicting the effects of transcortical holes in reducing bone strength: a 2mm hole will reduce the bending strength by 30% while it has little effect on torsional strength. It was also found that the critical distance value of bone is about 0.3-0.4mm, for both bovine and human bone, which is of the same order as the distance between structural features such as osteons and plexiform units. This shows the important role of osteons as a toughening mechanism of bone.

After showing that the TCD can be used to predict the bone fracture, it was applied to bone cutting. In this case, first the crack initiation point was estimated using the

TCD. After that, the indentation fracture force was predicted for different indenters and different directions of cutting. Finally, the amount of damage in the surrounding bone was estimated. The results were in excellent agreement with experiments which were performed on 8mm cubes of bovine bone, in a parallel PhD project. For example, the results showed that the cutting force in the longitudinal direction is significantly less than that in the transverse direction; this was shown to be due to deflection of the main crack in transversal cutting, an effect of the directional nature of material properties in bone.

Comparing the effects of the geometry of blades on fracture force showed that the radius of the indenter has more effect on the fracture force than the angle. Increasing in the radius up to a certain value (which depends on the angle) increases the fracture force. The study showed that for a given angle of blade, if the radius is larger than a certain value, increasing the radius does not have any effect on the cutting force. Also, there is not a significant difference between cutting force for a very sharp blade and 50 μ m-radius indenter however the damage zone caused by the 50 μ m indenter is twice as large.

This study has demonstrated for the first time that the TCD can be used to make predictions of the fracture of bone in a variety of different situations. The TCD is very easy to use in conjunction with FEA, so it can potentially be applied to many other problems in bone fracture.

Table of Contents

Chapter 1. Introduction	1
Chapter 2. Comparison of Four TCD Methods.....	7
2.1. Comparing the Critical Distances Methods.....	7
2.2. Stress-Based Methods	8
2.3. Fracture Mechanics Methods.....	10
2.4. Analytical Relationships between the Four Methods	12
2.5. Further Comparisons between the Methods: Notches and Anisotropic Materials	16
2.6. Discussion.....	22
2.7. Conclusions	24
Chapter 3. Brittle Fracture of Bone	27
3.1. Review.....	27
3.2. Previous Work Measuring Toughness and Critical Crack Size in Bone	30
3.3. Predicting Bone Fracture Using the TCD	35
3.3.1. <i>Methods</i>	35
3.3.2. <i>Tension</i>	36
3.3.3. <i>Torsion</i>	37
3.3.4. <i>Bending</i>	39
3.3.5. <i>Results</i>	40
3.4. The Toughness of Short Cracks.....	43
3.4.1. <i>Experimental data and predictions</i>	44
3.5. Effects of Thickness.....	46
3.6. Nanoindentation and the TCD	48
3.7. Discussion.....	51
3.8. Conclusions	53
Chapter 4. Indentation: Prediction of Crack Initiation	55
4.1. Summary of the Experimental Results.....	56
4.2. Indentation Fracture and Cutting: Background	58
4.3. Indentation singularities	60
4.4. Effects of Friction	65
4.5. Fracture Line.....	66

4.6. Conclusion	73
Chapter 5. Indentation- Cutting Fracture Force	75
5.1. Multiaxial Critical Distance Theory.....	77
5.2. Finite Element Modeling	79
5.3. Load-Displacement Model	80
5.4. Applying the TCD to Predict the Indentation Fracture Force	83
5.5. Longitudinal Indentation: Estimating α and L.	84
5.5.1. 20°-700 μ m Indenter	87
5.5.2. 20°-300 μ m Indenter	91
5.6. Estimating α and L.....	94
5.7. Sharp Blades	95
5.8. Prediction of the Fracture Force	98
5.9. Effects of Geometry on Fracture Force.....	99
5.10. Transverse Indentation	102
5.11. Tangential Indentation Fracture Force	115
5.12. Discussion.....	122
5.14. Conclusion	125
Chapter 6. Indentation: Damage Area	127
6.1. Methods	128
6.2. Damage and Acoustic Emission	128
6.3. Results	130
6.3.1. Experimental Results.....	130
6.3.2. Finite Element Predictions.....	135
6.4. Discussion.....	138
Chapter 7. Discussion	141
Chapter 8. Conclusions	151
Appendices	161

List of Figures

Figure 2-1. Principles of the stress-based methods. The Point Method (PM) uses the stress at a distance d_{PM} from the notch root; the Line Method (LM) uses the average stress over a distance d_{LM}	9
Figure 2-2. Flowchart of applying finite fracture method to the finite Element model .	12
Figure 2-3. Comparison of predictions from the four methods for the case of a circular hole in an infinite body, showing the effect of the hole radius ρ (normalised by L) on the fracture stress σ_f (normalised by σ_0).....	17
Figure 2-4: Comparison of predictions from the four methods for the case of a long narrow slot in an infinite body, showing the effect of the root radius ρ (normalised by L) on the measured fracture toughness K_{cm} (normalised by the true fracture toughness K_c).....	18
Figure 2-5: Comparison of the predictions of the four methods for the case of a long narrow surface slot in an effectively infinite body, for three different values of the anisotropy factor q : (a) $q=1$; (b) $q=1.85$; (c) $q=5$	20
Figure 2-6. Comparison of the four methods for the case of a hole in an effectively infinite body, in an anisotropic material ($q=5$).....	21
Figure 2-7. Prediction of effects of anisotropy of material containing long narrow slot in an infinite body using PM	22
Figure 3-1. Structure of bone in micro scale.....	28
Figure 3-2. Different orientations of specimens of bone according to ASTM E399, here, C-L is longitudinal, L-R: transverse and R-C tangential.....	30
Figure 3-3. Tensile specimen used by Bonfield and Datta 1976. The tensile axis of the specimen coincides with the longitudinal axis of the bone from which it was taken.	36
Figure 3-4. Finite element model of tensile test performed by Bonfield and Datta 1976	37
Figure 3-5. Example of the use of finite element analysis: stress-distance information is obtained on a line drawn from the hole surface in the expected direction of crack growth (at 45° in this example of a bone tube loaded in torsion). Note that the FE model has been cut away here to illustrate the plane on which the critical line is	

drawn. 1, 2 and 3 represent the longitudinal, circumferential and radial orientations of bone respectively.	39
Figure 3-6. Schematic of 4-point bending test on bone	40
Figure 3-7. Bonfield and Datta's experimental results: fracture stress as a function of the inverse square root of notch length. Predictions using the TCD with T=1 and T=1.33, using an L value of 0.38mm in both cases	41
Figure 3-8. Prediction of the effect of hole diameter on torsional strength of whole bones, using T=1.33 and L=0.32mm. The predictions are compared with the experimental results of Edgerton and the linear and nonlinear predictions of Hipp	42
Figure 3-9. Experimental data and TCD predictions for the effect of hole size on bending strength. T=1.33 and L=0.37mm	43
Figure 3-10. Predicted variation of fracture toughness with crack length, compared to data from Mullins.....	45
Figure 3-11. Transverse R-curve of bone, comparing the TCD predictions with Lakes experimental results	45
Figure 3-12. Predictions of the ΔK for a fatigue crack growth rate of $3\text{-}6 \times 10^{-8}$ mm/cycle using the TCD, compared to experimental data from Kruzic.....	46
Figure 3-13. The effect of thickness (B) on the critical distance (L) for bovine bone in three different stages. Plane stress stage ($B < 3$ mm), transition stage ($3 < B < 6$ mm) and plane strain stage ($B > 6$). The data also show the effect of crack propagation length on critical distance. L : plane strain critical distance($4.32\text{MNm}^{-3/2}$), a: crack length, w: width of specimen.....	47
Figure 3-14. Predicted R-curve for plane stress specimens, compared with data from Nalla et al (2004)	48
Figure 3-15. Prediction of relative toughness for short cracks using the line method and point method. The y-axis represents the ratio between the toughness and fracture toughness. The x-axis represents the ratio between the crack length and the critical distance. It shows that two methods predict roughly similar results.	49
Figure 3-16. There is a linear relationship between $Kc\text{m}^{-2}$ and $1/c$ obtained using nanoindentation as it was expected by the TCD. The intersection with y-axis and the slope of the fitted line represent Kc^{-2} and $L.Kc^{-2}$	50

Figure 4-1. Specimen holder for the indentation tests.....	56
Figure 4-2. Different indentation directions (longitudinal, transverse and tangential) ..	57
Figure 4-3. Three different zones formed during the elastic-plastic indentation	59
Figure 4-4. Damage zone at fracture for transverse indentation. The damage occurs underneath the indenter which is under high level of compression.....	61
Figure 4-5. Crack initiation spot for 20°-300μm blade for longitudinal indentation. The main cracks start at the boundaries of contact.....	61
Figure 4-6. Variation of maximum tensile and shear stress on the contact surface, for a 20° angle and 300μm radius blade. The distance is measured from the tip of the blade, and follows the material surface as shown in the diagram.	62
Figure 4-7. Schematic of the variation of first principal stress (S_1) and contact pressure along the boundary during indentation defining the two singularities. The distance is measured from the indenter tip along the surface of bone.....	64
Figure 4-8. Stress distribution in the presence of friction.....	66
Figure 4-9. The cement lines form the weakest constituent of bone. Crack propagation parallel to the osteons (shown with red lines) can occur much more easily in the longitudinal direction. Similarly, if a crack is propagating perpendicular to an osteon (horizontal red line), when it reaches a cement line it will change direction, the crack is blunted.	67
Figure 4-10. Crack propagation direction in longitudinal cutting. The main crack advances in the longitudinal orientation of bone.....	68
Figure 4-11. Crack growth during the transverse indentation. The main crack grows in the tangential plane.	69
Figure 4-12. Variation of normal stress and shear stress on the critical line for 20°-700 indenter at the fracture force.....	70
Figure 4-13. Contour of first principal stress for the 20°-300μm blade	71
Figure 4-14. Variation of tensile stress and contact pressure on the contact surface for longitudinal indentation using 20°-300μm indenter. The contact pressure drops to zero at the contact boundary. The distance is measured from the blade tip along the contact surface	72

Figure 4-15. Cracks in the longitudinal direction start from the boundary of contact, and then they merge and propagate in the longitudinal direction. Inelastic deformation at fracture can also be seen under the indenter.	73
Figure 5-1. Model of bone as a bi-linear material, the young modulus is taken from experiments and the tangent modulus is found such as to predict the best force-displacement curve measured from experiments.	81
Figure 5-2. Force-displacement during indentation using blade 20°-300μm to find the best model. It shows the force-displacement variation with Yield stress and tangential modulus and compare them with experimental results (darker curves).	82
Figure 5-3. Experimental force-indentation in longitudinal direction using 20°-300μm blade on four specimens.	85
Figure 5-4. Force-indentation of longitudinal indentation using 20°-700μm wedge performed on four different specimens.	86
Figure 5-5. Inelastic deformation and crack direction during the longitudinal indentation. The fracture line is selected in the longitudinal orientation.	87
Figure 5-6. Distribution of shear stress, tensile stress and the contact pressure on the contact surface for 20°-700μm indenter at the fracture force in longitudinal indentation. The contact pressure drops at the contact boundary. The tensile stress changes from compression to tension at the boundary. The shear stress is zero on the contact surface because of lack of friction but it changes at the boundary as a result of significant change in tensile stress.	88
Figure 5-7. Contours of shear stress and fracture line for 20°-700μm indenter at fracture force. The maximum shear stress occurs beneath the indenter at a distance from the boundary of contact.	89
Figure 5-8. First principal stress at the fracture force for 20°-700μm indenter. The stress beneath the indenter is extremely compressive. There is a small tensile zone on the surface.	89
Figure 5-9. Variation of normal stress and shear stress on the critical line for 20°-700μm indenter at the fracture force. The compressive stress is acting on the fracture line therefore a higher shear stress than the ultimate shear stress (69MPa) is required for failure.	90

Figure 5-10. Variation of maximum tensile, shear stress and contact pressure on the contact surface for 20°-300μm indenter at fracture force.	92
Figure 5-11. Maximum tensile stress under the 20°-300μm indenter at fracture force .	93
Figure 5-12. Shear stress distribution under the 20°-300μm indenter.....	93
Figure 5-13. Fracture stress ($\sigma+\alpha\tau$) on the fracture line for two different blades when $\alpha=0.3$. The critical distance found to be 0.32mm.....	95
Figure 5-14. Contours of maximum principal stress around the indenter tip for 20°-50μm blade. It shows the effects of different singularities on the stress distribution.....	95
Figure 5-15. Stress variation along the contact line at the fracture force for 20°-50μm indenter at fracture force. Stress distribution is affected by two kinds of singularities	96
Figure 5-16. The stress ratio for different crack initiation points, defined by distance from the indenter tip, for 20°-50μm indenter. The second and the fourth points are located at the geometric and boundary singularity respectively.....	97
Figure 5-17. Contour of critical stress at the crack tip with two different critical plane directions. The critical stress contour is growing with increasing the applied stress. The crack propagates if the critical stress contour reaches the critical distance in a certain direction	98
Figure 5-18. Predicted fracture force for different indenters in longitudinal indentation was found by assuming that the stress-distance curves at fracture force for each indenters passes through the critical point, as shown here.....	99
Figure 5-19. Experimental results and TCD predictions of longitudinal indentation force for blades with 20° angle and various radii.....	100
Figure 5-20. Effect of indenter angle on fracture force for longitudinal indentation. TCD prediction and experimental results.	102
Figure 5-21. Critical line for transverse indentation. The photo shows a sample just after the maximum cutting force. Part of the bone has removed due to the crack growth in the tangential plane.	103
Figure 5-22. Fracture line in the transverse indentation. The main crack grows in the tangential direction which is the weakest structural direction of bone.....	104

Figure 5-23. Finite element model verification with the experimental data for 20-50 blade in transverse direction	105
Figure 5-24. Fracture plane in transverse direction for sharp blade; photo taken just after fracture of the first piece of bone (from the left hand side).....	106
Figure 5-25. Stress on the contact surface of transversal indentation using 20°-300µm indenter	107
Figure 5-26. Possible critical lines for different crack initiation points (Transversal Indentation) he lines started from different points: the tip of the indenter, the largest compressive stress spot, an optional point and the boundary of contact ..	108
Figure 5-27. Fracture force factor for 20°-300µm indenter in transversal direction....	108
Figure 5-28. Fracture force factor for transversal indentation using 20°-50µm indenter. The three points show the indenter tip, the geometric and the boundary singularities respectively.	109
Figure 5-29. First Principal stress distribution of transverse indentation around the 20°-50µm indenter	110
Figure 5-30. 3rd Principal stress around the indenter of transverse direction for 20°-50µm blade	110
Figure 5-28. Transverse indentation fracture force for 20° indenter. Experimental vs TCD prediction. Error bars show standard deviation: dotted lines show maximum and minimum experimental values	111
Figure 5-29. Transverse indentation fracture force for 40° indenter. It compares the predictions using the TCD and the experimental results. The indentation fracture force increases with radius. Error bars show standard deviation: dotted lines show maximum and minimum experimental values.....	112
Figure 5-30. Transverse indentation fracture force for 60° indenters and different tip radius. Experimental results vs TCD predictions.	112
Figure 5-31. Fracture force of transverse indentation for indenters with radius 50 Micron	113
Figure 5-32. Fracture force of transverse indentation for indenters with radius of 700µm. The TCD predicts no change with increasing the angle. The statistic test rejects any significant difference between the experimental results for various angles.....	114

Figure 5-33. Load-displacement for 20°-50µm blade in tangential indentation..... 116

Figure 5-34. Load-displacement for 20°-300µm indenter in tangential indentation.... 117

Figure 5-35. Load-displacement for 40°-50µm indenter in tangential indentation 117

Figure 5-36. Load-displacement for 20°-700µm indenter in tangential indentation.... 118

Figure 5-37. Tangential indentation fracture force for blades with angle of 20° and different radii. 119

Figure 5-38. Tangential indentation fracture force for blades with angle of 40° and different radii. Error bars show standard deviation: dotted lines show maximum and minimum experimental values 119

Figure 5-39. Tangential indentation fracture force for blades with angle of 60° and different radii. 120

Figure 5-40. Tangential indentation fracture force for blades with radius of 50µm and different angles. The TCD predicts the experimental results for 20° and 40° blades well but there is no experimental result for 60 degrees blade to compare with the predictions. 121

Figure 5-41. Tangential indentation fracture force for blades with radius of 300µm. The TCD predicts no change with increasing the angle. The experimental data agrees with these predictions..... 121

Figure 5-42. Tangential indentation fracture force for blades with radius of 700µm. The TCD predictions are in good agreement with experimental data, which show that for this indenter, the angle does not have any effect on the indentation fracture force 122

Figure 6-1. Cumulative number of AE hits for bone specimen cut up to maximum fracture load. The onset of microcracking is associated with the non-linear phase. 129

Figure 6-2. Damage zone during the transverse cutting using a sharp blade. Two different damage zones, tensile and compression, are formed 131

Figure 6-3. Tensile and compression damage zones formed due to longitudinal cutting 132

Figure 6-4. Damage area for blade with 20° angle and different radii. (Three different cutting directions) 133

Figure 6-5. Damage area in different cutting directions..... 134

Figure 6-6. Estimating damage area using principal stresses for 20°-300µm indenter.
 Left: Damage due to compressive stress, Right: Damage due to tensile stress.... 135

Figure 6-7. Comparing damage area measured using FE model for longitudinal indentation of 20° blades, when critical stresses is 60% and 54% of ultimate stress with experimental results..... 136

Figure 6-8. Size of damage zone measured experimentally at transverse indentation fracture. It also shows the predictions using the FE model. The damage area in the FE model measured when the stress reaches 60% of ultimate stress..... 137

Figure 6-9. Size of damage zone at fracture in tangential indentation. it compares the FE prediction using 90% of ultimate stress. 138

Figure 7-1. Microstructure of compact bone..... 143

List of Tables

Table 3-1: Cortical bone fracture toughness results for transverse and longitudinal orientations.	29
Table 3-2: Orthotropic elastic constants of bovine femoral bone, Van Buskirk et al, ...	38
Table 5-1: Young's modulus of bovine femur in different directions (experimental data from Mr.Ger Reilly).....	82
Table 5-2: Predicted longitudinal fracture load using the TCD for different indenters (prediction error percentage). There is no experimental data for 60°-50µm blade to compare with the prediction.	99
Table 5-3: Transverse indentation fracture force for different indenters and the difference between average experimental results and FE predictions.....	111
Table 7-1: Cortical bone structural organization along with approximate physical scales	142

CHAPTER 1. Introduction

Bone is an important mechanical organ which must withstand high forces with limited amount of deformation, therefore, the health and quality of bone has always been a major concern. The health of bone is a function of its mechanical, chemical and biological properties. For example, bone is a porous material and its porosity increases with age. The increase in porosity and decrease in bone mineral density (BMD) raises the risk of fracture, which is a major problem. In 1990, 1.66 million people were suffering from hip fractures worldwide. In 1995, over half of these were documented to have occurred in Europe and North America [1]. It has been estimated that the number will increase by about 300% in 2050 [2]. Up to 20% of patients admitted with a hip fracture will die within 6 months and up to one third will become totally dependent and some will be permanently disabled. In 1990, over 1500 hip fractures were reported in Ireland due to osteoporosis in people over the age of 60. By 2002, this number was increased by over 110%. Due to the aging demographic in Ireland, the fracture risk assessment is becoming increasingly important and in need of being addressed.

Bone is a composite material with hierarchical structure. In continuum scale, it is known as an elastic material with small post yielding deformation. Linear Elastic Fracture Mechanics (LEFM) has been employed to study the fracture mechanics of bone, but it was shown that the LEFM is valid only for fracture in the longitudinal direction[3]. The Theory of Critical Distances (TCD) [4] is a relatively new method

which is based on LEFM, but it is generally more applicable. The TCD is easy to apply, which gives it an important advantage when compared to other fracture mechanics theories. The TCD was introduced to study the fatigue and brittle fracture of materials[5] and then it was developed to be employable to different ranges of loading, materials and geometries[6-20].

The TCD methods are based on the length characteristic parameter, L . These methods can be classified as either stress or energy methods. The Point Method (PM), Line Method (LM), Area Method (AM) and Volume Method (VM) are stress based whilst Finite Fracture Mechanics (FFM), and the Imaginary Crack Method (ICM) are energy based. These methods will be discussed and compared in more details.

Most fractures occur due to the high stress acting on the bone. A fracture usually starts from a weak spot or stress concentration point. Bones behave differently in the presence of stress concentrators, therefore effects of stress concentrators on bone have to be investigated. Such a study leads us to a better understanding of the mechanism of bone failure and the effect of surgical procedures which create stress concentrations.

Like other materials, bone can fail due to contact stresses: we call this indentation fracture. Cutting is one example of indentation fracture. The study of indentation is not new[21-29]. Indentation fracture and cutting have been widely employed to understand the failure mechanism of different materials[30-37]. They have also been used to obtain the mechanical properties of bones [38-40, 35, 36, 41, 42, 37, 43] and human enamel [44, 45]. Because bone is a brittle material, it fails during indentation in a catastrophic way, due to the growth of a main crack. The main crack nucleates at the contact surface which is under a high level of compression. It is difficult to predict the conditions needed to nucleate cracks in compressive zones.

Indentation fracture and cutting is used extensively for different purposes. In the food industries [46-49], finding the best crispiness and crunchiness for foods especially snacks [48, 47, 50, 46, 49] has a large effect on sales. In surgery, the cutting tools have to be sharp enough to reduce the fracture force and limit the damage in the surrounding

bone. Needle insertion and tactile sensor based on contact and indentation are used for virtual surgery[51].

The design of osteotomes has been developed since the 18th century. Drilling, cutting and sawing are important in surgery. The effects of cutting angle on the heat generation [52]and cutting energy [53-56]on bone has been extensively studied. Also, the drilling process was studied in order to reduce the heat generated [57-60]and cutting energy[61], but there has not been much investigation done on the effect of the wedge angle and tip radius of blades on the indentation fracture force of bone.

The present work was a theoretical study using computer simulations. It was conducted in parallel with an experimental study of indentation fracture, performed at the Institute of Technology, Sligo, by Mr. Ger Reilly. Therefore, whenever we are talking about experimental results of indentation, Mr. Reilly's results are presented. The theoretical predictions obtained in this study were compared with Mr. Reilly's results and also with other experimental results from the literature.

In this thesis, it is shown that the TCD can be used to study the failure of bone samples containing defects such as holes, notches and cracks, and to predict how the strength of bone changes due to these defects. Also, failure of bone under compression and indentation of bone, which are more complicated problems, were predicted using the TCD. Contact between a blade and bone, causes stresses in the bone. This stress concentration depends on the geometry of the components, especially the blade. Indentation fracture is an effect of this stress concentration. This is the first time that the TCD has been applied to predict the bone failure and also indentation and compression problems.

At the start of this project, some methods of fracture mechanics were examined. Different finite element techniques of fracture modeling were used. In some techniques, the crack must be simulated. The problem with these methods was that they are computationally expensive, especially in contact problems. The most important disadvantage of them is that they can not be used in our contact problem because of a

high compression stress at the fracture plane, which causes the cracks to close. Other methods, which generally are called smeared methods, do not need any crack introduction. In these methods, elements material properties change to show damage and cracks. The problem with this approach is that they are not fully accurate, especially for contact problems[62].

In chapter 2, the principles of the TCD are explained and the four different critical distance methods are compared. It will be shown that all TCD methods predict similar results, in particular for anisotropic materials. The advantages and disadvantages of the various methods and their application will be discussed.

In chapter 3, the TCD is applied to bone. Effects of stress concentrators like holes, notches and cracks are studied, and the critical parameters of bone are predicted. Furthermore, the effects of short cracks on the fracture toughness of bone are predicted using the TCD. This is the first time that the TCD is applied to bone. In this chapter it will be shown that the TCD works well to predict brittle fracture of bone, and also it is a potential method to study osteoporosis.

In chapter 4, the indentation problem is studied. We concentrate on the crack initiation spot under indentation. FE modeling is compared with experiments to explain the crack initiation point. It will be shown that stress concentrations play important roles in crack initiations. Two different singularities are defined and their effects on crack initiation are studied.

In chapter 5, crack propagation is considered. Using the experimental data, the crack propagation direction is defined and indentation fracture force is predicted using the TCD. The predictions are done for three different cutting directions as were used in the experiments: longitudinal, transverse and tangential. Effects of indenter geometry (radius and wedge angle) on fracture force are investigated. It is shown that the TCD can be used to predict the fracture force and also the location of crack initiation.

In chapter 6, the amount of damage during indentation is predicted. Experimental data on damage is compared with prediction using a simple theory. It will be demonstrated that the damage zone size is related to the critical distance of bone.

In summary, we will show that the TCD is able to predict the fracture of bone due to stress concentrations of various types, including indenters; the results also shed light on the physical significance of the critical distance in relation to the microstructure of bone.

CHAPTER 2. Comparison of Four TCD Methods

Critical distance methods were introduced for the purpose of studying the effects of stress concentration. Taylor[4] defined several different critical distance methods: some are stress based and others energy based, but they have two things in common: they are all linear-elastic methods and they all use the same length characteristic parameter, L . These theories have been used to study the fatigue failure of materials, as well as brittle fracture. They also have been applied to a wide range of materials. Here, four different critical distance methods are compared, which are so named: Point Method (PM), Line Method (LM), Finite Fracture Mechanics (FFM), and Imaginary Crack Method (ICM). It will be shown that the four methods predict results which are quite similar, but not always identical. Investigated also will be the effects of material anisotropy on fracture stress.

2.1. Comparing the Critical Distances Methods

Many different methods are used for the prediction of failure in bodies containing stress concentration features, such as notches. The wide variety of such methods and the large amount of research which is presently being conducted to further develop them demonstrates that this is a key area and one which requires continuing work. One

common feature of many modern methods of failure prediction is the existence of a material-dependant length scale. Such a length scale, which for the purposes of this work will be called the critical distance, expresses an important property of the material and strongly affects fracture behaviour when any feature of the notch geometry, such as its length or root radius, is similar in magnitude to the critical distance. Here we will consider four methods which are used to predict brittle fracture resulting from monotonic loading, and also high-cycle fatigue behaviour resulting from cyclic loading.

Two of these methods make their predictions using the stress field ahead of the notch. Starting from a simple elastic stress analysis (using either analytical solutions or FEA), a characteristic stress parameter is calculated and compared to a critical failure stress for the material. The critical distance appears in these models in the method of calculating the characteristic stress parameter. The other two methods which we will discuss are based on fracture mechanics; in these methods the critical distance appears in the form of an assumed initial crack length or an assumed increment of crack growth. The stress-based methods have been in use for over fifty years, and one of the fracture mechanics methods has been used for thirty years; however the other method, which we call Finite Fracture Mechanics (FFM), has been developed only recently.

The present work aims to show that these four methods, despite significant differences in their approaches, actually have much in common. This argument is developed first by showing, for some very specific cases, that the analytical solutions obtained from the two fracture mechanics methods are in fact identical to those from one of the stress-based methods, and that there is a simple relationship between the values of the various critical distances. Subsequently, a wider range of notch geometries and material types will be investigated, including notches in anisotropic materials with properties typical of those of fibre composites and human bone.

2.2. Stress-Based Methods

The two methods which will be called the Line Method (LM) and Point Method (PM), were originally developed by Neuber [63, 64] and Peterson [65], respectively for the purposes of predicting the fatigue limits of metallic materials. They were

independently invented some time later by Whitney and Nuismer [5] who used them to predict monotonic fracture in composite materials. The concept is shown in Figure 2-1. Failure is assumed to occur when a characteristic stress is equal to a critical value σ_o . For the line method the characteristic stress is the average stress along a line of length d_{LM} , thus:

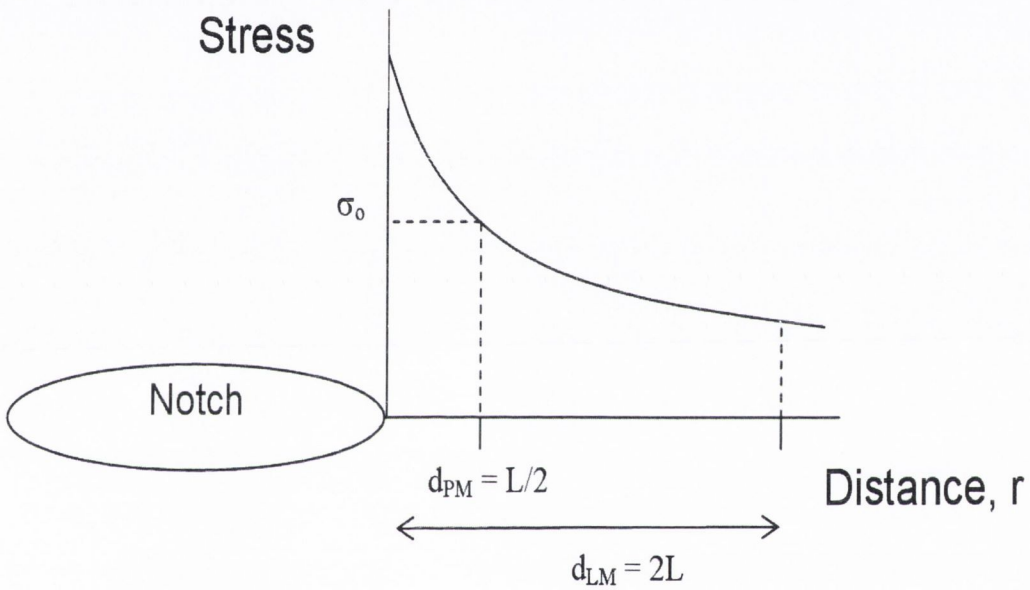


Figure 2-1. Principles of the stress-based methods. The Point Method (PM) uses the stress at a distance d_{PM} from the notch root; the Line Method (LM) uses the average stress over a distance d_{LM}

$$\frac{1}{d_{LM}} \int_0^{d_{LM}} \sigma(r) dr = \sigma_o \quad (2-1)$$

In the case of the PM, the characteristic stress is simply the stress at a particular point $r = d_{PM}$, thus the failure criterion is:

$$\sigma(d_{PM}) = \sigma_o \quad (2-2)$$

If the applied loading takes the form of simple tension perpendicular to the line which bisects the notch, then the relevant stress parameter to use will be the maximum principal stress, and the line on which calculations are performed will be the same as the notch bisector. In other cases involving multiaxial loading, these methods can still be used but different stress parameters and lines are required (see, for example [9]); These stress parameters can be considered as stress ranges in making predictions of fatigue behaviour.

2.3. Fracture Mechanics Methods

The method which we call the Imaginary Crack Method (ICM) was developed autonomously by several groups, which are as follows: ElHaddad *et al* for the use in predicting the effect of short fatigue cracks [66], by Lukas and Klesnil for predicting notch effects in fatigue [67], and by Waddups for predicting notch effects in monotonic fracture of fibre composites [68] . This method makes two assumptions. Firstly, that there exists a crack of a certain length a_{ICM} , at the root of the notch, and secondly, that the propagation of this crack conforms to Linear Elastic Fracture Mechanics (LEFM) theory, i.e. that brittle fracture occurs when the stress intensity K becomes equal to the fracture toughness K_c . Thus, the applied stress to cause monotonic fracture, σ_f , will be given by the following formula:

$$\sigma_f = \frac{K_c}{F\sqrt{\pi(a + a_{ICM})}} \quad (2-3)$$

Here F is a constant which depends on the geometry of the problem and the type of loading. Some workers have identified this crack with a real, physical crack or zone of damage which occurs in some cases prior to final failure, but it is worth noting that a physical crack of this length would, by definition, be too short to conform to LEFM. As a result of this, the use of the above two assumptions makes this crack essentially an imaginary one.

Another fracture mechanics method, which is called Finite Fracture Mechanics (FFM) was developed only recently [69, 15]. In this approach the normal Griffith energy balance of LEFM is modified, assuming that crack growth occurs in increments of finite length, Δa_{FFM} , rather than, as is conventional, assuming infinitesimal crack extension. This requires that we integrate the strain energy release rate, G , over the crack extension, and equate it to its critical value, G_c , thus:

$$\int_0^{\Delta a_{FFM}} G da = G_c \Delta a_{FFM} \quad (2-4)$$

It is useful to note that this can also be written in terms of stress intensity, thus:

$$\int_0^{\Delta a_{FFM}} K^2 da = K_c^2 \Delta a_{FFM} \quad (2-5)$$

Figure 2-2 shows how to apply the FFM on a finite element model.

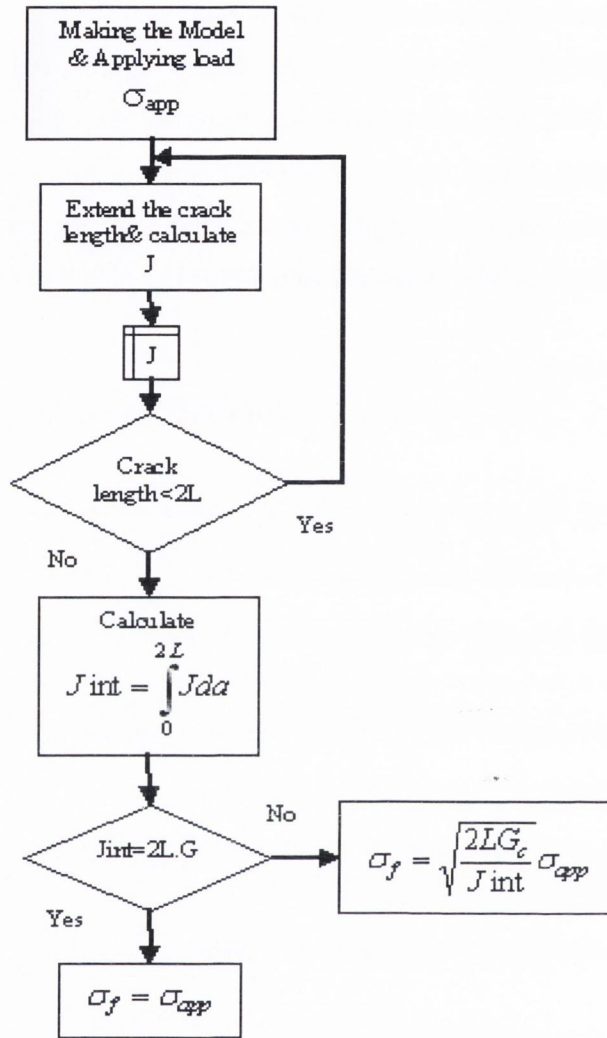


Figure 2-2. Flowchart of applying finite fracture method to the finite Element model

2.4. Analytical Relationships between the Four Methods

Some relationships have already been established between the critical distances used in the stress-based methods and the critical stress intensity factor K_c . These links were first noticed by Whitney and Nuismer [5] and subsequently re-invented in the fatigue area by other workers [70, 71]. The derivation starts from the idea that, since these methods are supposed to work for all kinds of notches, they should be applicable to sharp cracks. We know that the elastic stress distribution ahead of a sharp crack of

length a loaded to a stress intensity K can be approximated by a simple equation, provided we consider only distances $r \ll a$, thus:

$$\sigma(r) = \frac{K}{\sqrt{2\pi r}} \quad (2-6)$$

Noting that failure of the cracked body will occur when $K = K_c$, applying equations 2-1 and 2-2 shows that the critical distance for the Line Method, d_{LM} is equal to $2L$ and that for the Point Method, d_{PM} is equal to $L/2$, where:

$$L = \frac{1}{\pi} \left(\frac{K_c}{\sigma_o} \right)^2 \quad (2-7)$$

Applying these methods to the other extreme case, that of a plain specimen containing no crack or notch, one finds that σ_o is equal to the strength of the material (i.e. the Ultimate Tensile Strength in the case of monotonic loading and the fatigue limit $\Delta\sigma_o$ in the case of fatigue). These relationships are very useful because they provide a link between three material constants: the fracture toughness, the material strength, and L .

Experimental work has shown that these relationships do indeed hold for many practical cases, e.g. monotonic fracture of ceramic materials [12] and fatigue of metals [10], however there is a complication in the case of monotonic fracture in some materials, when σ_o takes on a value which is different from (and, it seems, always greater than) the plane-specimen strength; this occurs for example in metals and in polymers [11, 72]. This arises because the failure of plane specimens occurs by a different mechanism (e.g. the propagation of pre-existing flaws, or plastic instability) which does not occur when a notch is present. This matter is very interesting, however it is of no concern in this section because it does not affect the comparison between the different methods. Thus, we will proceed by assuming that σ_o is equal to the material's strength as measured using plane tensile test specimens. In the next chapters, it will be shown that in the case of bone, σ_o is slightly larger than plane specimen strength.

We will now develop some further links between these methods, using the same assumption that the methods are valid for the case of a body containing a pre-existing crack. In what follows, consideration will be given to the effect of crack length, including very short cracks where “ a ” approaches zero. Therefore, instead of the approximate relationship of equation 2-6, the precise result will be used, due to Westergaard, for the case of a central through-crack, half-length a , in an infinite body subjected to uniform tension:

$$\sigma(r) = \frac{\sigma}{\left[1 - \left(\frac{a}{a+r}\right)^2\right]^{1/2}} \quad (2-8)$$

If the Line Method is applied (equation 2-1) using this stress distribution, and noting that $d_{LM} = 2L$, the following will be obtained:

$$\sigma_f = \sigma_o \sqrt{\frac{L}{a+L}} \quad (2-9)$$

A prediction can also be made using the ICM (equation 2-3), noting that for the crack in question $F=1$ and that, for the case of zero crack length equation 2-3 reduces to:

$$\sigma_o = \frac{K_c}{\sqrt{\pi a_{ICM}}} \quad (2-10)$$

The ICM prediction is thus:

$$\sigma_f = \sigma_o \sqrt{\frac{a_{ICM}}{a+a_{ICM}}} \quad (2-11)$$

Comparing equations 2-9 and 2-11, it is obvious that they are identical and that the critical distance for the ICM is exactly equal to L . This result is by no means obvious,

since the LM is based on the local stress field of the crack, whilst the ICM is based on the change in stress intensity caused by the extra crack length. There is, however, a small difference between the two methods; further consideration will show that they are exact only for the case of a crack in which the geometry factor F is equal to unity, otherwise the two critical distances are related by $a_{ICM} = L/F^2$. In many practical cases, however, F lies closely to unity, for example it is equal to 1.12 for a surface crack and of the order of 0.7-0.8 for typical embedded elliptical flaws. In these cases the predictions from the LM and ICM will still be identical at the extreme cases of a plane specimen and a long crack, but slight differences will occur for intermediate crack lengths, especially around $a=L$.

Finally, use can be made of the FFM, taking the same case of a through crack (equation 2- 8). Please note that the strain-energy release rate, G , for this problem is:

$$G = \frac{dW}{da} = \frac{\sigma^2}{E} \pi a \quad (2-12)$$

Using equation 2- 5 gives the following result for the fracture stress:

$$\sigma_f = \sqrt{\frac{G_c E}{\pi \left(a + \frac{\Delta a_{FFM}}{2} \right)}} \quad (2-13)$$

Comparing this with equation 2- 3 (noting that $F=1$ in this case) it can be seen that the prediction using the FFM is identical to that of the ICM, with a critical distance Δa_{FFM} equal to $2L$.

In summary, the above analysis has shown that, for the particular case of a central through crack of any length, the predictions of the LM, ICM, and FFM are identical, and that the critical lengths are simply related, being $2L$, L and $2L$ respectively. For a more general case of a crack where F is not equal to unity, the predictions of the LM differ slightly from those of the fracture mechanics methods, for crack lengths close to

L. Again we note that these results are not at all obvious, since the fracture mechanics methods use quite different assumptions from those of the stress-based LM.

Figure 2-3 shows predictions of the effect of crack length when $F=1$, comparing the PM to the other three methods. Clearly, the PM gives slightly different predictions except at the extremes, though the differences between this and the other methods are small, being always less than 6%.

2.5. Further Comparisons between the Methods: Notches and Anisotropic Materials

Here the application of the four methods to various kinds of notches is considered. For some notches, closed-form solutions can be obtained, using previously-established relationships for the elastic stress fields and for stress intensities for the notch-plus-crack case. For example, the stress field around a circular hole in an infinite plate in tension can be found from the well-known Airy functions, whilst the stress intensity for a crack growing from the hole can be found from Murakami's handbook. Figure 2-3 shows predictions from all four methods for the effect of hole radius on fracture stress, normalised by the plane-specimen strength. For very large holes the result tends to $1/3$, reflecting the stress concentration factor of 3 close to the hole surface; for very small holes the results approach unity. As the figure shows, predictions obtained from the four methods are all slightly different. Clearly, it cannot be demonstrated the same kind of mathematical equivalence shown in the previous section for the case of short cracks, yet the differences between the methods are small – all four fall within a scatter band of plus-or-minus 7%, indicating that for all practical purposes the predictions are the same.

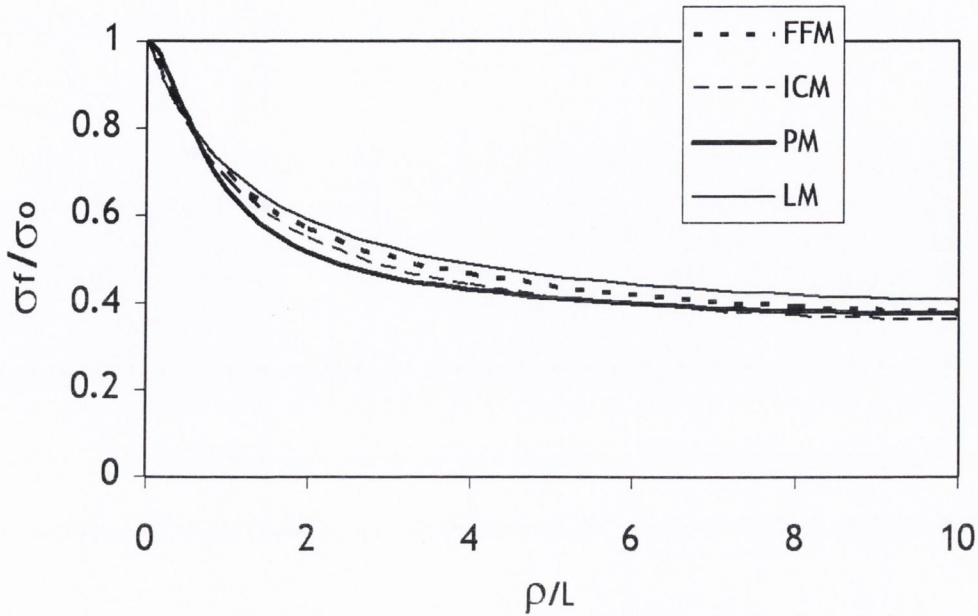


Figure 2-3. Comparison of predictions from the four methods for the case of a circular hole in an infinite body, showing the effect of the hole radius ρ (normalised by L) on the fracture stress σ_f (normalised by σ_0)

Another case of practical interest is that of a long, narrow slot, i.e. a notch of length D , which is much greater than its root radius ρ . The stress field for this type of notch, when located in an infinite body, was found by Creager and Paris [73]:

$$\sigma(r) = \frac{K}{\sqrt{2\pi x}} \left(1 + \frac{\rho}{2x} \right) \quad (2-14)$$

Here K refers to the stress intensity for a crack of the same length, D . The PM and LM can easily be applied to this equation, leading to closed-form solutions, and the ICM and FFM can also be used, taking solutions as before. Figure 2-4 shows the effects of changing the root radius, as a function of L . In this case it is convenient to express the results in terms of the ‘measured toughness’, K_{cm} , which is defined as the value of K_c which would be measured if the notch is assumed to be a sharp crack, therefore:

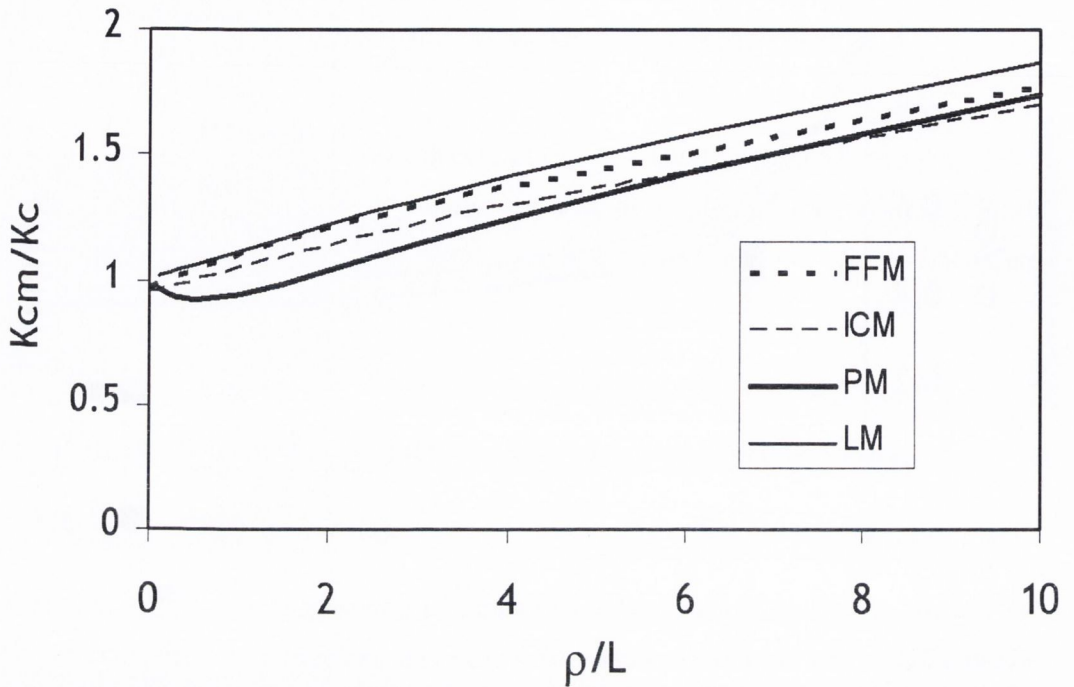


Figure 2-4: Comparison of predictions from the four methods for the case of a long narrow slot in an infinite body, showing the effect of the root radius ρ (normalised by L) on the measured fracture toughness K_{cm} (normalised by the true fracture toughness K_c)

$$K_{cm} = F \sigma_f \sqrt{\pi D} \quad (2-15)$$

Thus, the ratio K_{cm}/K_c tends to unity for a sharp crack ($\rho/L = 0$) and remains close to unity for small values of the root radius. Once ρ becomes significantly greater than L , K_{cm}/K_c increases, showing that the notch is no longer crack-like. Again it can be seen from the figure that the four methods, though not identical, yield similar results (within a scatter band of 5%).

In order to study some other cases for which convenient closed-form solutions do not exist, finite element analysis (FEA) must be used. The commercial software ANSYS was employed to create linear elastic models from which the stress fields near notches could be determined. In order to implement the ICM and FFM, cracks were introduced at the notch roots using quarter-point elements, and the stress intensity factors were

found using the J-integral facility in ANSYS, as well as calculating the stress intensity factor as explained in Appendix 1.

The FEA also allowed for the consideration of anisotropic materials. Some models were created with orthotropic elasticity, in which the elastic modulus in the direction parallel to the applied load axis was different from that in other orthogonal directions. The ratio between $E(\text{parallel})$ and $E(\text{perpendicular})$, termed q , was varied from 1 upwards to 5. Plane stress analyses were carried out, taking account of the different relationship between the stress intensity and the strain-energy release rate for materials having orthotropic elasticity, as developed by Sih et al [74].

Figure 2-5, Figure 2-6 and show examples of predictions for surface slots and central holes, in materials with q values of 1 (isotropic), of 1.85 (chosen because this value is typical of human bone) and 5 (typical of some industrial fibre composites). For slots, q has a strong effect on the form of the graph; for holes on the other hand anisotropy has only a small effect on the predictions. In all cases the four different methods again give similar predictions, with scatter bands no greater than plus-or-minus 10%.

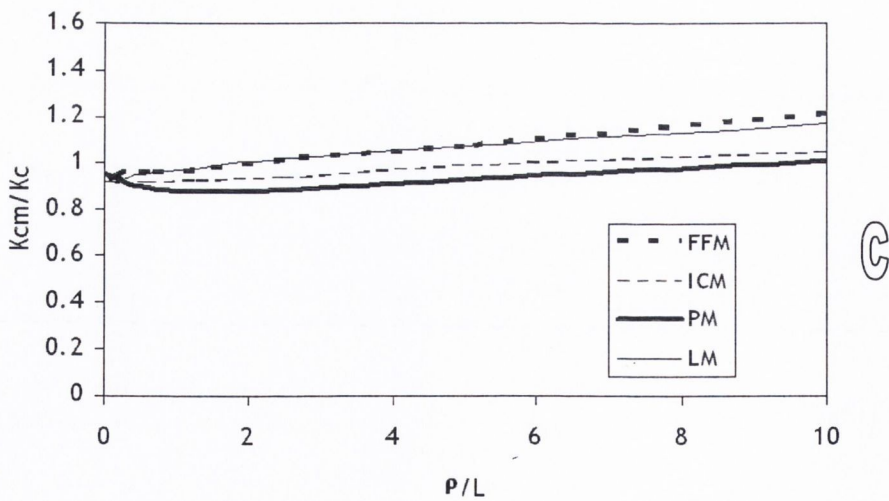
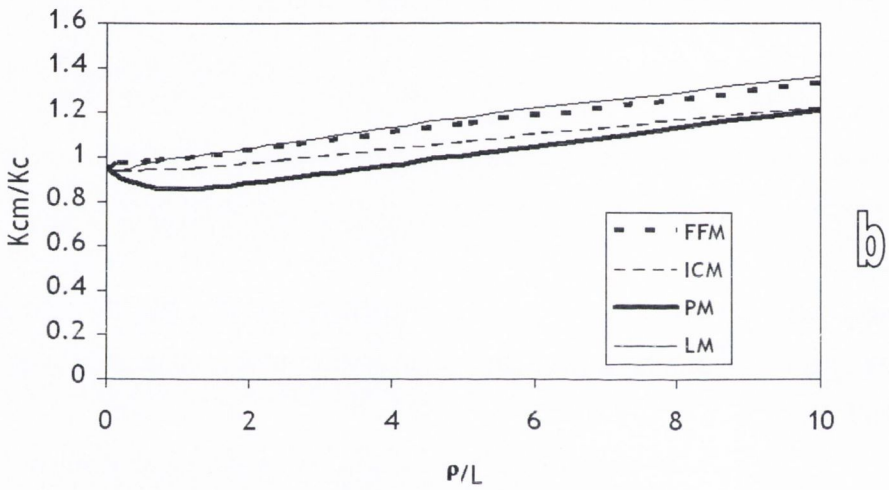
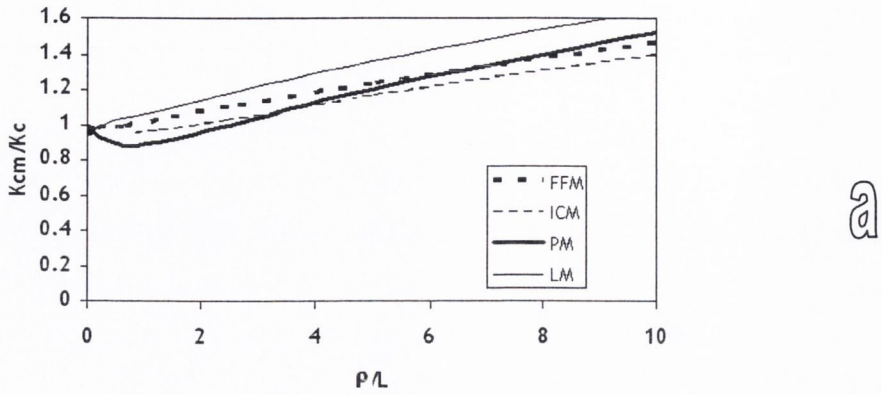


Figure 2-5: Comparison of the predictions of the four methods for the case of a long narrow surface slot in an effectively infinite body, for three different values of the anisotropy factor q : (a) $q=1$; (b) $q=1.85$; (c) $q=5$

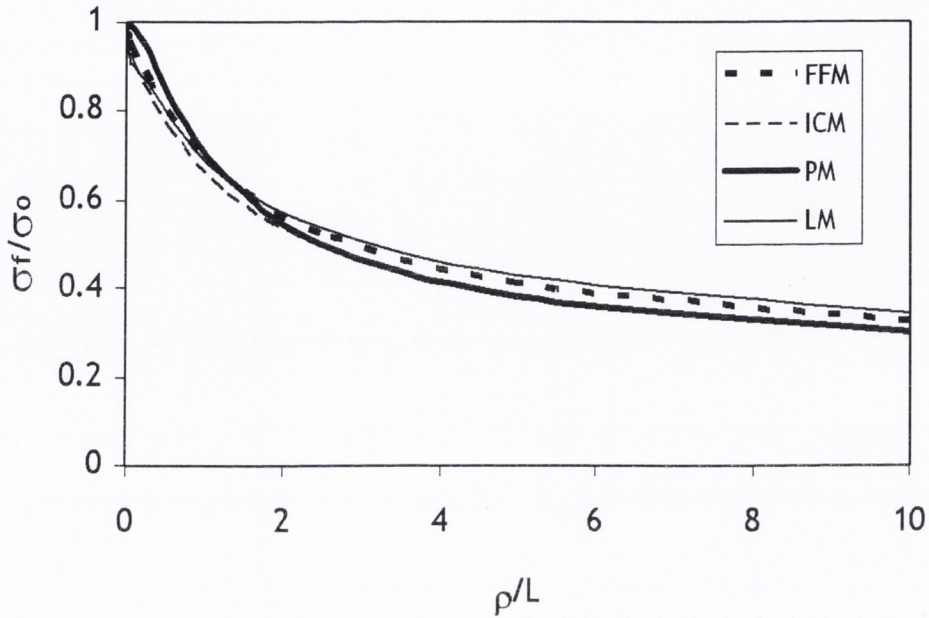


Figure 2-6. Comparison of the four methods for the case of a hole in an effectively infinite body, in an anisotropic material ($q=5$).

Figure 2-7 shows the effects of anisotropy predicted using the Point Method. PM predicts that with increasing the length of the slot, the effect of anisotropy on measured fracture toughness increases.

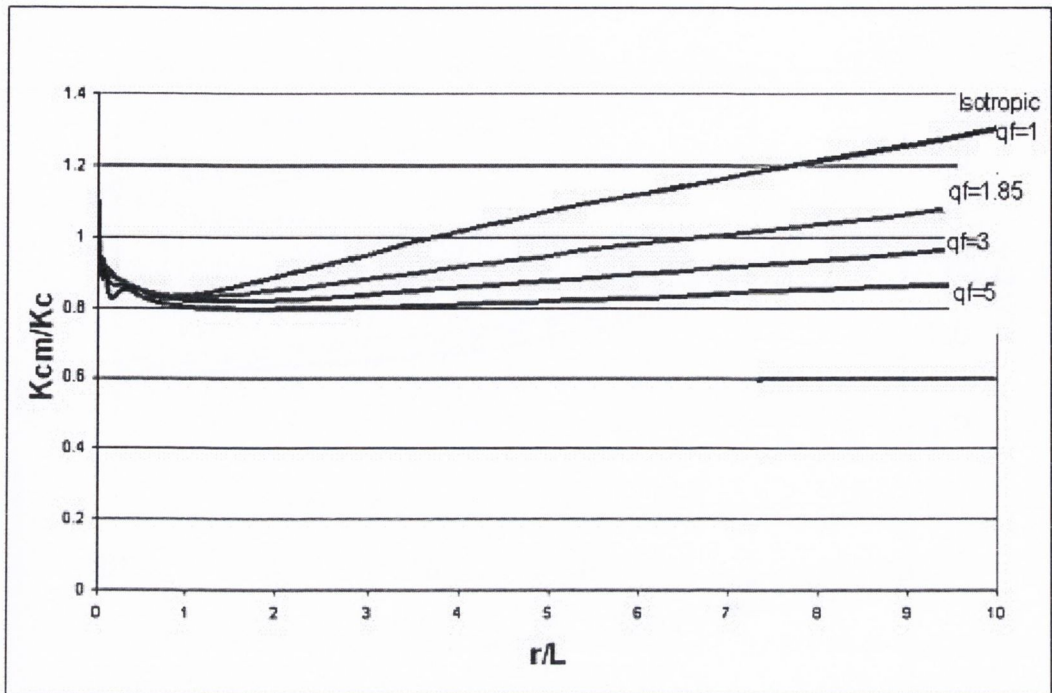


Figure 2-7. Prediction of effects of anisotropy of material containing long narrow slot in an infinite body using PM

2.6. Discussion

The above analysis has shown that these four methods have much in common; the critical distances involved are all closely related to the parameter L . Here, these predictions have not been compared to any experimental data. Many publications exist to testify to the accuracy of the PM, LM and ICM. For example, previous work has demonstrated that the PM and LM are highly successful in predicting the fatigue limits of notched specimens of metallic materials [75]. Likewise the ICM is more commonly used in the field of short-crack fatigue, where it is known as ElHaddad's method [66]. Awerbuch and Madhukar [76] conducted an extensive investigation into the accuracy of these and other methods as applied to predict monotonic fracture in fibre composite laminate materials containing holes and edge notches. The FFM is much newer, but work by Taylor [13] and by Seweryn and co-workers [69] has shown that the method is

capable of predicting experimental data on fatigue and brittle fracture, including multiaxial loading effects.

In this chapter the four methods have been formally compared, using both analytical and numerical methods. The similarity of these four approaches has two interesting consequences, one practical and one theoretical.

From a theoretical point of view, it is difficult to understand why the PM and LM are so successful. It is clear that the stresses in the vicinity of the notch are important in determining failure, but these methods use only limited information (i.e. the stress at a single point or averaged over a line) and consider only linear elastic stresses despite the existence of plastic deformation, microdamage, and other sources of non-linearity, which would considerably alter the stresses in this region. Likewise, the ICM can be criticised from a theoretical point of view on the grounds that the crack at the notch root is not a real crack. Some workers have identified this crack with a real feature, such as an area of damage or low strength at the specimen surface. However, this line of thought leads to a *reductio ad absurdum*, which is as follows: the crack which was introduced, being of length L , is by definition a short crack. So, in order to know whether it will propagate or not, the LEFM theory cannot be used. Logically, the crack should be assessed using the same method, i.e. another crack, length L , should be put at the tip of the first, and so on, *ad infinitum*. This is not done in the ICM. It is assumed that the small crack does conform to LEFM, implying that it must indeed be imaginary.

The FFM, on the other hand, faces no such theoretical barriers. It entirely conforms to LEFM theory, merely adding the assumption that crack growth occurs in increments of length $2L$; i.e. crack growth is not smooth and continuous, rather sporadic, occurring in jumps of finite length. This in fact reflects the known crack growth behaviour of many materials. Growing cracks tend to leap between microstructural features such as grain boundaries, or to jump through damage zones. This is particularly obvious in slow crack growth, such as the well-known 'stick-slip' growth in brittle polymers [77] and near-threshold fatigue crack growth in metals. Recently it has been demonstrated that a

similar phenomenon exists in the growth of cracks in bone at constant applied stress [78].

These observations lead one to the following conclusion: the PM, LM and ICM are successful because they give similar predictions to those of FFM. That is to say, FFM is the most accurate approach from a theoretical point of view, and the success of the other methods is due to the fact that they give approximately the same predictions.

These are also important from a practical standpoint. The fact that all four methods give similar predictions means that one is free to choose whichever method is most appropriate and convenient in any particular situation. For example, the PM and LM are very simple to implement in conjunction with FEA, so they can be used to predict failure in engineering components of complex shape. The PM is particularly straightforward to implement, but requires quite a fine FE mesh in order to accurately capture the stress at the point $L/2$ from the notch root. The LM, though marginally more difficult to implement, does not require such a fine mesh. The ICM and FFM are more problematical to apply within a FEA, but these methods can often be used in the form of closed-form solutions. This makes them more conveniently applied when studying the effect of parametric changes, such as the change in root radius or some other geometric feature. All four methods require only simple linear elastic analysis and limited material-property information.

2.7. Conclusions

When applied to the prediction of failure of a body containing a crack of geometry factor $F=1$, three different methods - LM, ICM and FFM - give identical predictions of the effect of crack length, including the effect of short cracks. Slight differences occur when using another method, the PM, and when the F factor differs from unity. The critical distance values for these four methods are all related to the same constant L , which is itself a function of the critical stress and stress-intensity parameters for the material.

Considering various notches (holes, central slots and surface slots) in effectively infinite bodies, the predictions of the four methods, whilst not identical, are always very close, falling within a scatter band of less than plus-or-minus 10%.

The methods also give very similar predictions when applied to materials having orthotropic elastic properties, typical of fibre composite materials and bone.

The FFM is theoretically rigorous and valid, and describes the discontinuous crack growth which occurs in many real cases. The other three methods are successful because they give approximately similar predictions to those of FFM.

The resemblance of these four methods allows them to be used interchangeably in practice, which is valuable when making predictions of fracture and fatigue in engineering components.

It was shown that all critical distance methods give the same predictions. In terms of application, PM is the simplest and more accurate method between them. It can be widely applied to different problems. ICM and FFM are more limited because of the crack introduction. For example, in a problem like indentation where the material fails in compression, with introducing a crack in the compression zone, the surfaces of cracks are in contact with each other. The friction between them, makes the problem much more difficult to analyze. Bone indentation is a good example for which the crack initiates in the compression zone. The PM, therefore, was employed to study the indentation fracture. Here after, the TCD is used to refer to the point method.

CHAPTER 3. Brittle Fracture of Bone

In this chapter, the TCD has been employed to predict the fracture of bone as affected by stress concentrations. First, papers which are related to the critical distance of bone are reviewed. This is subsequently followed by the study of the effects of stress concentrators, such as holes and cracks, on the strength of bone. This is the first time that the TCD is applied to bone for the purposes of predicting its failure. Strength of bone containing transcortical holes or notches under different loading conditions, torsion, tension and bending are studied. These examinations can especially be used when the effect of surgical procedures (e.g. plating, fracture fixation) is investigated. After looking at the effects of holes and notches, the crack growth resistance of bone is studied. The fracture toughness of bone increases with crack length, in both the transverse and longitudinal directions. It will be shown that this phenomenon can be predicted using the TCD.

3.1. Review

There has not been much research done about the critical distance of bone, as the best of our knowledge this is the first study to obtain its critical distance and apply the TCD to predict the effects of stress concentration.. There has, however, been research done to obtain the “intrinsic crack length”, which is also referred to as the “critical flaw

size” or “critical crack length”. It is a measure of the largest flaw that a material can tolerate before an unstable fracture occurs. This critical flaw size can be obtained using the same relationship as the critical distance, therefore these two parameters represent approximately the same value:

$$c_0 = L = 2r_c \quad (3-1)$$

Bone is a composite material (Figure 3-1), and as such, its properties, in particular fracture toughness and strength are very dependent on its structural orientation. It has not yet been shown how the critical crack length of bone varies with orientation. The fracture toughness for crack propagation in the transverse direction is almost twice the one in the longitudinal direction when the specimens are tested under the same constraints [79, 80]. Likewise bone’s tensile strength when it is loaded in the transverse direction is half the longitudinal one. Table 3-1 shows the fracture toughness in both directions for different types of bones.

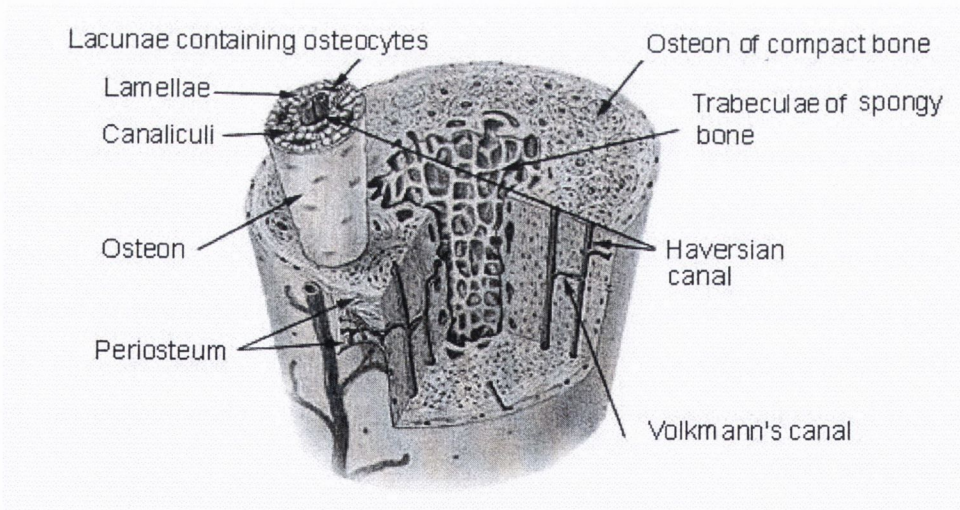


Figure 3-1. Structure of bone in micro scale

Table 3-1: Cortical bone fracture toughness results for transverse and longitudinal orientations.

Bone	Crack Direction	K_{Ic}	Ref
Bovine Femur	Transverse	5.8±0.5	[81]
Bovine Femur	Transverse	3.48-5.05	[79]
Bovine Tibia	Transverse	4.53-6.64	[79]
Bovine Tibia	Transverse	6.5	[80]
Bovine Femur	Transverse	5.7±1.4	[82]
Bovine Tibia	Transverse	11.2	[83]
Bovine Femur	Transverse	2.2-4.6	[84]
Bovine Femur	Longitudinal	2.3-2.89	[79]
Human Tibia	Longitudinal	4.05-4.32	[85]
Bovine Tibia	Longitudinal	6.29-6.73	[85]
Bovine Tibia	Longitudinal	3.2	[80]
Bovine Tibia	Longitudinal	6.3	[86]
Bovine Tibia	Longitudinal	4.5-5.4	[87]

The objective of this review is to acquire an idea about the value of the critical distance of bone, as well as the relationship between critical distance in the longitudinal and transverse directions.

Work-to-fracture, bending and tensile tests are methods that have largely been applied in to cause cracking in one of two different directions, transverse (L-R) and longitudinal (C-L) as shown in Figure 3-2. Various workers, including Bonfield et al [84] and Robertson [82] have conducted tests on bone samples containing cracks or very sharp notches, which give similar results in practice. This work has shown that, within certain constraints, traditional fracture mechanics concepts can be used to predict the effect of crack length on fracture stress. There is no obvious way, however, in which fracture mechanics theory can be applied to consider features which are not cracks or very sharp notches, features such as circular or elliptical holes, square holes, spherical cavities, and blunt notches.

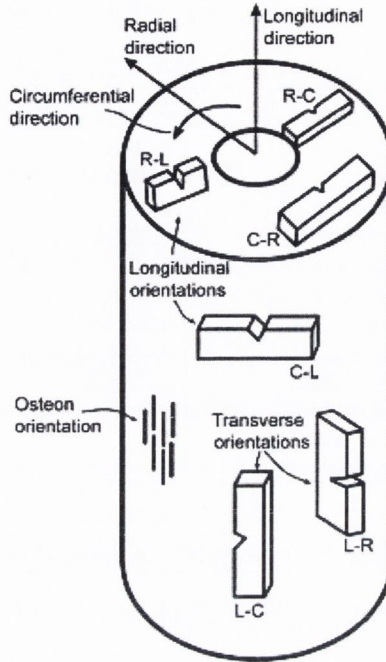


Figure 3-2. Different orientations of specimens of bone according to ASTM E399, here, C-L is longitudinal, L-R: transverse and R-C tangential.

3.2. Previous Work Measuring Toughness and Critical Crack Size in Bone

Bonfield and Li [88] studied the fracture characteristics of bone under impact and tensile loading in 1966. They showed that the fracture properties of bone are a function of orientation and are also notch sensitive. They illustrated that the presence of cracks on the surface significantly reduces the energy absorbed during the fracture of bovine femur and tibia under impact conditions independent of direction. Study of the dependency of fracture factors on temperature demonstrates that strength of bone is very dependent on temperature within the range of -70°C and 100°C . The maximum strength is at 0° when the specimen is parallel to the bone axis (longitudinal). These results agree with other results reported in the literature [89]. They performed the experiments at the temperature range of $3-50^{\circ}$, and showed that the maximum fracture toughness take place at 0° .

The fracture of bovine femur was studied by Piekarski at two different strain rates, using the three point bending test [90], with specimens having a crack perpendicular to the long axis of the bone (transverse). This is the first published data about the critical crack length of bone. He applied the Griffith crack theory to obtain the critical crack length using typical values for fracture stress ($\sim 100\text{MPa}$) and elastic modulus ($\sim 20\text{GPa}$). The critical flaw size for the slow-controlled crack propagation and fast-uncontrolled propagation was calculated to be 76.5 mm and 1.3mm respectively. As a 76.5mm long crack can not exist, he suggested that slow crack propagation is essentially a “pull-out” type mechanism which needs a great amount of energy during the fracture, therefore Griffith theory does not apply. He observed, however, that a rapidly propagating crack has the typical appearance of a brittle fracture, but there was no pre-crack length of 1.3mm in the internal discontinuities they had seen.

Bonfield and Datta [84] in 1976 looked at tensile specimens of bovine bone, with a gauge length of 24.5mm, a width of 18mm, a thickness of 2mm, and transverse crack direction. The experiments were at a strain rate of $3 \times 10^{-4} \text{ sec}^{-1}$. They found a linear relationship between the fracture stress and $c^{-1/2}$ for a crack length range of 1.25 to 14mm as follows:

$$\sigma_f = A.c^{-1/2} - B \quad (3-2)$$

In which $A=2.6 \text{ MNm}^{-3/2}$ and $B=13.5\text{MPa}$ are constants. For un-notched specimens tested under identical conditions a mean fracture stress of 120 MPa was obtained. The critical crack length (intrinsic crack length) was calculated for the edge of the crack as 0.37mm by substituting the fracture stress of intact bone into the equation 3-2.

They also showed that the fracture stress was approximately independent of the crack tip radius. This research gave a value of $2.2\text{-}4.6 \text{ MNm}^{1/2}$ for fracture toughness. Furthermore, they applied the notch factor to their result and found a value of 0.34mm, but as the critical distance is a material property and thus independent of notch size, the value will be used before applying the geometry factor.

V-notched specimens of bovine bone with the crack in transverse direction were tested at a temperature of 37° by Robertson (1978) [82], using three-point bending. A critical crack length, perpendicular to the tensile stress axis, was determined to be 0.36mm at the strain rate of 7×10^{-6} to $3 \times 10^{-2} \text{ sec}^{-1}$. Experiments using three different types of specimens: (1) notch, (2) notch with a pre-crack at the root of that, and (3) without notch (natural cracks), illustrated that the existence of a pre-crack does not have a significant effect on fracture toughness.

Behiri and Bonfield, 1984[86], studied the effects of density, thickness and crack velocity for cracking in the longitudinal direction in bovine tibiae. They found a significant dependence of fracture toughness and strain energy release rate on bone density, whereas K_c increased from 2.2 to $4.82 \text{ MNm}^{-3/2}$ when the density increased from 1.85 to $2 \text{ Mgm}^{-1/3}$. Variation in thickness of specimens (0.5-2mm) did not have any effect on fracture parameters. The absence of a thickness effect for bone in the range of 1.85-3.8mm was demonstrated by Wright and Hayes (1977). They also found that, for a given density, increases in the crack velocity between 1 and $120 \times 10^{-5} \text{ ms}^{-1}$ cause an increase in K_c from 2.8 to $6.3 \text{ MNm}^{-3/2}$.

Moyle and Gavens analysed bovine plexiform tibia with different crack length (4-12mm) and tip radii in the transverse direction[83]. They found the same form of equation as Bonfield and Datta (1) with different constants ($A=7.12$ and $B=54.2 \text{ MPa}$). Their results showed a large effect of crack length on the fracture stress, as it decreased from 54.2 MPa to 8.12 MPa when the crack length increased from 4mm to 12mm. The crack tip radius had no major effect on fracture toughness. They found a mean fracture stress of $112.7 \pm 5.9 \text{ MPa}$ for un-notched specimens. Using this fracture stress value and equation 1 with new constants (A and B) they obtained $11.2 \text{ MNm}^{-3/2}$ and 1.8 mm for K_c and intrinsic flaw size respectively. They mentioned that there are no naturally occurring voids of the size of this intrinsic flaw in the bone. In fact in plexiform bone, due to the lamellar structure, the vascular canals lie around the circumference of the bone. The cracks in the specimens propagate parallel to these canals and they may act as extension of the crack tip.

Silvia and Fortes (1987), also found the linear relation between the fracture stress and $c^{-1/2}$, with the constants $A=4.77$, $B=39.51$ (MPa) and the mean K_c of 5.9 ± 0.72 $\text{MNm}^{-3/2}$ [91].

Bonfield (1987) compared their results for critical crack length with those of Moyle. He stated crack paths as a reason for the significant difference between their results and Moyle's for K_c and critical flaw size. Bifurcation in the Moyle and Gavens specimens is in contrast to the relatively straight, single crack produced in the Bonfield and Datta tests. The intrinsic flaw size estimated by Moyle and Gavens is also beyond the scale of any natural flaws.

Another reason for this difference could be due to the difference in structures of specimens as Moyle and Gavens had used plexiform bone and Bonfield and Datta used Haversian bone. Norman et al [85], compared the fracture toughness and strength of bovine tibia and human Haversian bone. They found a ratio of 1.5 between strength of bovine tibia and human Haversian, but their fracture toughness is proportional to their strength, implying that the critical distance of human bone equals the critical distance of bovine tibia. This is an interesting result, as the microstructures of these two types of bone are different. It will be shown below that the same critical distance can be used for both types of bones.

It was also found that, for controlled slow crack propagation, fracture toughness increases from $3.2\text{MNm}^{-3/2}$ for fracture in the longitudinal direction to $6.3\text{MNm}^{-3/2}$ for fracture in the transverse direction[3].

Behiri and Bonfield published the fracture toughness value of bone in different orientation from longitudinal to transverse. They performed tests on specimens with 6 different angles respective to the long axis of bone. They found that fracture toughness increases from 3.2 to $6.5\text{MNm}^{-3/2}$ with variation in orientation from longitudinal to transverse [80]. These values agree with the result from Melvin and Evans (1973). The fracture toughness of bone in longitudinal and transverse direction were found to be as 3.21 and $5.58\text{MNm}^{-3/2}$ respectively [92]. Unfortunately, they didn't publish any data about the fracture stress of bone by variation of orientation.

Lucksanasombool et al[79] compared the longitudinal and transverse fracture toughness using the single-notch bending test. They reported values of $3.48 \pm 0.33 \text{ MNm}^{-3/2}$ and $2.30 \pm 0.27 \text{ MNm}^{-3/2}$ for transverse and longitudinal fracture respectively.

Reviewing all the above papers, two different ranges of the critical distance of bone in the transverse direction were found. The disparity between these two critical distances is significant. The first agrees with the Bonfield and Datta's results, giving values of about 0.36mm. This critical distance is similar in size to the microstructure of bone. The other range is about 1.3mm which agrees with Moyle's results.

The linear relationship of equation 3-2 was reported by several researchers with different constants as mentioned above. This equation is the form of Griffith equation for finite width specimens. In this equation B is the same unit as stress and

$$A = \frac{K_c}{2\pi} \quad (3-3)$$

If we assume $\sigma'_f = \sigma_f + B$ then equation 3-2 changes to:

$$\sigma'_f = A.c^{-1/2} = \frac{K_c}{2\pi}.c^{-1/2} \quad (3-4)$$

Which, is the same relation as Griffith.

Equation 3-4 implies that, in order to calculate the critical distance, a corrected fracture stress has to be applied.

The ratio of fracture toughness in the transverse and longitudinal directions is about 2 and the tensile strength of un-notched specimens is almost the same ratio (typically 120/50). Therefore, because the critical distance related to the ratio of fracture toughness to tensile strength, it could be expected that the critical distance in the longitudinal and transverse directions will be approximately the same.

3.3. Predicting Bone Fracture Using the TCD

A catastrophic fracture of bone after loading with limited plastic deformation or micro-cracking demonstrates the brittle fracture in bone. The TCD can be employed to analyse this type of fracture as it has been shown for other materials. Here, effects of holes and notches on strength of bone are studied. This is particularly relevant when a long bone contains transcortical hole subjected to bending or torsion. This study would be useful when we face surgical problems such as the attachment of plates or fracture fixation devices, as it can suggest the appropriate hole size to reduce the effects of stress concentrations.

Data from tests carried out in tension (Bonfield and Datta)[84], bending (McBroom) [93] and torsion (Brooks) [94] are studied. It is assumed that mode I fracture will occur under these three loading conditions. The effective stress, therefore, is the first principal stress. The fracture line and the type of bone used for each test are different, therefore the critical distance is not assumed to be constant for the various cases.

3.3.1. *Methods*

The critical stress σ_0 to be used in the TCD analysis is defined by T (ratio between the critical stress and the ultimate tensile stress) which is assumed to be a constant for bone. The critical distance may change with orientation and type of bone. Here, three sets of experimental data (tensile, torsion and bending) were employed.

In accordance with previously-established procedures for the TCD, stress/distance curves were drawn, starting at the locations of maximum stress (i.e. the surface of the hole or notch) and moving in a direction perpendicular to the direction of maximum principal stress. The stress parameter used was the maximum principal stress as this is normally the factor which controls brittle fracture.

The two material parameters L and T were varied systematically in order to optimise the accuracy of the predictions. In this regard attention was paid to minimising the

least-squares fit to the individual data points whilst maintaining key features of the results, especially the differing effects of small holes in torsion and tension.

3.3.2. Tension

In the Bonfield and Datta tests[84], tensile specimens with gauge length of 25.4mm, a width of 18.0mm and a thickness of 2.0 mm, were prepared from 2-3 yr old bovine tibia section. A slit perpendicular to the tensile axis of width 0.38mm (with a range of lengths from 1.25 to 14.0mm different specimens), was drilled from the midpoint of the specimen edge (Figure 3-3). The tip of each slit had a constant radius of a curvature of 0.38mm. For the FEA we made a half model (Figure 3-4) containing the gauge length of the specimen as shown in. Bone was modelled as an orthotropic material as table 3-2.

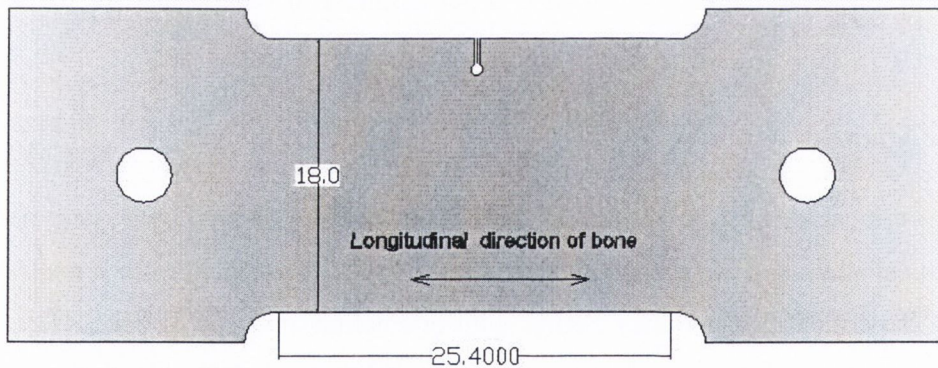


Figure 3-3. Tensile specimen used by Bonfield and Datta 1976. The tensile axis of the specimen coincides with the longitudinal axis of the bone from which it was taken.

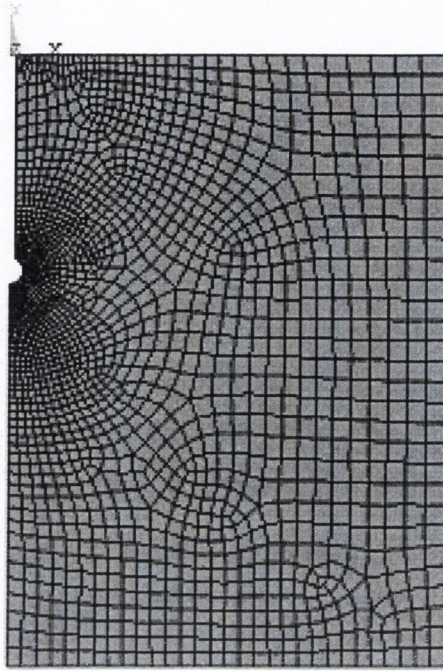


Figure 3-4. Finite element model of tensile test performed by Bonfield and Datta 1976

Bonfield and Datta performed the test such that the crack grew perpendicular to the tensile loading. They did not employ the data when the crack grew in other directions. A line from the crack tip perpendicular to the loading direction was used as the fracture line. With this assumption there is no shear stress acting on the fracture line. It turns the problem to a mode I fracture. The critical stress is assumed to be the ultimate stress which was reported as 120MPa.

3.3.3. Torsion

Bone usually breaks under tension. When bone is loaded in torsion, it also breaks on planes of maximum principal stress. The torsional model which was examined here is based on Edgerton and co-worker's experiments[95]. Hipp et al[96] presented a simple model of bone to study the effect of the transcortical holes; he showed that a nonlinear model can predict the Edgerton's result better. The same as presented by Hipp et al was employed in this study.

The basic model which served as the foundation for parametric consisted of a cylindrical tube with inner and outer diameters equal to the average endosteal, 12.8mm, and periosteal, 19.6 mm diameters of the sheep femoral tested by Edgerton. Torsion was applied by fixing one end and applying distributed torsion loads to the opposite end. The loaded end was also constrained to rotate about the centre of the cylinder, simulating typical boundary conditions for an in vitro torsional test. Six different hole sizes were modelled, with the hole size varying from 10% to 60% of bone diameter. The experiments showed that the crack initiates and propagates at a 45° angle. It was therefore assumed that the fracture line is the line maximum principal stress. This is a uniaxial fracture problem as the only stress on the fracture line is the tensile stress. A linear orthotropic material using data from Van Buskirk et al [97] (Table 3-2) was applied to the FE model. In the case of elastic-plastic model they used an isotropic model with the yield stress of 129MPa.

Table 3-2: Orthotropic elastic constants of bovine femoral bone, Van Buskirk et al,

E1=21.9 GPa	N23=0.38	G23=5.29 GPa
E2=14.6 GPa	N13=0.206	G13=6.29 GPa
E3=11.6 GPa	N12=0.307	G12=6.99 GPa

Figure 3-5 shows a bone containing a hole, loaded in torsion. In this case the stress/distance curve is evaluated on a line in a plane at 45° to the bone's axis, as illustrated in this cut-away diagram.

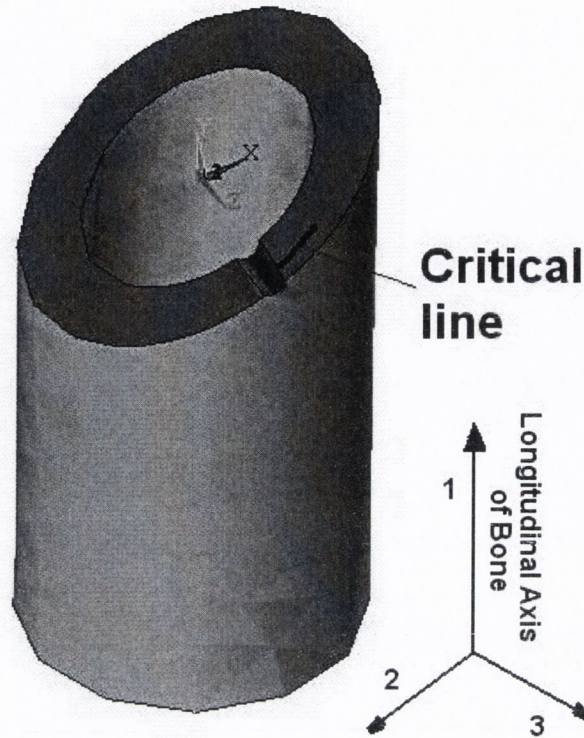


Figure 3-5. Example of the use of finite element analysis: stress-distance information is obtained on a line drawn from the hole surface in the expected direction of crack growth (at 45° in this example of a bone tube loaded in torsion). Note that the FE model has been cut away here to illustrate the plane on which the critical line is drawn. 1, 2 and 3 represent the longitudinal, circumferential and radial orientations of bone respectively.

3.3.4. Bending

Here the data from McBroom et al [93] who tested whole femora of 52 adult dogs under bending was used. To study the bending, three dimensional finite element models were generated. An idealized geometry was employed to simplify the finite-element mesh based on an assumption of tubular geometry for the diaphysis of the canine femur. The holes created in the femora with the drill bits were cylindrical holes through one cortex. The idealized geometry, under bending loads as in the experimental model, contains two symmetry planes. With the proper boundary displacement constraints this allowed for representing the tube and hole using one quarter of the full geometry. The inner and outer diameters were 14.64mm, 19.7mm respectively. The

hole sizes varied between 10% to 70% of bone diameter. The distance between the outer and inner pairs of supports was 210 and 76mm respectively (Figure 3-6).

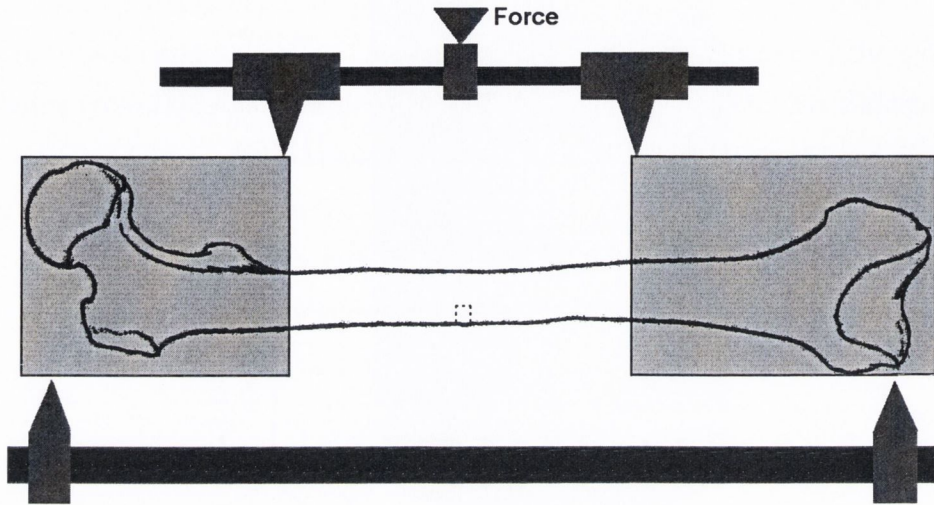


Figure 3-6. Schematic of 4-point bending test on bone

3.3.5. Results

It was found that all data could be predicted with reasonable accuracy using a single constant value of the parameter T of 1.33, and values of L which varied only slightly, in the range 0.32-0.38mm.

Figure 3-7 presents the experimental data of Bonfield and Datta, who tested tensile specimens containing notches of varying length with a constant root radius of 0.38mm. The fracture stress is plotted as a function of the inverse square root of notch length, in which form there is an approximately linear relationship. Predictions are shown using $L=0.38\text{mm}$ with two different values of T : 1.0 and 1.33.

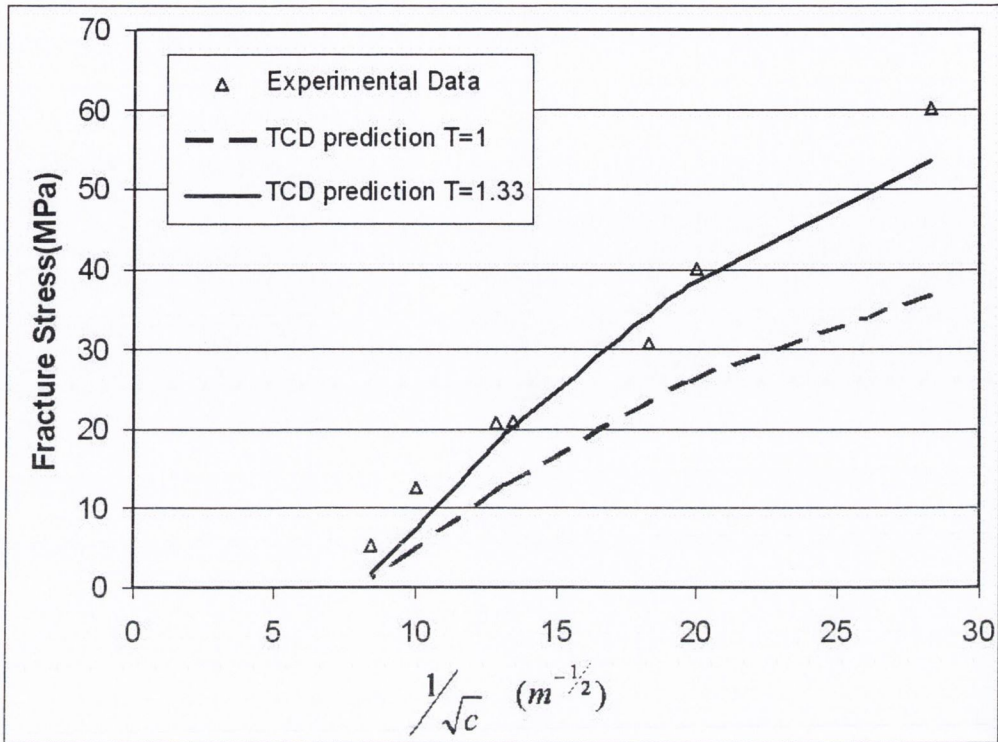


Figure 3-7. Bonfield and Datta's experimental results: fracture stress as a function of the inverse square root of notch length. Predictions using the TCD with $T=1$ and $T=1.33$, using an L value of 0.38mm in both cases

Figure 3-8 shows the experimental data of Edgerton, for whole bones containing holes and loaded in torsion; fracture stress (expressed as a percentage of the strength of intact bones) is plotted as a function of the hole diameter, normalized by dividing by the diameter of the bone. The figure also shows TCD predictions using $L=0.32\text{mm}$ and $T=1.33$. Also shown are two predictions due to Hipp et al[96], in which failure was predicted based on the maximum stress at the hole surface, calculated using either a linear or a non-linear material model.

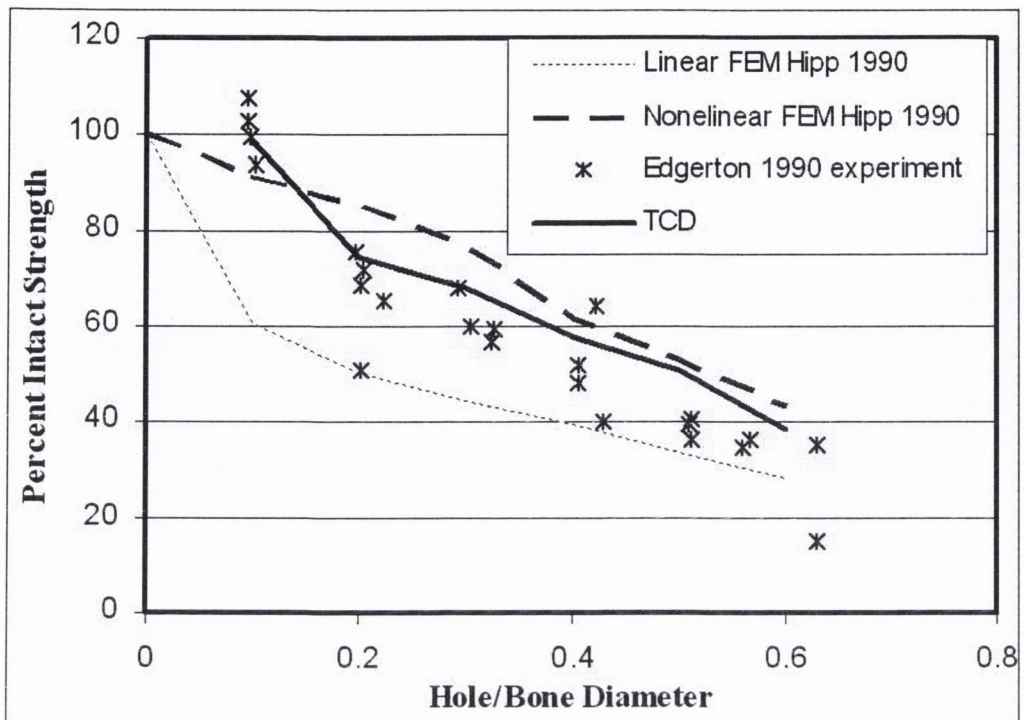


Figure 3-8. Prediction of the effect of hole diameter on torsional strength of whole bones, using $T=1.33$ and $L=0.32\text{mm}$. The predictions are compared with the experimental results of Edgerton and the linear and nonlinear predictions of Hipp

Figure 3-9 shows results for holes in bending [93], using a similar format to the previous figure. Predictions were made using $T=1.33$ and $L=0.37\text{mm}$. The general trend was well predicted, as was the position of the data for small holes; there was a slight systematic error for larger holes, whereby the fracture stress was underestimated by 20-30%. A larger value of critical distance can estimate the effect of larger holes but it does not accurately predict the effects of the small holes. In the presence of the large holes, the tensile damage zone meets compressive damage zone. The damage area, therefore, is much larger and it leads to a larger value of critical distance.

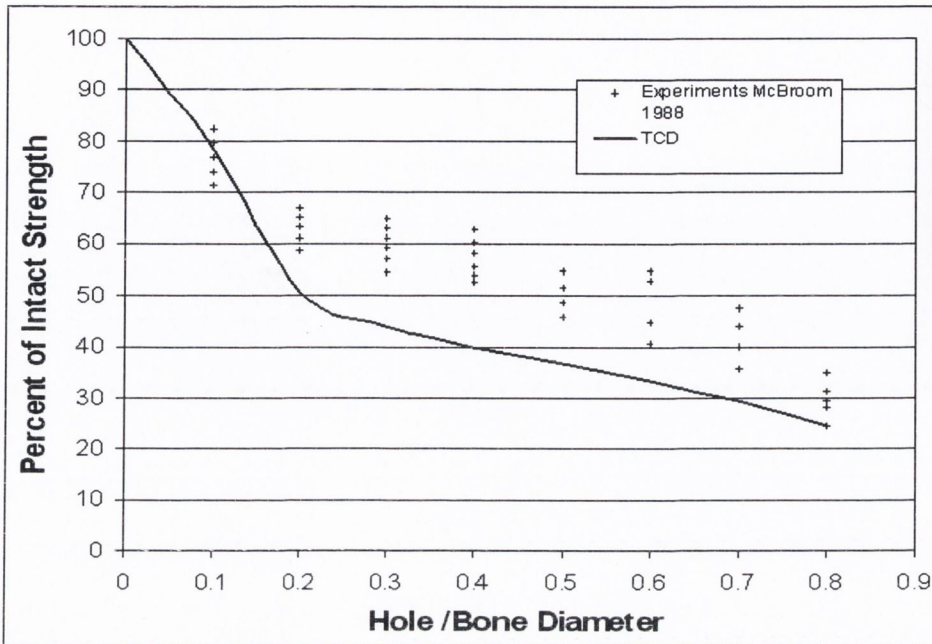


Figure 3-9. Experimental data and TCD predictions for the effect of hole size on bending strength. $T=1.33$ and $L=0.37\text{mm}$

3.4. The Toughness of Short Cracks

In some substances, the microstructure is formed such that it becomes more difficult for a crack to grow as it gets longer. This especially can be seen in composite materials. Different mechanisms cause this kind of crack-growth resistance, including micro-cracking, blunting, and bridging. In some materials, such as bone, the failure mechanism varies with orientation due to their microstructure.

Fracture mechanism of bone can change from brittle to quasi-ductile[98]. When the crack is advancing in a direction perpendicular to the osteons, resistance against crack growth is highest. This is because of the different mechanisms[99], such as bridging [100] or crack deflection[101].

Plane strain fracture toughness increases with crack length and then it becomes constant for a long enough crack length. This constant value of fracture toughness, K_{IC} ,

is no longer a function of crack length and is a material property. The TCD can be employed to explain the effects of short cracks[12, 14].

Here, the effects of short cracks in bone are predicted using the TCD. This is the first time that this theory is utilized to study the R-curve of bone, i.e. the curve showing the increase of toughness with crack length. Experimental data from the literature are employed. In all cases, the Westergaard equation for the stress field ahead of the crack is used.

3.4.1. Experimental data and predictions

Mullins et al [37] measured fracture toughness of bone in the transverse direction for short cracks using nano-indentation. Figure 3-10 shows predictions of their results using the TCD. The prediction has been done using $L=0.38\text{mm}$ as used in the previous predictions, and a long crack toughness $K_c=5.5 \text{MPa(m)}^{1/2}$ which is typical of values found in the literature, for tests in which crack propagation occurred in the transverse direction [3]. It can be seen that this approach accurately predicts the results of Mullins et al [4]. The same approach, with the same material constants, also predicts data from Lakes et al [5], who tested bone samples containing small, sharp notches oriented in the transverse direction (Figure 3-11).

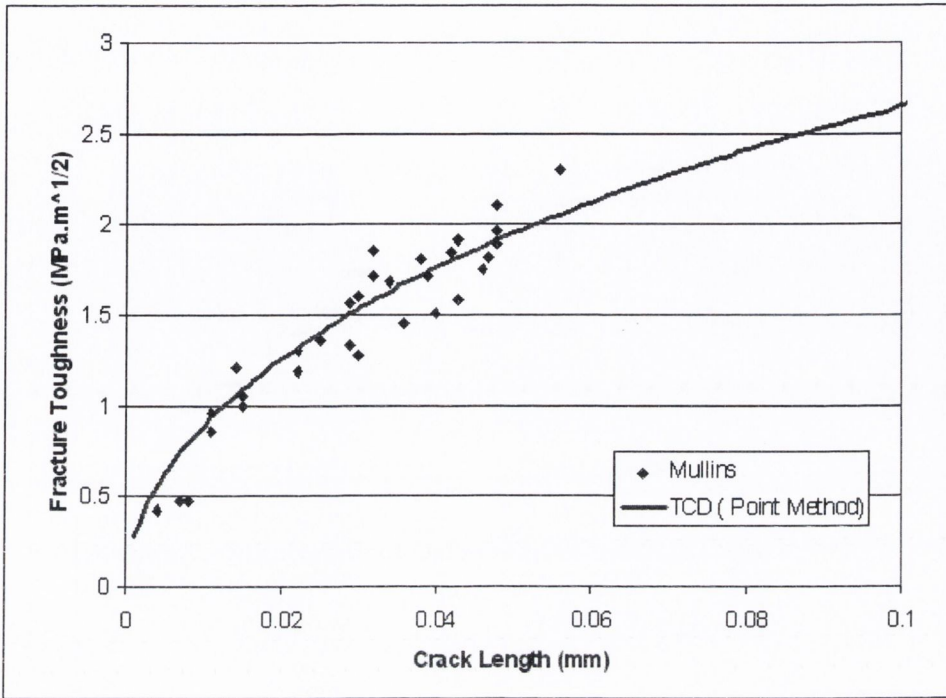


Figure 3-10. Predicted variation of fracture toughness with crack length, compared to data from Mullins

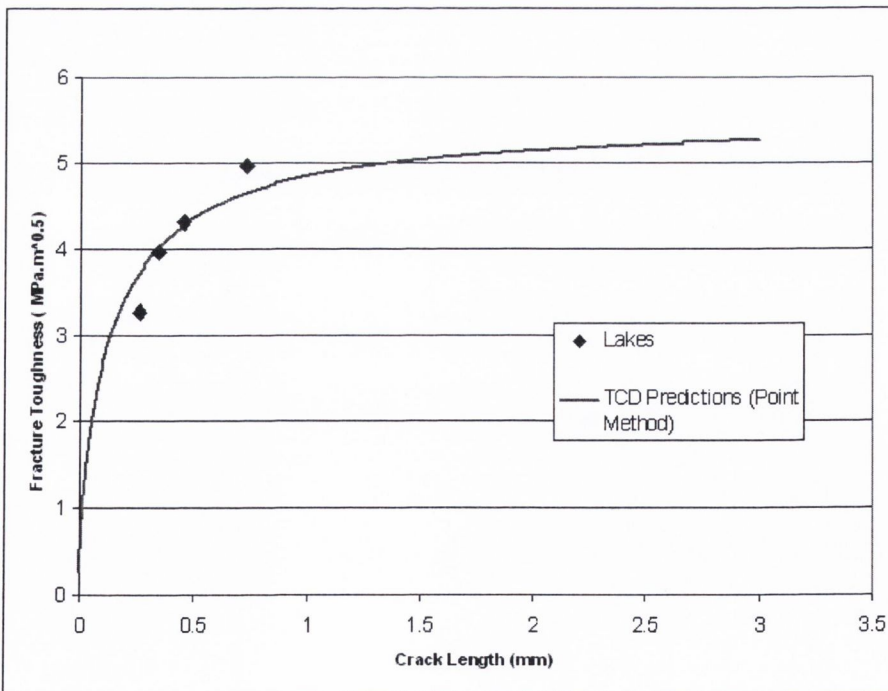


Figure 3-11. Transverse R-curve of bone, comparing the TCD predictions with Lakes experimental results

The TCD was also employed to predict the effects of short cracks under fatigue loading in bone. Figure 3-12 shows predictions of the ΔK required for a da/dN value of $3-6 \times 10^{-8}$ mm/cycle, compared to experimental data compiled by Kruzic et al [102]. The value of $L=0.38$ mm and the published long-crack ΔK value ($0.95\text{MPa}\cdot\text{m}^{1/2}$) were used for prediction. Again it can be seen that the predictions are very accurate. The cracks tested here were small, semi-elliptical surface cracks.

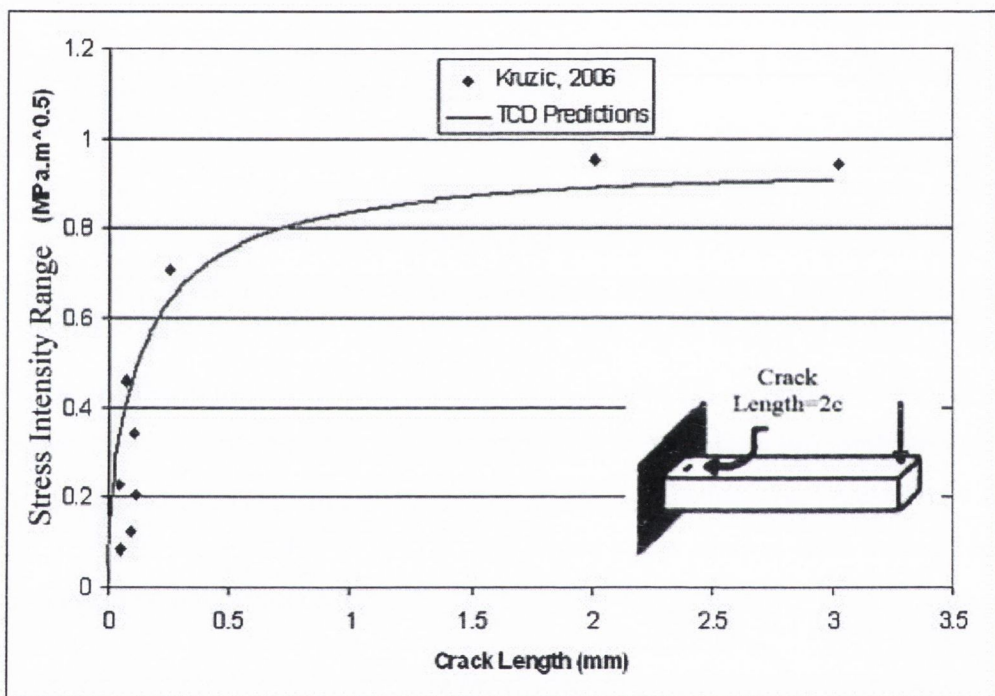


Figure 3-12. Predictions of the ΔK for a fatigue crack growth rate of $3-6 \times 10^{-8}$ mm/cycle using the TCD, compared to experimental data from Kruzic

3.5. Effects of Thickness

K_{IC} represents the fracture toughness under plane strain conditions. When the specimen is not thick enough to satisfy the plane strain conditions, the fracture toughness is much higher than K_{IC} , therefore the critical distance will be affected by the

thickness of the specimen. It has been shown that the critical distance of plane stress specimen in metal can be as much as 7 times higher than plane strain[4]. Bone stop being in pure plane strain when the thickness is less than 6mm. The bone behaves between plane strain and plane stress until a much smaller thickness[85].

Figure 3-13 shows the variations of critical distance with thickness of bone when the crack was propagating in the longitudinal direction. These are based on data from Norman[85]. It is seen that the critical distance is much higher than the plane strain critical distance as an effect of the specimen's geometry. The graph also shows the effect of the crack length propagation on critical distance.

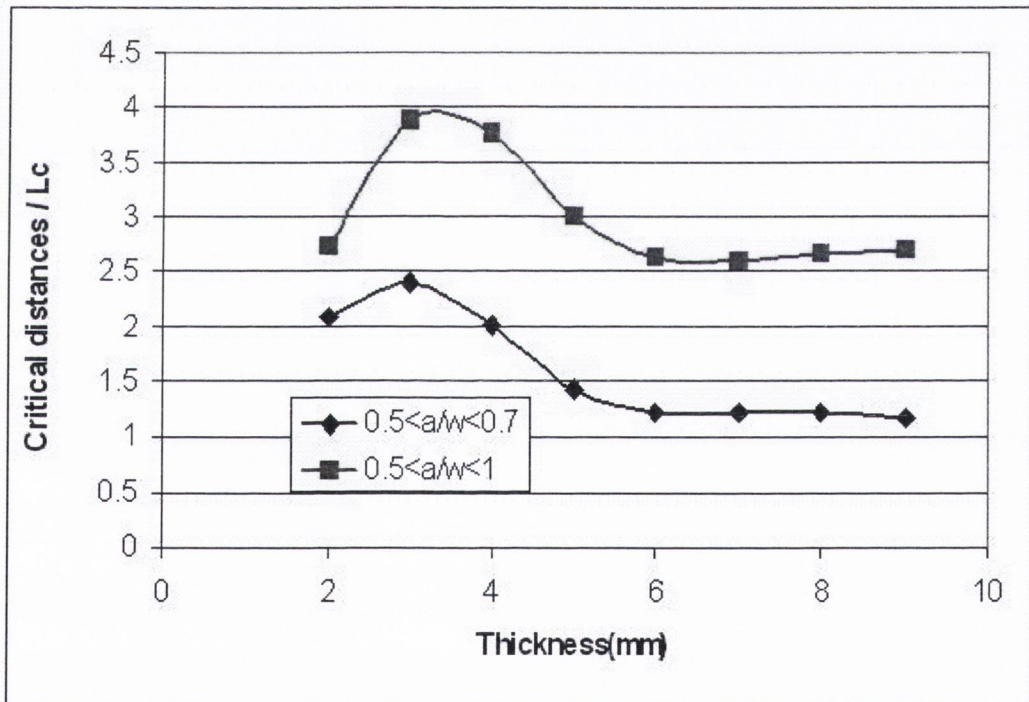


Figure 3-13. The effect of thickness (B) on the critical distance (L) for bovine bone in three different stages. Plane stress stage ($B < 3$ mm), transition stage ($3 < B < 6$ mm) and plane strain stage ($B > 6$). The data also show the effect of crack propagation length on critical distance. L : plane strain critical distance ($4.32 \text{ MNm}^{-3/2}$), a : crack length, w : width of specimen

Nalla et al [103] measured the R-curve of bone for specimens with 3mm thickness. In fact, the fracture toughness is much higher in this case, as well as the critical

distance. On the other hand, what they measured was not the absolute crack length but the crack extension, commencing from a starter notch of several millimeters in length, with the crack growing in the longitudinal direction. Their K_{IC}/a relationship is much more linear and does not level out to a constant long-crack value. The fracture toughness typical value of $4.5\text{MPa}\cdot\text{m}^{0.5}$ was chosen and the critical distance was changed to get the best fit. Figure 3-14. The results show that a critical distance of 2.5mm can predict the R-curve. It is almost 6.5 times larger than the critical distance of a plane strain specimen.

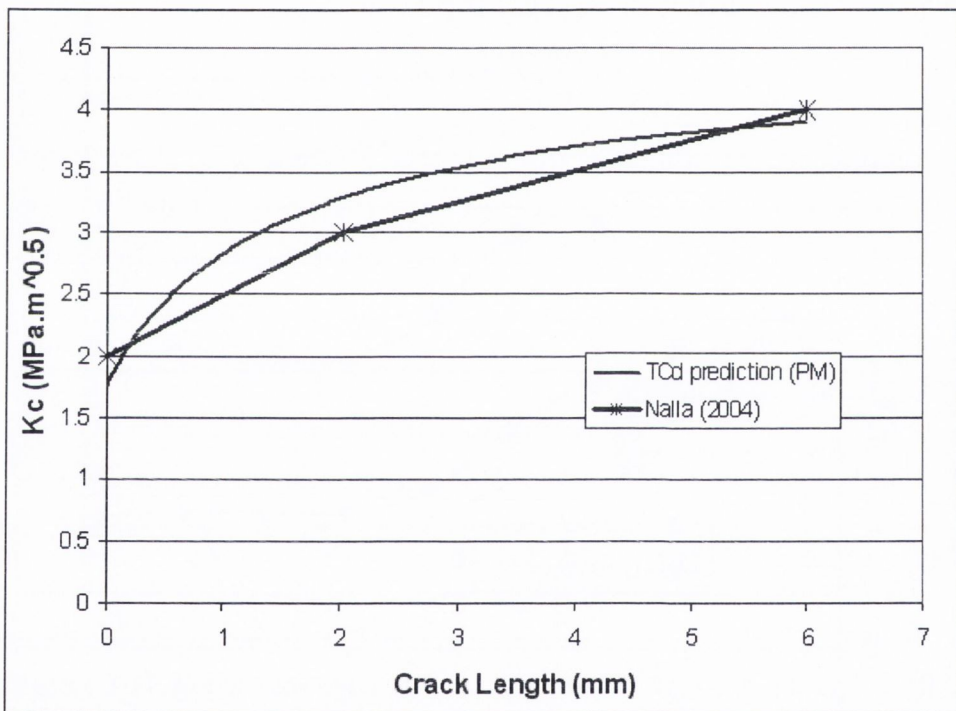


Figure 3-14. Predicted R-curve for plane stress specimens, compared with data from Nalla et al (2004)

3.6. Nanoindentation and the TCD

Since we are able to predict the toughness of short cracks, measured by indentation, using the TCD then we have to be able to find the critical distance using the nanoindentation data. Performing the test on small samples is an advantage of nanoindentation test compare to other tests. The need for a large sample size is the

disadvantage of this method. It was shown earlier that the critical distance approach can be employed to study the effects of short cracks in bone.

It was seen that the PM is capable of predicting the effect of short cracks on toughness. The LM predicts the similar results. Figure 3-15 comparing the toughness of short cracks predicted using the PM and LM. The graph also demonstrates that the minimum crack length for the long crack assumption is 7 times larger than the critical distance (less than 5% errors in toughness). In this section the LM is employed as the equations are simpler than the PM. Using the Line Method the toughness of short cracks can be calculated as follow:

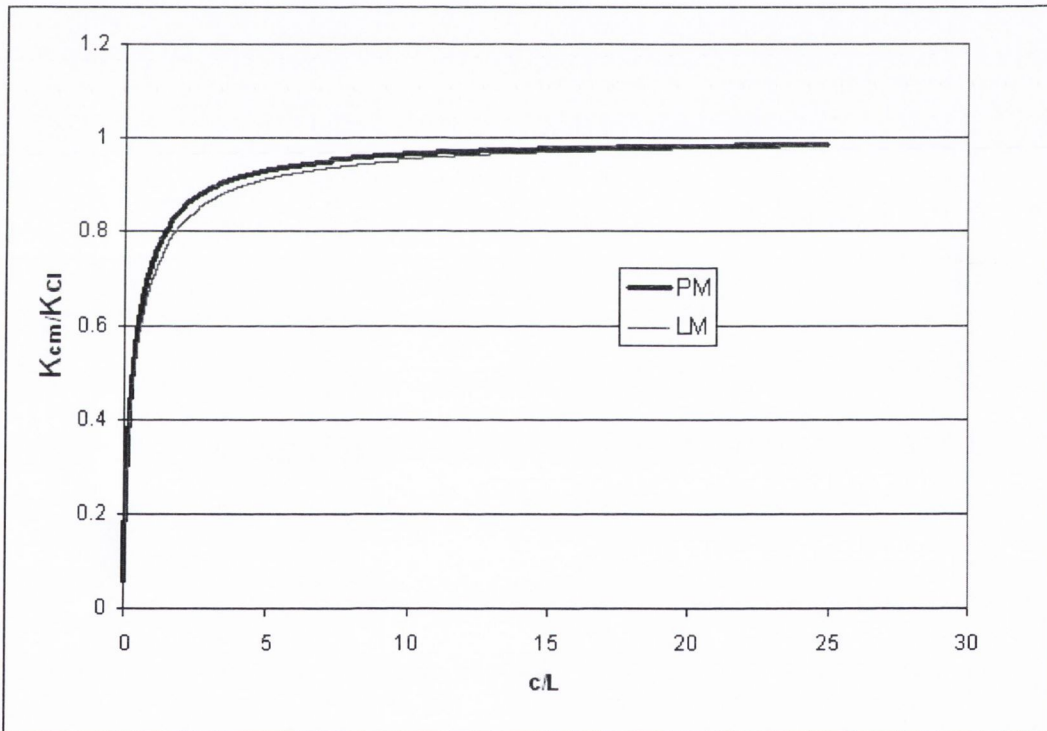


Figure 3-15. Prediction of relative toughness for short cracks using the line method and point method. The y-axis represents the ratio between the toughness and fracture toughness. The x-axis represents the ratio between the crack length and the critical distance. It shows that two methods predict roughly similar results.

$$K_{cm} = K_{IC} \sqrt{\frac{c}{c+L}} \quad (3-5)$$

With rearranging the above equation states that there is a linear relationship between $\frac{1}{K_{cm}^2}$ and $1/c$.

$$\frac{1}{K_{cm}^2} = \frac{1}{K_{IC}^2} + \frac{K_{IC}^2 L}{c} \quad (3-6)$$

With using the data from Mullins et al [37] and equation 3-6 we can estimate the fracture toughness and critical distance. Fitting a line between the data (Figure 3-16) gives the $K_{IC}=8.7 \text{ MPam}^{0.5}$ and $L=1.38\text{mm}$. This error was expected as all data are for short cracks. A larger sample size is required for more accurate results. Longer crack will reduce the errors as the critical distance give better predictions for long cracks; therefore it is suggested to use a bigger indenter to produce larger cracks.

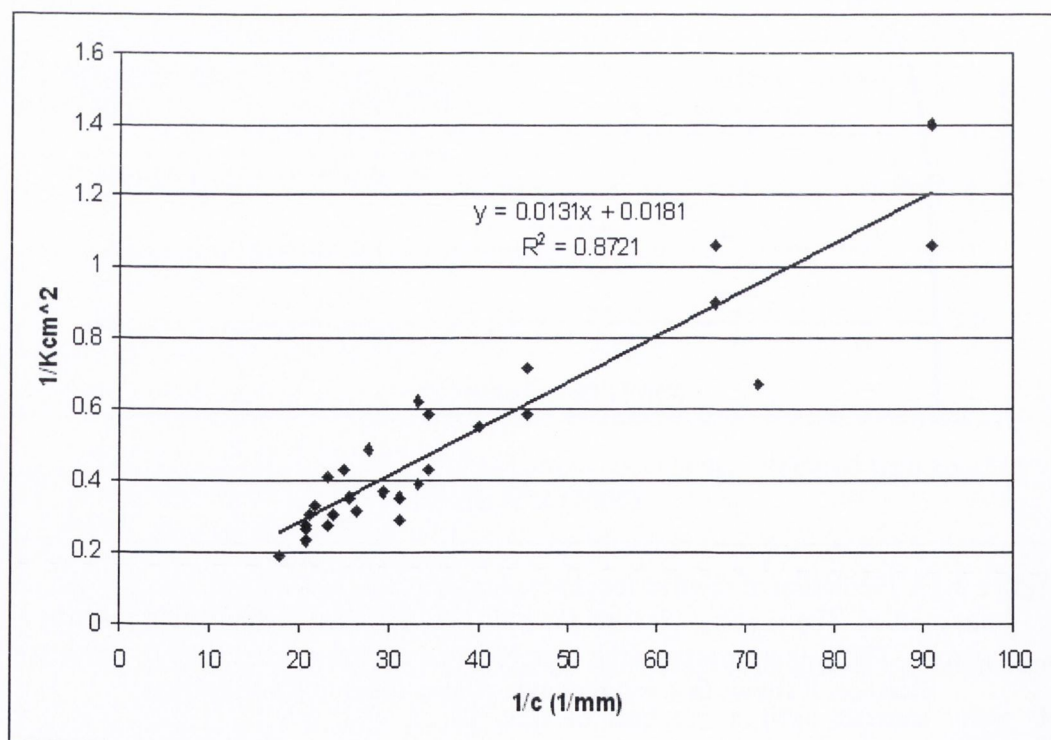


Figure 3-16. There is a linear relationship between K_{cm}^{-2} and $1/c$ obtained using nanoindentation as it was expected by the TCD. The intersection with y-axis and the slope of the fitted line represent K_{IC}^{-2} and $L \cdot K_{IC}^{-2}$

With changing the fracture toughness, the critical distance value changes to find the best fitted line using the nanoindentation data. The fracture toughness of bone in transverse direction was reported between 4.5 and 6 MPam^{0.5}, these values give the critical distance range of 0.25 to 0.46mm. The average value of fracture toughness is about 5MPam^{0.5} which gives the critical distance of $L=0.32\text{mm}$.

3.7. Discussion

The results show that good predictions can be made using this theory. In regards to the material parameters, a constant value of T (1.33) could be used, and values of L varied only slightly (0.32-0.38mm). The critical distance is expected to be a material constant reflecting the size of the damage zone at failure. Works which have been carried out on other materials suggest that the value of L is related to the size of microstructural features which affect crack propagation and thus control toughness. For example, L is equal to the grain size for steel failing by brittle cleavage fracture [4]. In the tests discussed here, cracks propagated in the transverse direction (or 45° to it in the case of torsion), cutting through the longitudinal structural units such as osteons. The size and spacing of osteons is of the order of 0.2mm, so our result for L implies that these have a significant role in bone toughening, as suggested previously by Nalla et al [104]. The slightly different value of L which was found for torsion testing may be due to the different orientation of crack growth (nominally at 45° to the bone's axis), though it may also be due to other factors, such as age, species, etc. Our results are also in agreement with recent data showing that the measured toughness of bone increases with increasing crack length, up to crack lengths of several millimeters [105, 99], due to the involvement of increasing numbers of toughening units (osteons) as the crack grows.

Previous work on the TCD has shown that in some materials, for example ceramics[12], the critical stress is the same as the ultimate tensile stress (i.e. $T=1$), whilst in other materials, for example polymers [76, 11], it takes larger values of 2 or more. The physical significance of T is unclear, but increased values of T may be related to nonlinear material behavior (e.g. plasticity and non-linear elasticity) or to inhomogeneity (e.g. porosity), both of which tend to reduce the effect of a stress concentration below that predicted by a simple linear, homogeneous material model

[93, 106]. Bone displays some porosity, and a small amount of non-linear deformation behaviour before fracture, which explains why its T value is slightly larger than unity.

The intrinsic crack length, mentioned above, is essentially the same as L if calculated assuming $T=1$. This explains why Robertson and Bonfield & Datta both calculated intrinsic cracks lengths similar to our L values. These researchers assumed that the intrinsic crack length corresponded to actual cracks that were pre-existing in the material, whose propagation caused failure during a simple tensile test. This is not exactly valid because cracks of this length will not conform of linear elastic fracture mechanics, especially at loads above the material's yield strength. Our work provides a more precise interpretation for this length parameter: it relates to the size of the damage zone just prior to fracture, a parameter which is in itself connected to the material's histological structure, and especially to those features which cause improved toughness, such as osteons.

The critical distance method can predict an interesting effect of loading type: small holes have a much stronger effect when loaded in bending (essentially creating tensile loading at the hole) compared to torsion (creating shear loading). This distinction is important because our bones are loaded in both bending and torsion, to varying degrees depending on the bone itself and the activity in question. The source of this difference is the higher gradient of stress created by the torsion loading. The fact that the theory can predict the effect of these two types of loading separately implies that it will also be able to predict fracture under combined bending and torsion, since the analysis will involve only the superposition of the two linear elastic models.

This work has shown that the TCD can predict some important short crack effects in bone. The significance of this finding is twofold. Firstly, the approach has practical applications, for example it can be used to estimate the effect of defects such as microcracks, which are known to exist in bone. This can be useful in the treatment of stress fractures in professionals and fragility fractures in older people, and in understanding "brittle bone" conditions such as osteoporosis. Secondly, the result helps in our fundamental understanding of bone's mechanical behavior.

Data from Nalla [103], could not be predicted using the critical distance range of 0.3-0.4mm. A reason for that could be the thickness of the specimens. The thickness is very low and causes plane stress conditions in the material[85]. Plane stress increases the value of critical distance[4]: here is seen that a much larger critical distance was able to predict these results. Furthermore, a different mechanism may be operating. The cracks tested by Nalla et al were growing in the longitudinal direction, which is approximately parallel to the osteons, but in practice the orientation of individual osteons varies, lying typically at 10-20° to the longitudinal direction, and in some cases up to 30°. Thus, it is possible that some osteons remain unbroken and pass through the plane of the crack, causing toughening by a bridging mechanism, as observed by Nalla et al. This suggests that the operative value of L in this case will be much larger than that for cracks in the transverse direction. It has to be taken in consideration that the critical distance is sensitive to the strain rate and temperature. In order to have a complete set of data for this case one would have to examine much longer crack lengths, and currently these data are not available.

3.8. Conclusions

The Theory of Critical Distances (TCD) can be applied to predict the effect of holes, notches and other stress concentrations on the fracture of bone. It is simple to use in conjunction with linear elastic finite element analysis and therefore can easily be employed to study problems of clinical interest.

Using three sets of data from the literature, the critical distance L was found to be almost constant, ranging from 0.32 to 0.38mm; the critical stress was found to be slightly larger than the material's UTS, by a constant factor $T=1.33$. This factor probably arises due to the non-linear and inhomogeneous material behavior displayed by bone.

The critical distance values were not significantly different for the transverse direction (bending and tension) and 45° (Torsion). It is expected that the value of the critical distance, does not vary greatly with changing the direction in spite of

differences in the toughening mechanism. It had also been shown that for composite materials the critical distance does not change along or across the fibers[76].

The TCD can predict the effects of short cracks and thickness in bone. It is useful to study the effect of natural voids in bone as well as fragility and osteoporosis.

CHAPTER 4. Indentation: Prediction of Crack Initiation

In order to study fracture mechanics, there are two major problems that first need to be addressed- crack initiation and propagation. Of these two, crack propagation has been well-researched [28, 27, 107] but the crack initiation is still a large issue that demands further study. In brittle materials, the failure generally occurs and propagates at a void, crack or perpendicular to loading direction. In the case of indentation, initiation is more complicated because of the extremely high stress gradient in the contact near field. The flaws on the surface concentrate the stress on the surface of material due to contact; therefore, there is a certain dependence on the surface flaw and microcracks [28]. In addition, very high stress concentrations stem from the shape of indenter and contact between indenter and substrate material due to the high pressure gradient and local geometry. Here we call those “singularities”. The aim of this work is not to study the effects of the surface flaws on the fracture, but the effect of the geometry on the fracture load. It is assumed that there is no pre-crack on the surface to cause stress concentration and then the fracture. It is also assumed that the indenter tip does not make any crack on the surface at the contact point. In other words, the indenter is not sharp enough, it has a smooth surface, and also the cutting conditions do not make an initial crack. In the indentation, it will be shown that high stress gradient spots- singularities- can be analysed to predict the fracture force using the TCD.

4.1. Summary of the Experimental Results

Indentation tests were carried out on 8mm cubes of cortical bone from bovine femora, indented in three directions with different blades. The indentation was performed at a rate of 2mm/min at room temperature.

Indenters were wedges made from stainless steel with 8mm depth. Various indenters were employed for tests. The wedge indenter is defined by wedge angle and tip radius. Different angles of 20°, 40° and 60° were picked. In surgery, small angles of about 20° are used, but here we were interested in effects of the wedge angle on cutting. Four different tip radii were considered, one of which was very sharp (we call that here 0 μ m, but the radius is in fact about 8 μ m), also 50 μ m, 300 μ m and 700 μ m. The 300 and 700 μ m indenters were very blunt. Indenters were lubricated before each test such as to reduce the friction between materials. From this point forward, by stating 20°-300 μ m blade, we mean a blade with a wedge angle of 20° and tip radius of 300 μ m.

Figure 4-1 shows the device used to hold the specimens. 1mm at each side, at the bottom of each specimen, was constrained using the holder. The experimental results demonstrated that the velocity of the indenter did not have a marked effect on the fracture load when the loading rate changed between 2mm/min and 50 mm/min: all tests thereafter were performed at 2mm/min.

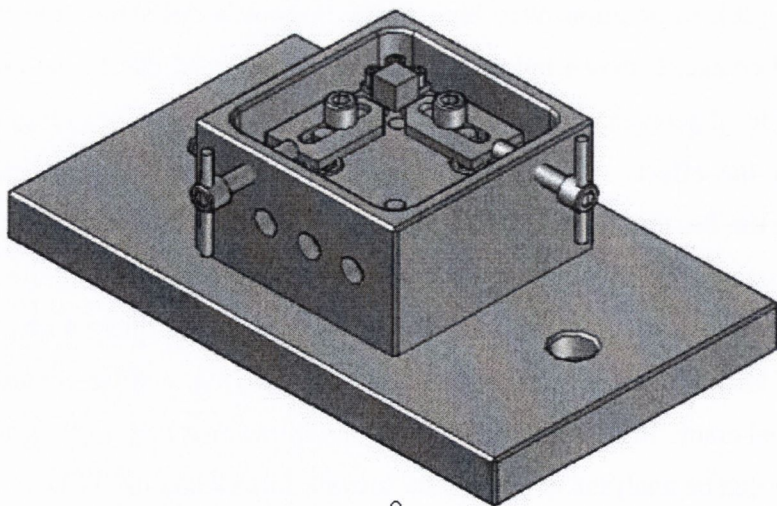


Figure 4-1. Specimen holder for the indentation tests

Indentation tests were performed in three different directions as shown in Figure 4-2, which shows the orientation of the specimen and of the indenter, with respect to the bone tube.

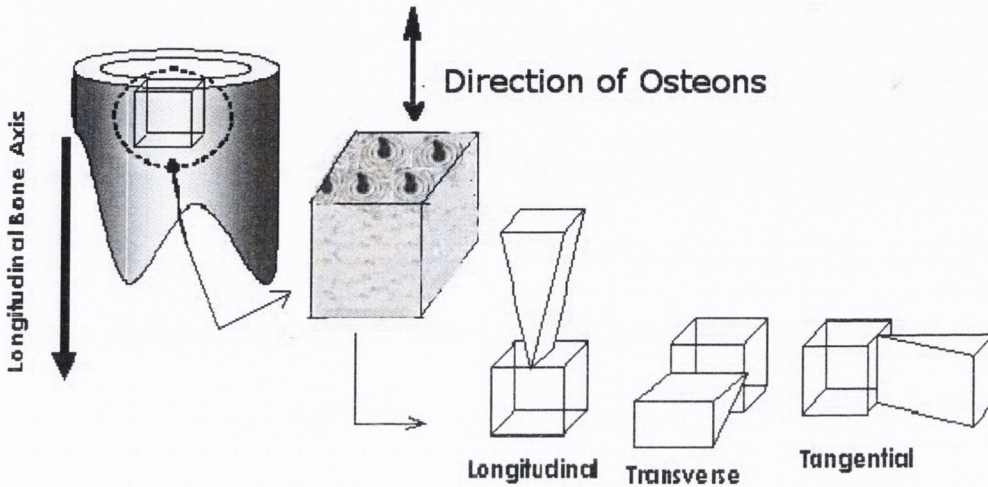


Figure 4-2. Different indentation directions (longitudinal, transverse and tangential)

The surface of a brittle material generally contains a wide distribution of microcracks. Some of these may control the main crack nucleation and propagation. Also from the work in the previous chapter, we would expect that microcracks of length much less than L will have no effect on the strength of the material, so the surface roughness and surface flaws were kept at values much less than L . To do this, there was an attempt to improve the surface of specimens before testing. During the indentation, a critical stage will be reached at which point microcracks initiate and one of them will suddenly extend and cause a fracture. The aim of this research is to predict this critical load. Experiments showed that the crack initiates and grows in parallel with the longitudinal direction of the bone, which is roughly the same as the osteons' orientation and the weakest direction in the bone. It is independent of the indenting direction.

Bovine femora were obtained from 30 months old animals. Whole bones were stored at -18°C until the day of specimen preparation. Before preparation, bones were allowed to thaw under a damp cloth. Beams of 8mm wide and 100-120mm long were taken from a medial surface. They were prepared at low speed to reduce heat and bone

damage. Between 8 and 10 specimens were cut from each beam. These bone cubes were stored in individual bags in the freezer.

4.2. Indentation Fracture and Cutting: Background

The study of the indentation and cutting fracture are of fundamental for the understanding of failures mechanism of materials. Understanding the mechanism of indentation fracture and cutting helps for the advance of indenters and cutting tools. The minimum cutting force and damage with the smooth surface are desirable in cutting process. This is a concern especially in surgery for an easier cut with less damage on the tissues. The Cutting is an special case of indentation when the indenter becomes sharper, therefore understanding the indentation fracture mechanism help us to gain a better understanding of cutting.

Finite element models have been developed for indentation [21]. The finite element method has proven to be an excellent approach for solving elastic-plastic related problems which give a quantitative estimation for the indentation stress field [24]. To find the cutting force, usually the crack propagation is simulated until the formation of an unstable crack which is computationally expensive. The model we will employ is based on the analysis of deformation, therefore we will not model any crack.

For an indentation test, it must be noted that the condition of the materials at the time of the test are very important. For example, drying has large effects on the mechanical properties of bone, as it increases the elastic modulus and hardness of interstitial lamellae and osteons. It also reduces the fracture toughness and strain to fracture[39].

There has been much research done on indentation fracture at a larger scale. Lawn et al., [27] studied different types of indentation. They defined the sharp and blunt indenter depending on whether or not there is irreversible deformation at contact. They also explained the ductile and brittle fracture of indentation. In the case of ductile material, the compressive stress on the shear plane must be high enough to allow the material to experience a considerable shearing strain before fracture. Brittle indentation

is completely different and also depends on the shape of the indenter. When a brittle material is loaded by an indenter, three different zones are formed. Figure 4-3 shows different zones formed by a spherical indenter. A hydrostatic core is formed immediately below the indenter, which is due to the high tri-axial compressive stress. Outside the compressive zone, a large strain zone is developed due to the pushing action of the core. In some materials, tensile cracks may form due to pre-existing flaws. Outside these areas, the material behaves elastically.

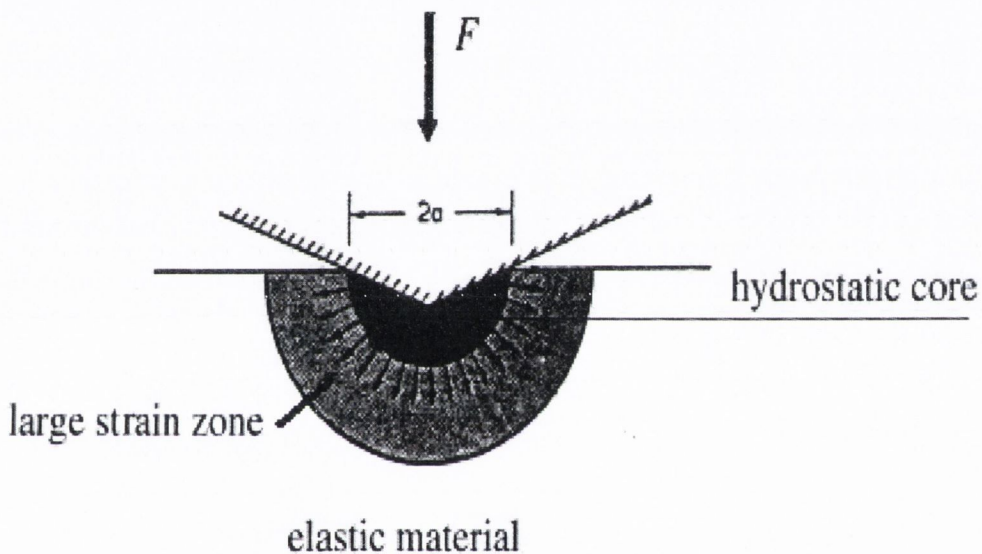


Figure 4-3. Three different zones formed during the elastic-plastic indentation

Chiaia [34] studied the cutting process in quasi brittle materials, using different hypotheses for microscopic failure behavior, namely a simple frictional mechanism, plastic crushing, and linear elastic fracture mechanics. In general, plastic rocks are only crushed and penetrated by indenters, giving linear curves, whereas more brittle rocks are cracked with the formation of chips, giving nonlinear and discontinuous curves[108].

In the case of bone indentation using cylindrical indenters, there is an inelastic deformation; therefore using the above definition for blunt and sharp indenter is

confusing. In this thesis as an initial definition we use a relative definition for sharp and blunt indenter; the smaller the angle and radius of indenter, the sharper the indenter.

The finite element method is appropriate to determine the contact stress field, though it is usually time-consuming.

4.3. Indentation singularities

During the indentation, the material beneath the indenter is under large amounts of compression, which is followed by a tensile area at greater distances from the surface. In some materials like ceramics, there are no microcracks observed in the compressive area, but they are formed in the tensile zone. Therefore the crack initiates and propagates from a point in the tensile region [28]. In some other materials, depending on the indenter shape, a crack nucleates from a region of the surface of the material which is under tension. This tensile spot is at a distance from the contact boundary [27, 28]. Contrary to these materials, the experiments on bone show that diffuse damage zones are formed in the compressive zone but failure occurs from a main crack which is started from the contact surface, see Figure 4-4. Indentation fracture of bone is a occurs by catastrophic failure, therefore it is expected that this type of breakdown can be predicted using the TCD. Figure 4-5 shows the indentation at fracture. It can be seen that the main crack starts from the point on the contact surface approximately at the boundary. At this point normal stress changes from compressive to tensile. In bone, both compressive and tensile failure can occur, but in different ways. Yield stress is higher in compression than in tension. Yield damage is microscopically quite different in compression from yielding in tension. Also shear lines appear in compression [109]. These shear lines show a strong tendency to initiate at large stress concentrators, such as blood channels. When the specimen is loaded in the longitudinal direction, the lines are formed at angles of 30° to 40° with respect to the long axis. These lines probably represent very small scale buckling of lamellae or fibrils in osteonal bones [110]. During the indentation a crack, therefore, can be initiated at the stress concentration spot when the material is under compression.

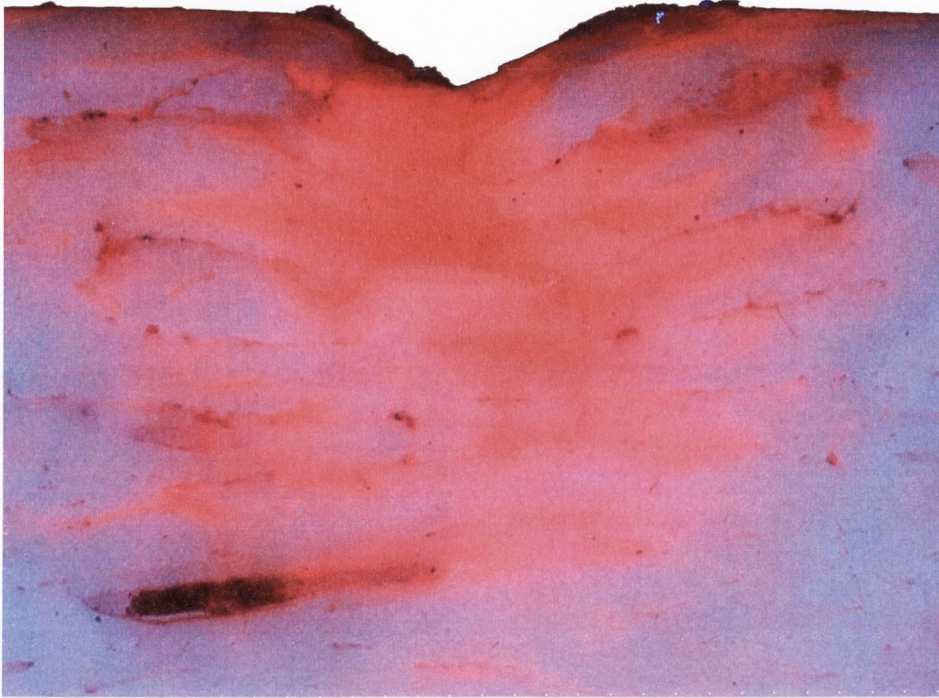


Figure 4-4. Damage zone at fracture for transverse indentation. The damage occurs underneath the indenter which is under high level of compression.

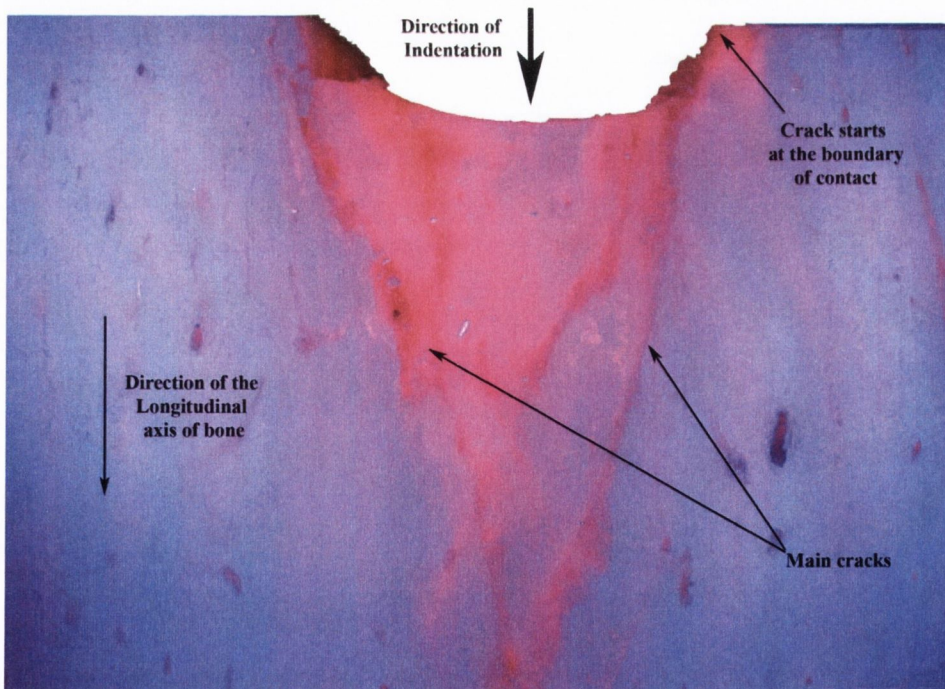


Figure 4-5. Crack initiation spot for 20°-300 μ m blade for longitudinal indentation. The main cracks start at the boundaries of contact.

Figure 4-6 shows the variation of stress along the contact line for a $300\mu\text{m}$ radius, 20° angle blade at the fracture force. Looking at the distribution of stress along the contact line, it shows a high gradient of stresses. The contact pressure drops at the contact boundary to zero. In this thesis, the absolute value of the contact pressure is shown in all the graphs however the contact pressure is compressive. The normal stress along the contact line is highly compressive and it has a minimum value at the boundary of contact. It turns to tensile stress (outside of contact area) and increases until a peak value and then decreases gradually. The maximum tensile stress therefore occurs outside of the contact area, though the value of tensile stress is large enough to cause damage, yet experiments show that the crack rarely initiates from this zone.

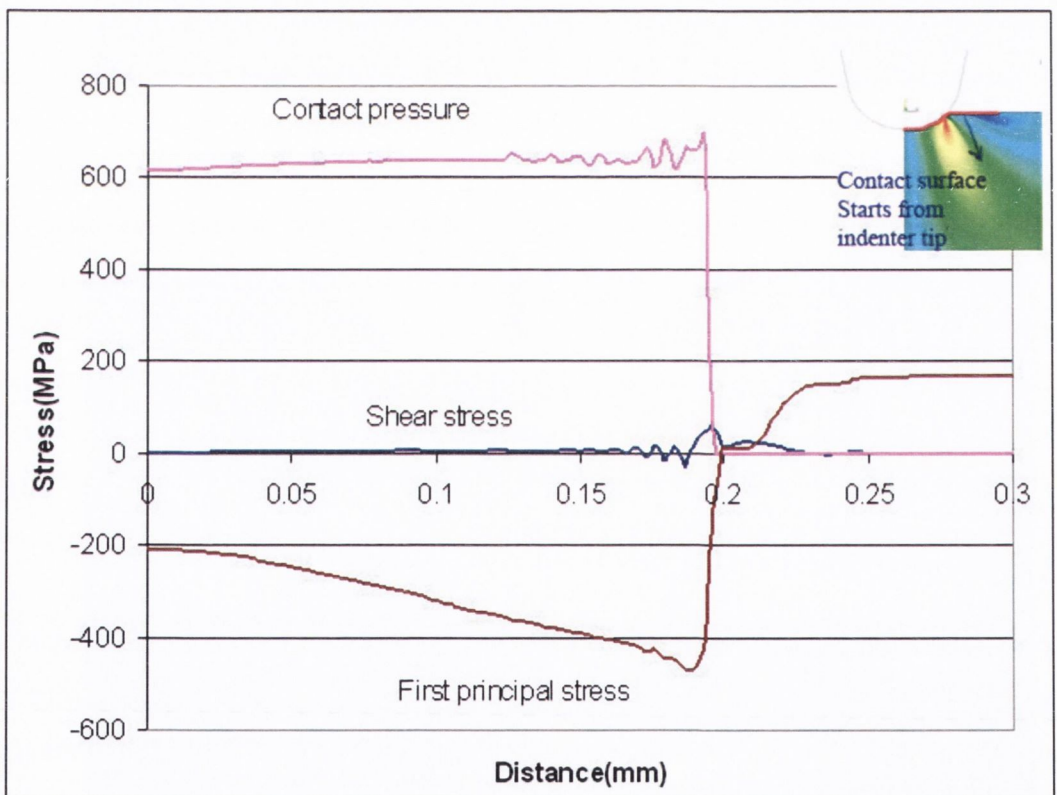


Figure 4-6. Variation of maximum tensile and shear stress on the contact surface, for a 20° angle and $300\mu\text{m}$ radius blade. The distance is measured from the tip of the blade, and follows the material surface as shown in the diagram.

Assuming that the bone is a homogenous material under indentation makes it easier to define the crack initiation position. During the indentation there are some spots with a high gradient of stress. We call them singular points, however stress at these points do not go to infinity. There are two different types of singularities in a blade- boundary and geometric singularities. The former is defined as the place on the contact surface where the indenter is separated from the material. At this point stress changes due to a sudden alteration in pressure on the material from a finite value (in the contact zone) to zero (outside the contact zone). This type of singularity depends on the contact area between the two bodies and also their material properties. The latter singular point occurs at the point along the indenter geometry where the radius of curvature changes. In fact, even for a perfect indenter, with smooth sides, the radius of boundary curvature varies from a finite value at the tip to an infinite value at a certain point. This variation in the curvature causes a singularity during contact due to changing the pressure distribution on the contact surface. Figure 4-7 shows the singularities on the contact surface. As it can be seen the normal stress on the contact surface changes markedly as a result of shifting of contact pressure at singular points. Singularities concentrate stress during the indentation and they are probable locations for crack initiation. It will be shown later on in this thesis that, in the case of longitudinal and tangential indentation, the boundary singularity plays an important role.

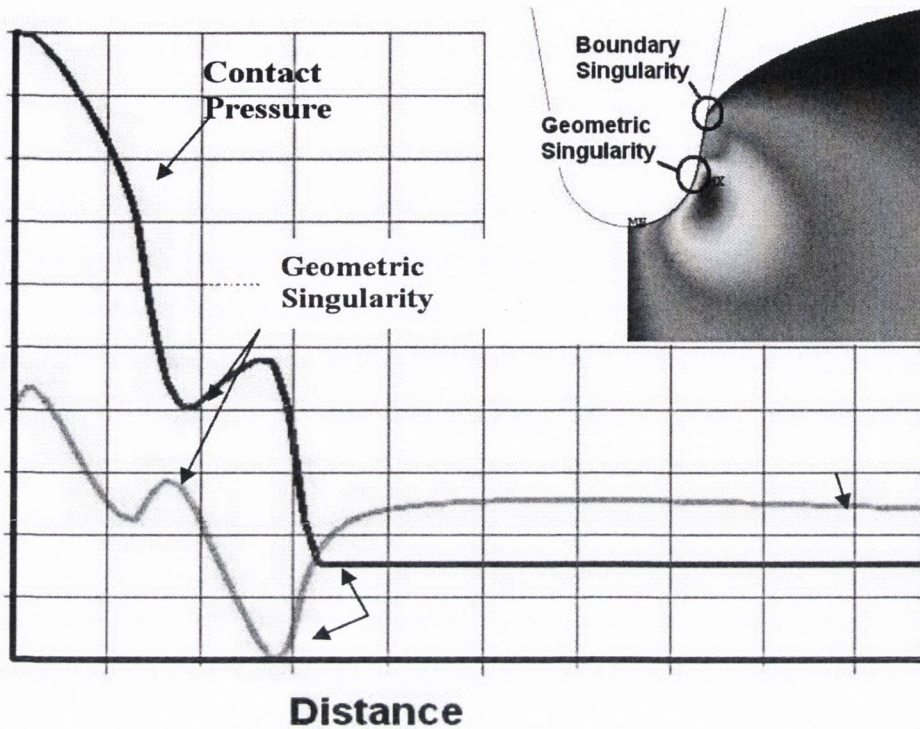


Figure 4-7. Schematic of the variation of first principal stress (S_1) and contact pressure along the boundary during indentation defining the two singularities. The distance is measured from the indenter tip along the surface of bone.

The maximum tensile stress occurs at a distance from the boundary conditions. For example, in a 20° - $300\mu\text{m}$ blade, at the fracture force contact occurs up to a distance of 0.19mm from the symmetry line and the maximum tensile stress occurs at the distance of 0.32mm . It might be expected that the crack initiates from the maximum tensile stress point but this does not agree with the experiments, as will be shown below.

As the strength of cortical bone is less in shear than in tension and compression, particularly in the longitudinal plane, it would be expected that the crack initiates from this point [111-113]. In case of indentation, the main crack starts at the boundary of contact for blunt blades. At this point the shear stress reaches the maximum value and the compression stress is minimum in value.

4.4. Effects of Friction

In the previous section, the effects of the blade geometry on the stress were studied, along with possible effects on crack initiation. Besides the singularity points and due to the geometry of the blades, friction in the contact areas will affect the stress distribution. The role of friction is more important for sharper blades. In fact, the crack does not always initiate at the point close to the boundary singularities, but sometimes at a spot along the contact line. These nucleation spots can be an effect of the friction force. During the experiments it was attempted to minimize the effects of friction by using lubricants and polishing the surface of contacts. Friction between the indenter and bone will change the stress distribution on the surface of the material. Maximum local shear and tensile stress points vary with the friction factor. Friction therefore makes a new maximum point which, apart from the singularity point, is another probable point for crack initiation. Figure 4-8 shows the stress distribution along the contact area when the Coulomb friction factor is assumed to be 0.15, which is acceptable when the blade is lubricated. It is seen that shear stress reaches a maximum point somewhere along the contact line. At this point the normal stress is less compressive than at the boundary points, which makes it a more likely place for crack initiation. Therefore, using the fracture line starting from this point will change the prediction force for fracture. Unfortunately, there are no experimental results to show the effects of the friction on the indentation fracture force in bone.

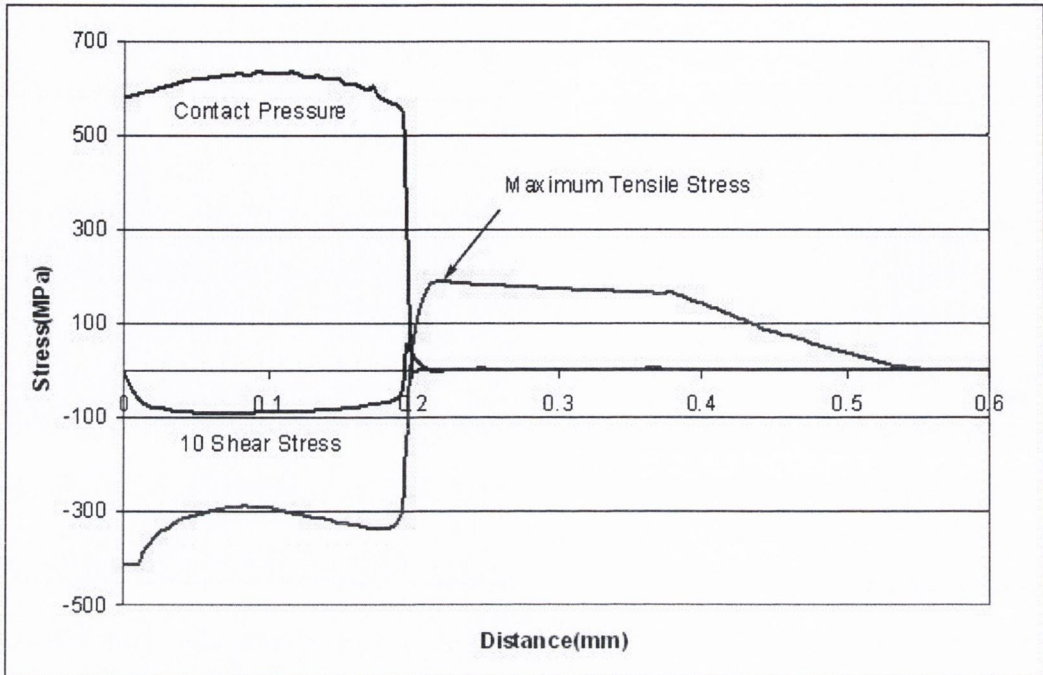


Figure 4-8. Stress distribution in the presence of friction

4.5. Fracture Line

Crack propagation has been well-studied for many materials and it is well-known that maximum tensile stress plays an important role in crack growth during brittle fracture[28]. In the case of crack propagation of bone, there is still no global agreement. Two general theories are applied to bones. The first one assumes that the crack propagates in the direction perpendicular to the maximum principal stress. For example, it has been observed that the crack grows at the 45° when it is loaded under torsion [94, 114]. The other theory states that the crack will grow in the weakest directions [8]. There are two factors that must be noticed in order to find the weakest plane in the bone- loading and structure. Bone strength is weaker under shear than tension and compression in a longitudinal direction. In transverse and tangential directions, the shear and tensile strength are close[113, 111, 112]. The weakest direction, therefore, depends on the type of loading that is acting on the fracture plane. The failure may be caused by shear or tension especially in the tangential direction where the difference between the shear and tensile strength is small. In this case we say that the crack advances in the “weakest possible direction”. The weakest possible direction means the

weakest plane on which there is enough stress acting to cause failure. From a structural point of view, considering the three planes- tangential, longitudinal and transverse- the tangential is the weakest while transverse is the strongest. This was confirmed by measuring the fracture toughness of a crack growing in each direction[115, 116, 3, 79, 117]. The fracture toughness for a crack introduced in tangential direction is almost half that in transverse. In fact, the resistance of material against crack growth is used to characterise the material. Fracture toughness, therefore, is used to find the weakest direction in the material. In osteonal bone, cement lines are the boundaries between secondary osteons and the surrounding interstitial lamellae in cortical bone. It is known that the weakest direction is the plane parallel to the osteons, in the tangential plane[115]. This is shown in Figure 4-9. Therefore according to the second theory, bone fracture should occur in the same direction as the osteons independent of loading.

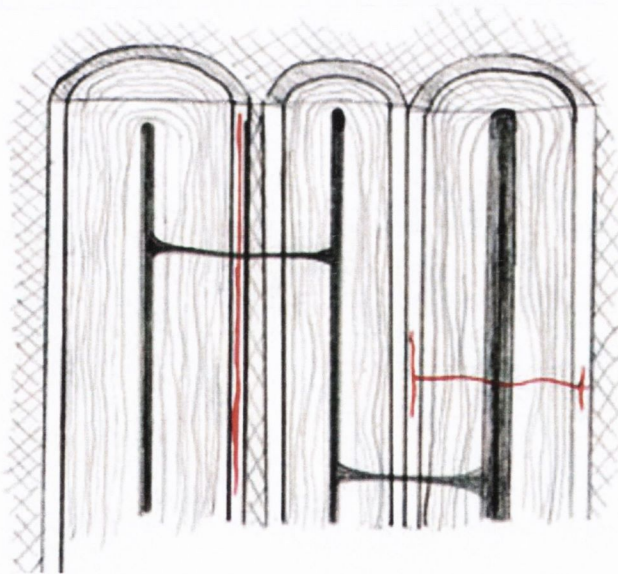


Figure 4-9. The cement lines form the weakest constituent of bone. Crack propagation parallel to the osteons (shown with red lines) can occur much more easily in the longitudinal direction. Similarly, if a crack is propagating perpendicular to an osteon (horizontal red line), when it reaches a cement line it will change direction, the crack is blunted.

In the case of indentation, the first theory is not applicable, as the material is under high amounts of compression at the contact area where the crack starts. The second theory correctly predicts the direction of crack growth, as will be shown below. In the longitudinal indentation, the shear and tensile stress acting on the tangential plane is negligible while the longitudinal and transverse plane are under intense shear and compression. It is therefore expected that bone will fail under shear in the longitudinal direction. In transverse indentation, there is not as much stress acting in the longitudinal plane, but high shear and compressive stress acting on the transverse and tangential plane. In this case, the crack is expected to grow in the tangential plane, which is perpendicular to the indentation direction. In tangential indentation, high shear stress is acting on the tangential plane, which causes crack propagation in this plane.

Experimental results concur with the prediction using the second theory. It was shown that the crack propagates in the weakest loaded direction of bone independent of the cutting direction. For example, Figure 4-10 shows the crack propagation in longitudinal cutting. As expected, the crack grows in the longitudinal direction of bone.

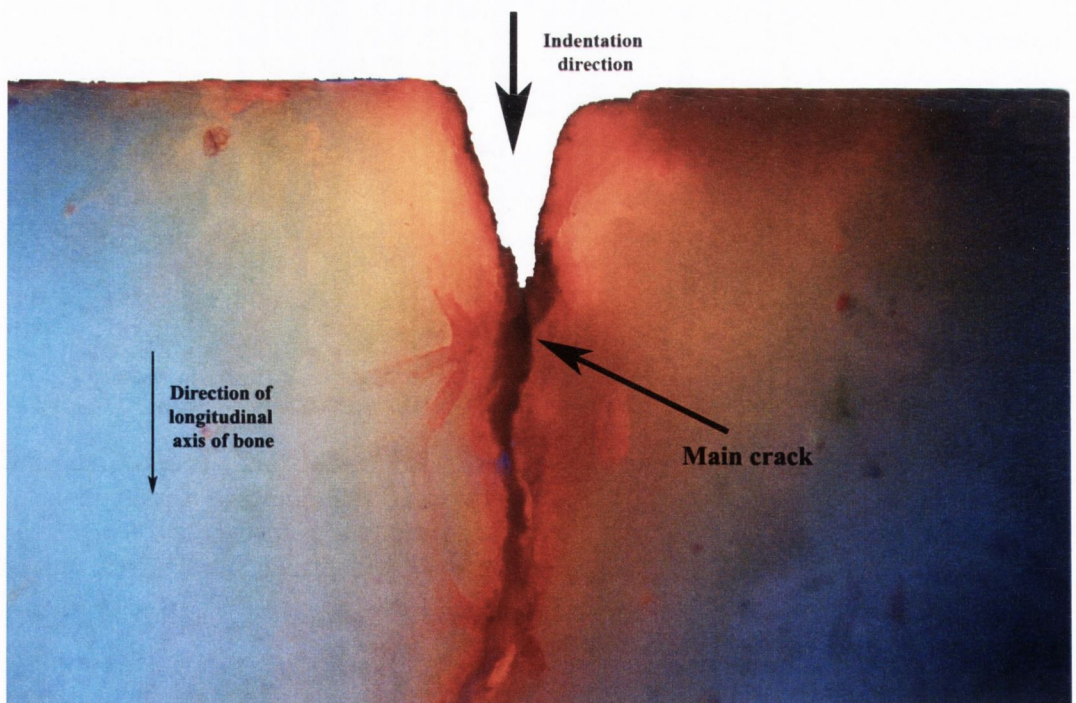


Figure 4-10. Crack propagation direction in longitudinal cutting. The main crack advances in the longitudinal orientation of bone

Figure 4-11 shows the crack direction during the cutting performed in the transverse direction of bone. During the indentation, many large cracks grew in the tangential plane, as it can be seen on the figure. A main crack developed in the tangential plane (perpendicular to the cutting direction) and removed a piece of material. The chipped off section on the right hand of the figure shows the direction of the crack propagation.

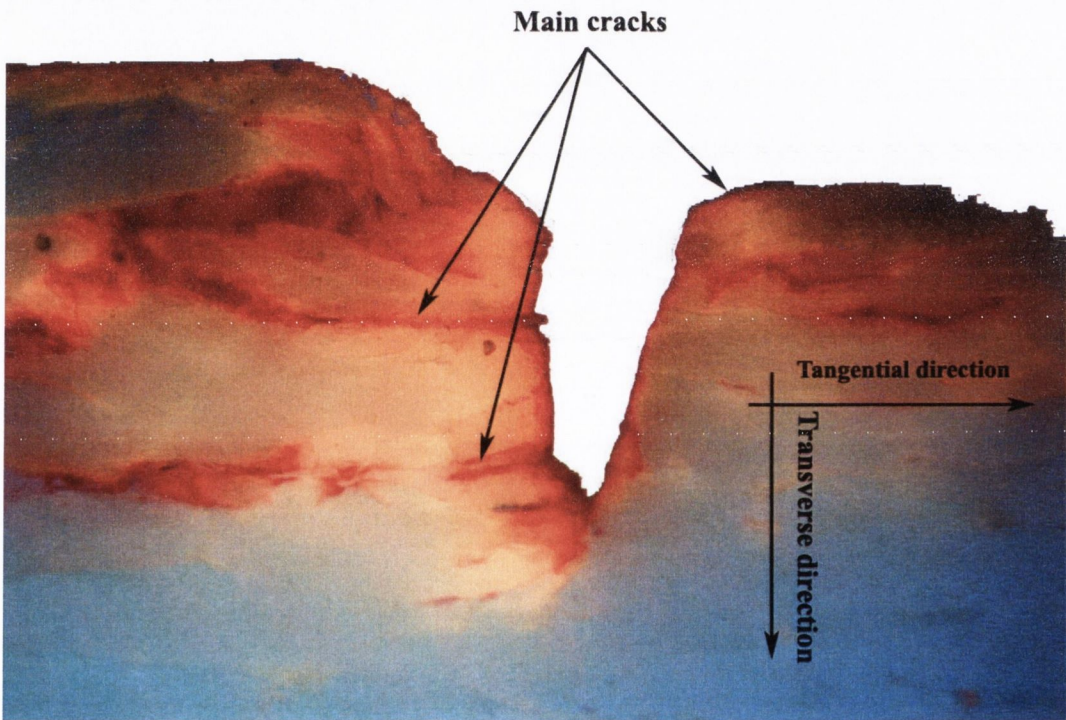


Figure 4-11. Crack growth during the transverse indentation. The main crack grows in the tangential plane.

Looking at the shear and normal stress on the fracture line for longitudinal indentation at the fracture force demonstrates that on the fracture line the material is under high amounts of compression (Figure 4-12). The fracture line starts at the contact boundary in the longitudinal direction. (In Ansys, when a path is defined, normally the distance is measured in the un-deformed geometry. In this case, we are interested on the distance after deformation because of the large deformation. Appendix 2 explains how to measure the deformed distance). The shear stress as can be seen in the following figure, increases over a small distance and then decreases gradually. The peak in the

stress curve is due to the fact that the maximum stress happens at a distance from the contact surface. The shear stress on this line is higher than the shear strength of bone. If we assume that the fracture happens because of the shear stress, then it could be said that in the presence of compressive stress a higher shear stress is required for failure.

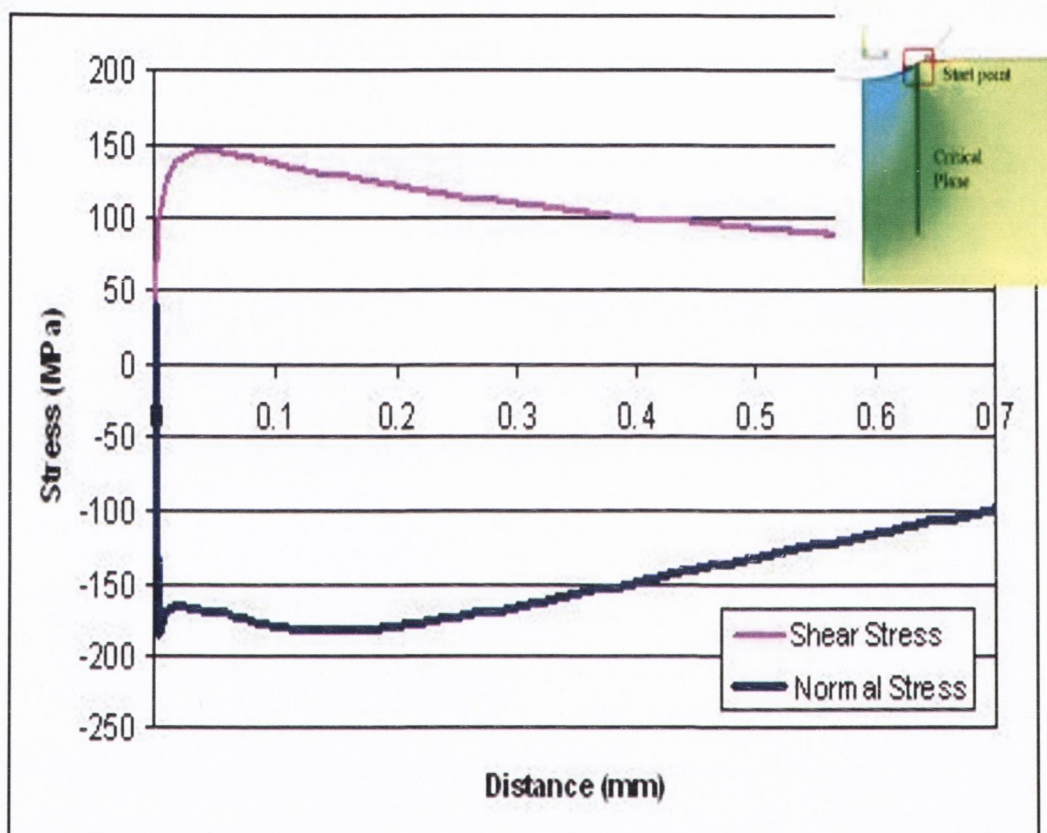


Figure 4-12. Variation of normal stress and shear stress on the critical line for 20°-700 indenter at the fracture force

Under indentation, part of the material beneath the indenter is under high compression. Figure 4-13 shows the contour of maximum principal stress at fracture. The indenter 20°-300 μ m is quite blunt, therefore the contact area and compression zone are large. In some ceramic materials, however, microcracks were not seen in this compression zone [28] but experiments on bone shows that there are diffuse cracks in this compression zone. There is a large tensile zone next to the compressive area. The tensile stress on this area decreases from the centre (under the indenter) to the sides.

The tensile stress in this zone, however, is not large enough to cause fracture, but it is a probable zone to form microcracks.

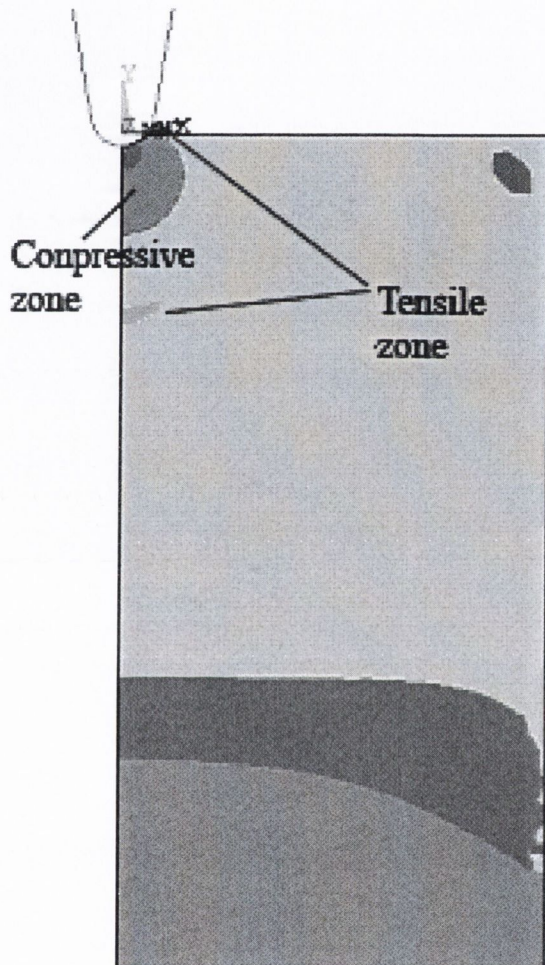


Figure 4-13. Contour of first principal stress for the 20°-300 μ m blade

The pressure distribution on the contact surface for the 20°-300 μ m indenter is shown in Figure 4-14. As can be seen, in the absence of friction, there is only one marked change in the pressure. This means that the boundary singularity is the only one present for this indenter before fracture, therefore there is no geometry singularity for blunt indenters as it lies out beyond the contact boundary. In other words, it is to be expected that there is no effect of angle on the fracture force. This occurs for the indenters with large tip radii.

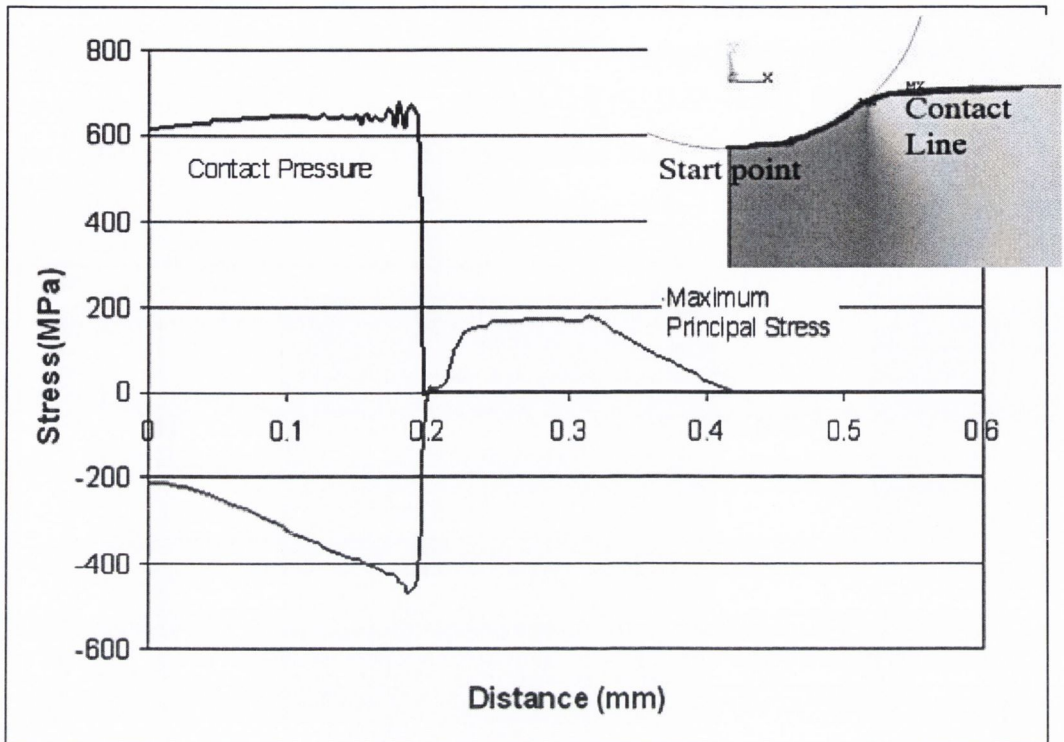


Figure 4-14. Variation of tensile stress and contact pressure on the contact surface for longitudinal indentation using 20° - $300\mu\text{m}$ indenter. The contact pressure drops to zero at the contact boundary. The distance is measured from the blade tip along the contact surface

The fracture plane is shown in Figure 4-15. It shows that two large cracks grow in the longitudinal direction and then converge at a point in the middle of specimen along the indenter. It is hard to know why these two cracks join instead of growing radially as in a metal under spherical contact. It might depend on the microstructure of bone and the maximum shear stress direction and the fact that a crack in the bone tends to grow in the weakest plane. As can be seen in the above figure a diffused damage zone was formed below the indenter. It is different from some other materials, like ceramics, in which diffuse cracks are not formed in the compression zone. There is also a high tensile stress below the compressive zone. No microcracks have been seen in this area, though the tensile stress is enough to build up the microcracks. This is because of the catastrophic crack growth after crack initiation on the surface. This type of growth does not give time for microcracks to be built up in the tensile region. The high tensile stress in this area can be another reason that the two cracks converge together.

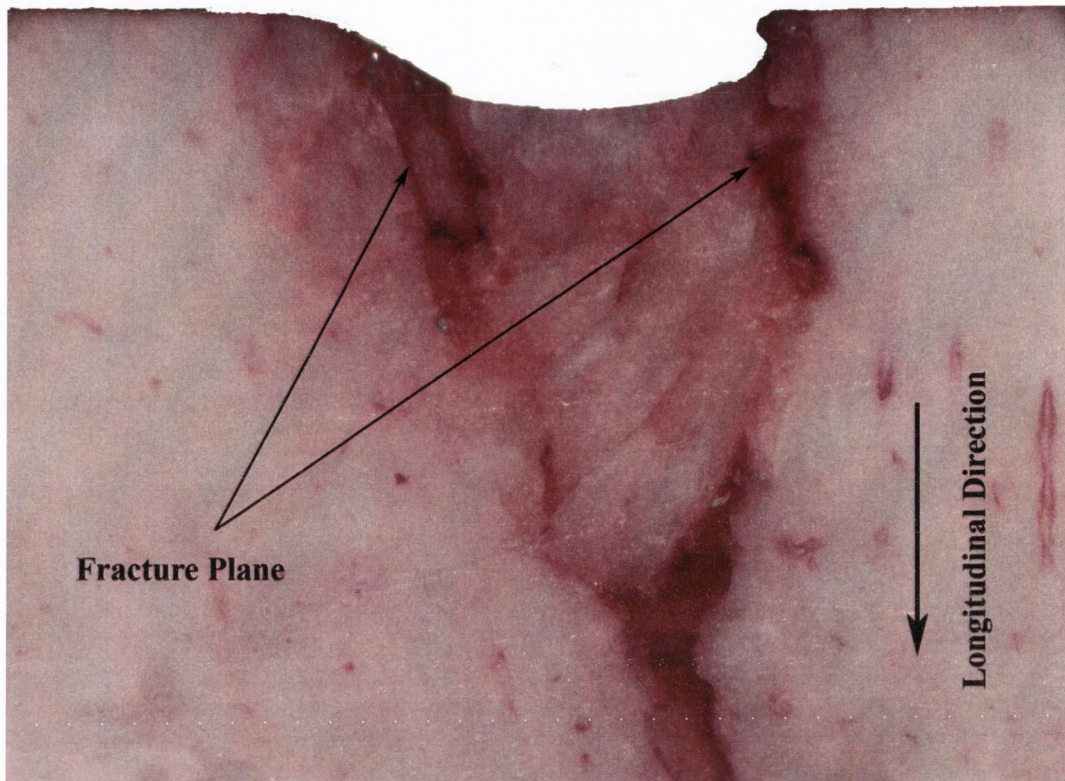


Figure 4-15. Cracks in the longitudinal direction start from the boundary of contact, and then they merge and propagate in the longitudinal direction. Inelastic deformation at fracture can also be seen under the indenter.

4.6. Conclusion

Indentation fracture in this material occurs by growth of a macro crack nucleated from the surface of contact. There is inelastic deformation in bone before failure which could be because of plasticity, micro-cracking or crushing. The amount of inelastic deformation depends on the geometry of the indenter. Diffuse damage has been seen in the compression zone beneath the indenter. As the main crack starts from the contact surface which is in the compression zone, it can be said that the shear stress plays an important role in the final fracture of bone. The contact singularity spot is defined as the first estimation for the crack initiation in the absence of friction. In the next chapter it will be shown that the initial point can be estimated as well and it will verify this assumption. The crack propagation plane is parallel to the force axis in the case of tangential and longitudinal indentation and perpendicular to the indentation direction for the transverse indentation. In the next chapter, the ideas developed here about crack

initiation and crack growth will be applied, along with the TCD, to predict fracture forces and other experimental results.

CHAPTER 5. Indentation- Cutting Fracture Force

Analysis of indentation stress fields and fracture cracking in brittle materials have been carried out by many researchers following the work of Hertz and Griffith. To investigate the bone cutting mechanism, various cutting operations, such as drilling, [57, 59, 60, 58], sawing[52] and orthogonal cutting [54, 53, 56] were studied. Also, the critical parameters that influence heat generation during cutting were examined. In orthogonal cutting, the force components are a function of cutting tool geometry, depth of cut, and relative orientation between the cutting edge and bone structure, therefore such a study can help to optimize the cutting tools. The 'specific cutting energy' was defined as the energy to remove a unit volume of bone by cutting. It was shown that the specific cutting energy decreases with increasing the rake angle, and speed of cutting [53, 54].

Indentation fracture (including nanoindentation) has been widely used to measure the mechanical properties of materials, especially the fracture toughness. It has been proven to be a useful tool for characterizing the mechanical properties of micro-structural components of bone, such as individual osteons and trabeculae[40, 41, 38, 35]. The micro-indentation technique was also employed to estimate the fracture toughness of human enamel [44, 45]. The process of indentation is completely different in the case of the brittle materials and depends also on the shape of the indenter [27].

For example, the required force to produce a crack in bone using a cube-cornered indenter is up to 1000 times less than using Berkovich or Vickers tip [32]. Fan et al [36] looked at the consequences of anisotropy on nanoindentation measurements for cortical bone using a three dimensional finite element model. There was no pile-up observed during the indentation [36, 118]. Pile-up in elastic-plastic material is related to the young's modulus, yield stress, and strain hardening [33]. Young's modulus and yield stress are roughly constant for bone, therefore a pile-up phenomenon is due to the lack of strain hardening. Thus, it is a fair assumption that by applying strain-hardening to the model, it will eliminate pile-up in bone simulation.

Cortical bone has a complicated material structure. Its material properties, however, might not be described well by the classical elastic-plastic model, but there is not proper material model available for cortical bone. In most indentation FE studies, bone was simulated as a classical elastic-plastic solid with isotropic or anisotropic properties [36].

Wesley et al [118] looked at the cross section profile of microindentation in wet and dry bone using the Knoop pyramid. They found that there no pile-up on the short diagonal sides, and a crack formed along the apex of long axis of the microindentation in the case of both dry and wet bone. They summarized that indentation compacts the material, leaving it locally more dense and fractured.

Indentation on a larger scale on other materials has also been investigated. The cutting of wood [119, 31], PMMA [23, 22], bone [54, 55, 50], and needle insertion have all been studied to understand the mechanism of fracture, while also improving the cutting tools.

Indentation on rocks [108] showed that in general, plastic rocks are only crushed and penetrated by the indenter, leaving linear curves, whereas more brittle rocks are cracked with the formation of chips, thus yielding nonlinear and discontinuous curves.

In the previous chapter it was shown that, in the experiments conducted in parallel with the present study, the main crack is inclined to nucleate at stress concentration spots and propagate in the weakest available direction. Furthermore, the main crack starts at the contact zone, which is under high levels of compression and where the shear stress is also high and effective. In this chapter, the force required to cause indentation fracture is predicted using a specially-devised multiaxial critical distance method. Firstly, a fracture criterion model is proposed based on the TCD in combination with the Coulomb-Mohr fracture criterion. Then, the unknown parameters are estimated using two sets of the experimental results. Subsequently, the model is applied to predict the indentation fracture force for the other cases studied experimentally. Also, the crack initiation point is estimated using the critical distance method and is compared with the experimental observation.

5.1. Multiaxial Critical Distance Theory

Engineering components are usually subjected to a complex loading system. Even in many simple loading structures, failure can not be determined by a single tensile or shear stress. In simple situations, having a notch or crack mostly results in a multiaxial stress field. In other words, the stress on the fracture plane are a combination of shear and normal stresses. In some failure approaches, the fracture plane or critical plane has been used to predict the multiaxial fracture. The critical plane or fracture plane is the plane on which the initial crack forms and grows. In the critical plane approach, it is attempted to reduce the stress tensor to a scalar quantity. Here, we call this scalar quantity “**fracture stress criterion**”.

The TCD has previously been extended to multiaxial stress fields using the critical plane approach, to study metal fatigue problems [9]. For a multiaxial TCD, a fracture stress criterion should be defined. This decisive factor depends on the failure mechanism of the material under different loading conditions. Unfortunately, there is no universally-agreed procedure for failure prediction. In fact, the failure mechanism in materials is highly dependent on the type of loading. In most brittle materials, tensile

and compressive behaviors are very different, therefore many fracture stress criteria were defined for given material and loading conditions [120, 9, 121-123, 19]. The fracture stress criterion is usually a combination of shear and normal stress acting on the critical plane.

Indentation is a multiaxial problem. A complex field of stress, including shear and normal stress, is acting on the critical plane. A compressive zone is formed beneath the indenter. This compressive stress can not even open a crack but forces voids and cracks to be closed and produces friction between the sides of the voids. The shear stress, therefore, is playing an important role in causing fracture. The greater the shear stress acting on the fracture plane, the greater the compressive stress required to avoid fracture. In effect, the internal friction is an important issue which has to be factored in. To study the bone fracture, the Coulomb-Mohr criterion was employed, which was initially proposed for brittle multi-axial fractures, and which is related to the stress acting on fracture planes and inherent friction. The Coulomb-Mohr theory has been widely used to model the failure of porous materials, especially rocks [124, 125]. It is assumed that the critical stress is a linear combination of normal and shear stress on the fracture line, as shown in equation 5-1. The equivalent critical stress is assumed to be the nominal shear strength, τ_u , as the equation is satisfied if there is no normal stress on the critical plane (σ).

$$|\tau| + \alpha \cdot \sigma = \tau_u \quad (5-1)$$

τ and σ are shear and normal stress acting on the fracture plane (for more details see appendix 4). α is a material constant which depends on the relative strength of material under different stress states. It is related to the tensile (σ_{ut}) and compressive (σ_{uc}) strength with equation 5-2.

$$\frac{\alpha}{\sqrt{1 + \alpha^2}} = \frac{\sigma_{uc} + \sigma_{ut}}{\sigma_{uc} - \sigma_{ut}} \quad (5-2)$$

and nominal shear strength, τ_u , is related to the shear strength (τ) using equation 5-3:

$$\tau_u = \tau \sqrt{1 + \alpha^2} \quad (5-3)$$

By assuming the typical values for shear, tensile and compressive strength for bone as 69, 150, and -250MPa respectively, the material constants are calculated to be $\alpha=0.35$ and $\tau_u=73\text{MPa}$.

According to this equation, a greater compressive normal stress is expected to cause more friction between the opposite faces of flaws, thus increasing the shear stress necessary to cause fracture. As the bone is highly under compression during indentation, a high shear stress is expected to act on the fracture plane; this shear stress is much higher than the shear strength of bone. It must be noted that this form of Coulomb-Mohr criterion is not suitable when the tensile and compressive strength of material are similar. In this case the criterion is restricted by some other constraints.

5.2. Finite Element Modeling

The elastic stress fields arising from indentations with point loads, spheres, cylindrical and flat punches are well-known analytically [24, 29, 26, 23, 36]. For elastic-plastic materials, simplifying assumptions are required for theoretical analysis. Furthermore, the stress field for more complicated geometries may not be calculated analytically. The finite element method, is a useful tool to simulate these indentation problems[24, 126, 25].

A 2D finite element model of indentation was created using ANSYS software. Bone was modeled as a bilinear isotropic material. The indenter was modeled as a rigid material in order to show the difference between Young's modulus of the indenter and bone. Also, it was assumed that there is no damage to the blade during indentation. This is a fair supposition because the indenters are used just for a few tests, and also they are relatively blunt.

Specimens were cubes of side 8mm. A 2D plane strain model can be employed because of the symmetric conditions. The tests were conducted in displacement control (2mm/min), therefore force was measured as a function of displacement. In the modeling, either force or displacement can be applied to a model and the other one is

found from the simulation. These two methods of loading are slightly different when the convergence of nonlinear problems is considered. Here, displacement was applied to the indenter; reaction force was determined to validate the model. All nodes on the bottom surface of the bone sample were constrained in the vertical direction. Along the sides for the lower 1mm were constrained in the horizontal direction. A map mesh using element PLANE82 was used around the contact area. PLANE82 is an eight-node element which is suitable for this analysis due to the bending of elements around the indenter. High deformation around the contact area tended to cause a mesh destruction error. To avoid this problem a mesh ratio up to 1:2 was used in this region. Contact surfaces were modeled using CONTA172 and TARGE169 with standard behavior. The penalty method was employed as a solver. Mesh was refined until there was no marked difference in the results. (Appendix 2, 3 contain more details of the FE model and a sample of the Macros used with it)

5.3. Load-Displacement Model

Here we are focusing on two important points upon which to model the bone indentation- load-displacement and pile-up phenomena. These two criteria are considered to model the material of bone as an elastic-plastic model. It is well-known that pile-up is related to the work hardening of material, yield stress and elastic properties[36]. If the elastic modulus and yield stress are known and constant then hardening controls the pile-up. Also an elastic- perfectly plastic model for bone predicts pile-up along the sides of indenter. There is not a material model that can effectively explain the behaviour of bone. Some researchers have used an isotropic hardening model to represent the load-displacement and pile-up [36]. Here we assume a linear hardening model for bone. On the other hand, load-displacement depends on the material properties, as well as the geometry of specimens. To model the load-displacement, it was assumed that the Young's modulus of bone is roughly constant and also the moduli of elasticity in tension and compression are the same[127, 106], then for the given dimensions of the specimens, we found the yield stress and tangent modulus as the best fit for prediction with experimental results. A bi-linear material behaviour

with Von-Mises yield criterion was used to model bone (Figure 5-1). Two dimensionless parameters, Y/E and E_t/E were varied until the force/displacement relationship of experimental results was obtained. The Young's modulus of bone was assumed to be 18GPa in the longitudinal direction. This value was taken from test results performed by Mr. Reilly (Table 5-1). Plane strain conditions were assumed due to the large thickness of specimens (8mm) [85]. Figure 5-2 shows the Force-displacement of experimental results as well as the FE model for different Y/E , and E_t/E . The investigation results show that during the indentation the top surface of the specimen was displaced in the cutting direction by about 0.15-0.25mm. This amount of displacement in bone specimens, which is happening gradually during the indentation, should not be counted as the blade indentation. It was due to the uneven surface of specimens at the bottom part where it is in contact with the holder or at the contact surface. There are two ways to show this effect in the FE model. The first is to change the constraint at the bottom surface of specimens to allow it to move about 0.2mm. Another way is that, as the displacement is occurring gradually, a factor should be applied to the experimental displacement. This is defined by the ratio between the specimen displacement and the maximum displacement of the indenter. It will be applied to all the experimental results in all directions.

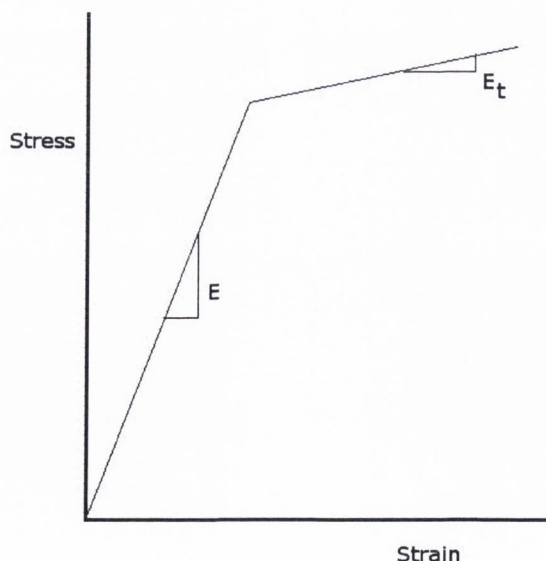


Figure 5-1. Model of bone as a bi-linear material, the young modulus is taken from experiments and the tangent modulus is found such as to predict the best force-displacement curve measured from experiments.

Table 5-1: Young's modulus of bovine femur in different directions (experimental data from Ger Reilly)

Direction	Longitudinal	Transverse	Tangential
Young's' Modulus (GPa)	17.9	10.8	9.1
Standard Deviation	1.57	0.934	0.99

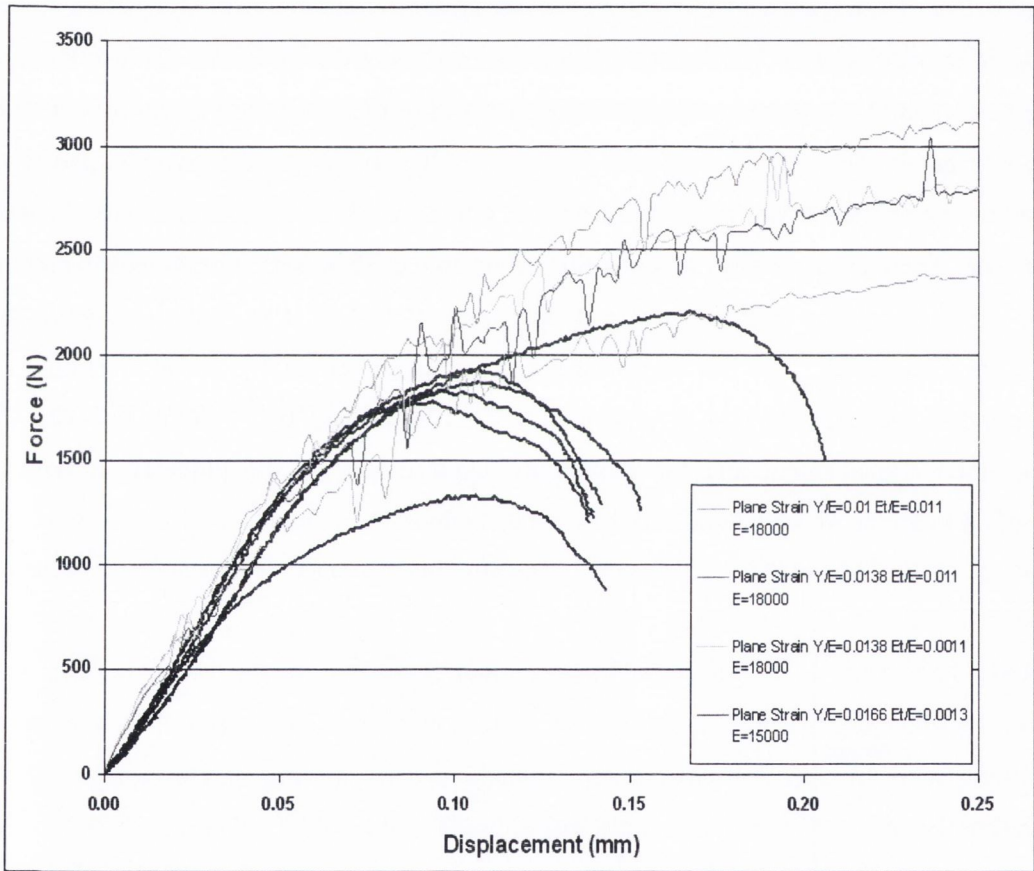


Figure 5-2. Force-displacement during indentation using blade 20° - $300\mu\text{m}$ to find the best model. It shows the force-displacement variation with Yield stress and tangential modulus and compare them with experimental results (darker curves).

5.4. Applying the TCD to Predict the Indentation Fracture Force

In chapter 3 we showed that the TCD is applicable to predict the brittle fracture of bone. Here we are going to predict the indentation fracture of bone using the TCD. As the TCD is applied on the critical line, finding the fracture line is the first step. The critical line can be defined by its origin and direction. These two characteristics are identified by the crack initiation point and the growth direction. There is not a general agreement made over the direction and beginning point of the main crack. In contact problems, tensile stress controls the fracture when usually the crack initiates from a point outside the contact area or at a distance from the contact zone below the indenter. The shear stress often has important effects when the crack starts at the contact surface or the compression area underneath the blade. This is due to the type of stress formed in the different zones during the indentation. Microstructure of bone also has an effect on its failure control. In most loading conditions, it has been seen that the crack tends to grow in the weakest possible direction. In addition, it is known that the shear strength of bone is much less than the tensile strength, especially in the longitudinal direction (tensile longitudinal strength, 135 MPa , shear strength, 65-71 MPa) [112].

In compact bone, the tangential direction, which is parallel to the osteons' orientation, is the weakest direction. Likewise, the longitudinal plane is weaker than the transverse plane. In the indentation problem, it is seen that no matter what the indenting direction is, the main crack grows in the weakest possible direction. The weakest direction depends on loading conditions and can be the tangential (in the case of tangential or transverse cutting) or longitudinal (for longitudinal cutting) as it was explained in chapter 4. After defining the crack initiation and critical plane, a defined fracture stress criterion is applied. Fracture force is predicted as the force which causes this criterion to be satisfied at the critical point. To apply the TCD to study the indentation problem, the unknown parameter, α , in equation 5-1 has to be calculated. The other parameter is the critical distance of bone. We will estimate the critical distance of the used bone (plexiform bone), however we believe that the critical distance is in the range of 0.3-0.4mm for many different types of bone as was shown,

in the previous chapter. This is another study to show that a critical distance in the above range can predict the fracture of bone. By assuming a value for the shear strength from the literature ($\tau_u=69\text{MPa}$) [112], two other parameters are therefore unknown: α and L . The value of α is obtained here and it is compared to the theoretical estimation which was found earlier ($\alpha=0.35$).

To estimate these two parameters, using equation 5-1, we require the experimental results of at least two different indenters. Experimental results of 20° - $300\mu\text{m}$ and 20° - $700\mu\text{m}$ indenters were employed. We also used the fact that the crack grows in the longitudinal direction for longitudinal indentation. According to the TCD, the stress acting on the critical plane has to pass through the critical point, therefore stress curves on the critical line against distance for two different indenters, have to meet each other at the critical point (equivalent critical stress, τ_u , and critical distance, $L/2$). Changing α will change the intersection of the two curves. Accordingly, α is changed such that the curves meet each other at the critical point. Consequently, α and the critical distance can be calculated using two groups of data. Appendix 2 contains some details of path defining in Ansys.

5.5. Longitudinal Indentation: Estimating α and L .

In this section, we look at two different indentations in the longitudinal direction to calculate the unknown parameters, α and L ; 20° - $300\mu\text{m}$ and 20° - $700\mu\text{m}$ indenters were thus selected. We have already estimated both parameters previously: we calculated α to be approximately 0.35 using known strength values for bone, and critical distance variances of between 0.3-0.4mm using brittle fracture predictions. The strength of the tested plexiform bones are not the same as that of osteonal bone, therefore α might be slightly different. L was estimated in chapter 3 for different type of bones. For indentation test bovine bone (plexiform) was employed which is different from the type of bone was used in the previous study (chapter 3).

First, we must look at some examples of the experimental results. Figure 5-3 and Figure 5-4 show force-indentation variation during indentation using 20° - $300\mu\text{m}$ and 20° - $700\mu\text{m}$ indenters, respectively. It can be seen that the force-indentation is almost linear for low forces and then it becomes nonlinear. Then, after a peak, the force decreases suddenly as a result of fracture. The average fracture force for these blades was $1892\pm 172(\text{N})$ and $2578\pm 156(\text{N})$ respectively. The statistical analysis shows strongly that these two fracture forces are significantly different ($p=0.001$). It means that the tip radius of the indenter has a large effect on the fracture force during longitudinal cutting.

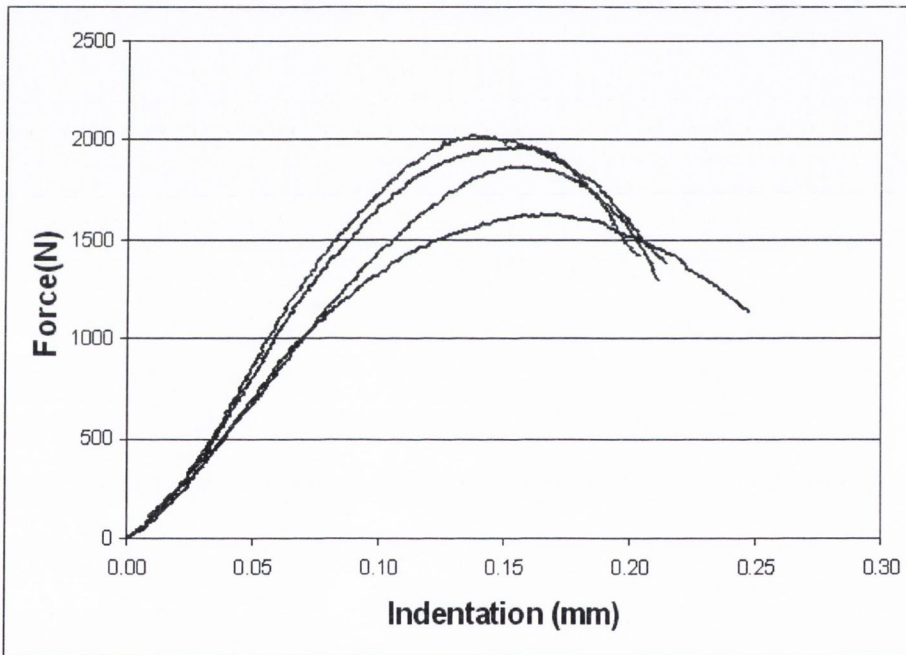


Figure 5-3. Experimental force-indentation in longitudinal direction using 20° - $300\mu\text{m}$ blade on four specimens.

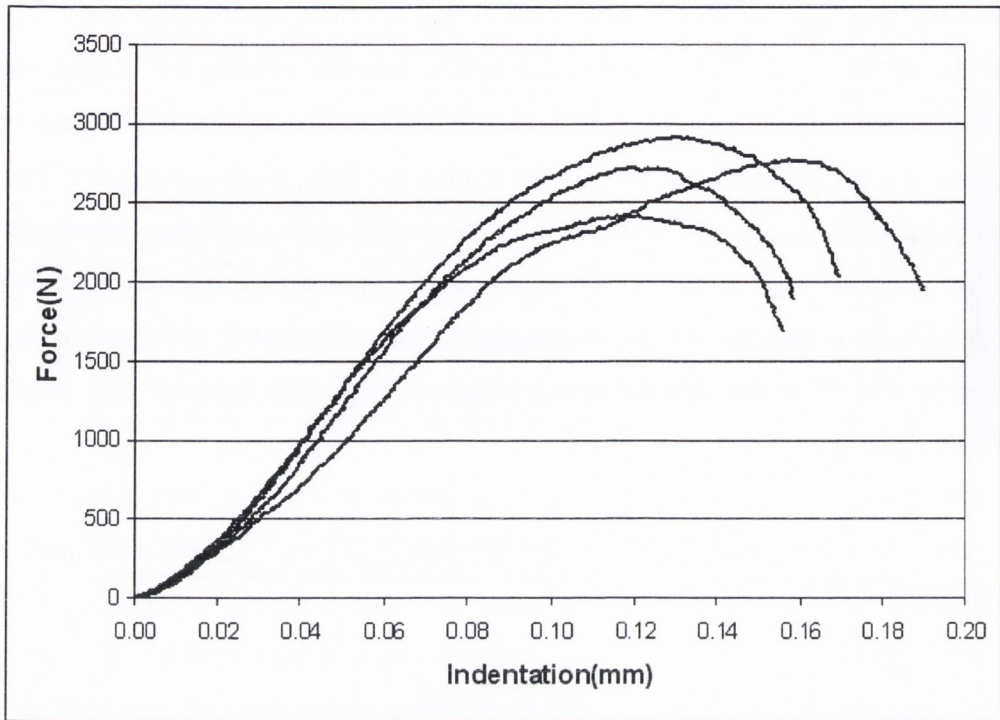


Figure 5-4. Force-indentation of longitudinal indentation using 20° - $700\mu\text{m}$ wedge performed on four different specimens.

Figure 5-5 shows a typical specimen after fracture. It is clear that the middle part of the specimen has separated and moved down. The cracks initiated at the surface of bone and then grew in the longitudinal direction, which is the weakest possible direction under stress in this case.

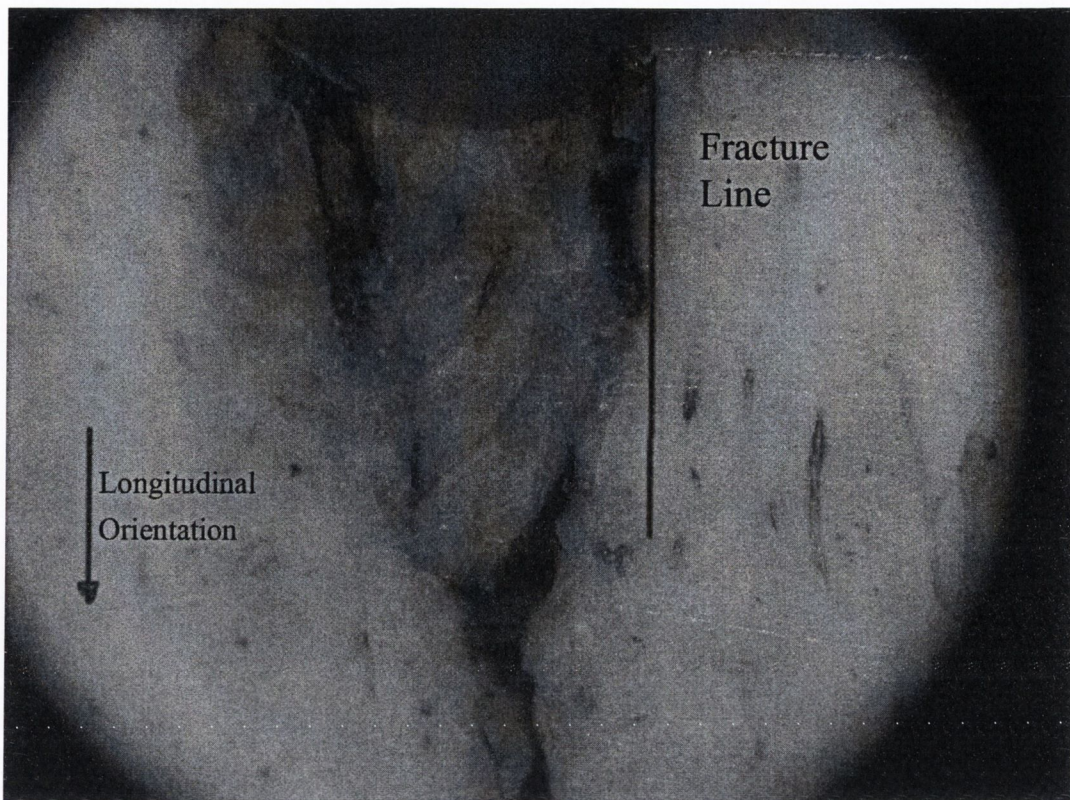


Figure 5-5. Inelastic deformation and crack direction during the longitudinal indentation. The fracture line is selected in the longitudinal orientation.

5.5.1. 20°-700 μ m Indenter

It has been shown that a boundary singularity point is a probable spot for crack initiation. Based on the experimental results, it was assumed that the critical plane (i.e. the crack growth plane) lies in the longitudinal direction. During the longitudinal indentation, the experimental results show that the main crack grows in the longitudinal direction and then deviated with an angle of about 30 degree. This divergence could be because of the shear lines. Figure5-6 shows the variation of shear and first principal stress on the contact surface for 20°-700 μ m indenter. It can be seen that stresses change significantly when the contact pressure drops to zero (we defined this previously as the boundary singularity). The normal stress is compressive at the contact area and turns to tensile stress out of the contact zone. The experiments show that the crack initiates in the contact area close to the boundary singularity. A fracture line, therefore, was defined as parallel to the longitudinal axis of bone starting from a boundary singularity.

The maximum contact pressure at fracture is about 530MPa. It is related to the blade geometry and fracture load.

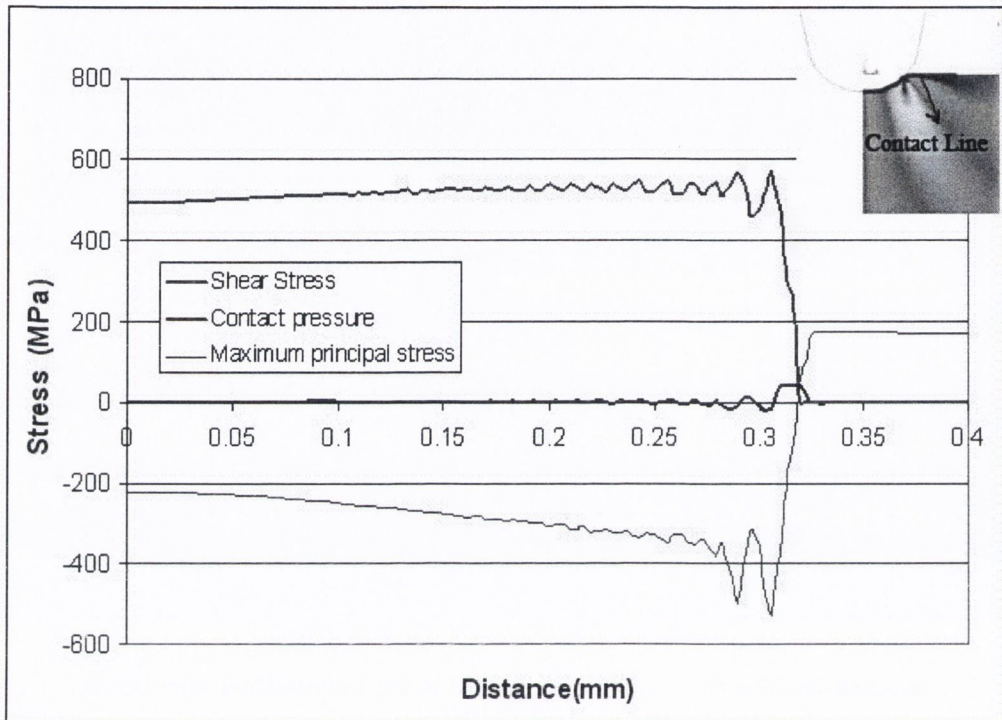


Figure5-6. Distribution of shear stress, tensile stress and the contact pressure on the contact surface for 20° -700 μ m indenter at the fracture force in longitudinal indentation.

The contact pressure drops at the contact boundary. The tensile stress changes from compression to tension at the boundary. The shear stress is zero on the contact surface because of lack of friction but it changes at the boundary as a result of significant change in tensile stress.

The contour of shear stress around the indenter tip can be seen in Figure 5-7. It also shows contact and fracture lines. Fracture line is along the longitudinal direction of bone which is the same direction as indentation. The figure also shows that the maximum shear stress does not happen on contact surface, rather takes place at a distance from that point. This maximum shear stress is beneath the surface contact at the boundary singularity. Figure 5-8 shows distribution of maximum normal stress underneath the indenter tip at fracture force for the same indenter. It shows that maximum tensile stress is mostly distributed outside of the contact area. The part of the bone which is in contact with the indenter is under high compression. The size of this

zone strongly depends on the indenter radius and applied force. For a given force, the larger the indenter radius, the larger the compressive zone. It also shows that the fracture plane is under high compression.

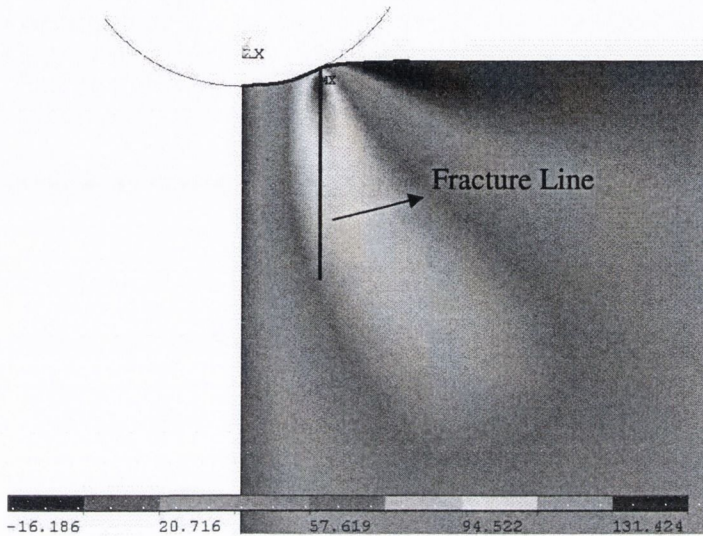


Figure 5-7. Contours of shear stress and fracture line for 20° -700 μm indenter at fracture force. The maximum shear stress occurs beneath the indenter at a distance from the boundary of contact

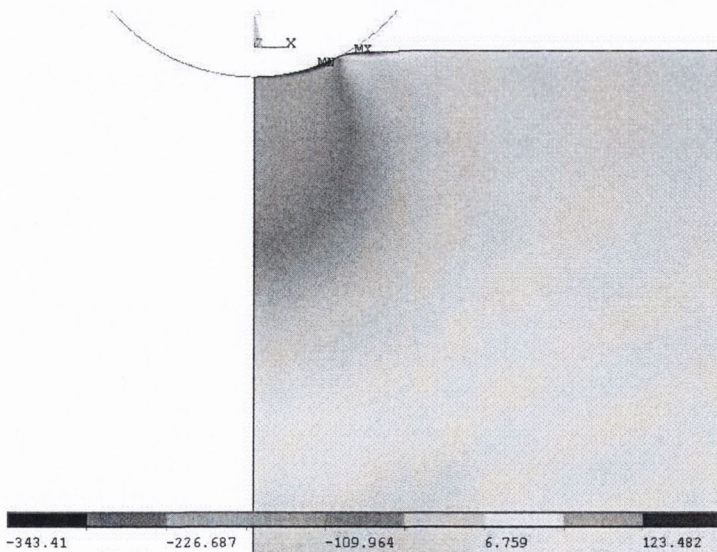


Figure 5-8. First principal stress at the fracture force for 20° -700 μm indenter. The stress beneath the indenter is extremely compressive. There is a small tensile zone on the surface.

Figure 5-9 shows the variation of shear and normal stress on the fracture line for longitudinal indentation with the 20° -700 μm indenter at the fracture force. It demonstrates that on the fracture line material is under a high level of compression. Shear stress on this line is higher than the shear strength of bone. This is possibly due to the frictional resistance of microcracks to sliding. It is also in agreement with equation 5-1, as a higher shear stress is required for failure in the presence of compression. As it can be seen, the shear stress increases over a small distance and then decreases gradually. The peak in the stress curve is due to the fact that the maximum stress occurs at a distance from the contact surface. In this case the angle of the indenter does not play any role in the stress distribution, as will be discussed further below.

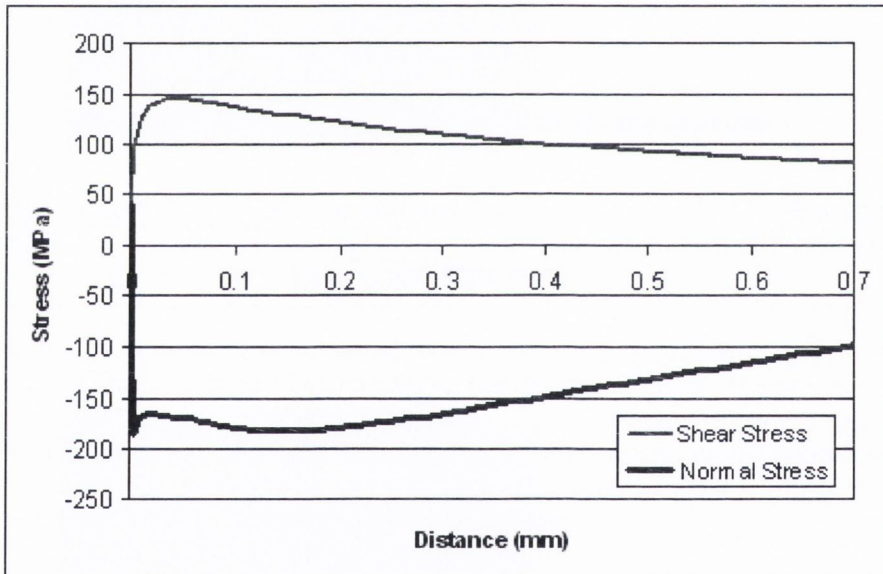


Figure 5-9. Variation of normal stress and shear stress on the critical line for 20° -700 μm indenter at the fracture force. The compressive stress is acting on the fracture line therefore a higher shear stress than the ultimate shear stress (69MPa) is required for failure.

5.5.2. 20°-300 μ m Indenter

The 20°-300 μ m indenter is quite blunt, therefore the contact area and compression zone are large. In some materials, however, microcracks do not form in the compression zone [27, 22, 31, 23, 25] but experiments on bone have shown that there are diffuse cracks in the compression zone beneath the indenter. The area on the bottom part of bone is also compressed because of the constrained conditions on the sides and bottom part of bone. There is a large tensile zone between the two compressive areas. The tensile stress in this area decreases from the centre (under the indenter) to the sides. The tensile stress in this zone, however, is not enough to cause fracture, but it is a probable zone to initiate and grow microcracks, yet no micro-cracks have been seen in this region.

Figure 5-10 shows the contact pressure and stress distribution on the contact area. It can be seen that stresses at the boundary change significantly. This graph also confirms that the angle of the indenter is not expected to have any effect on the fracture force for this blade, as there is only one singularity on the stress distribution. The average contact pressure is just over 600MPa at the fracture force, which is less than the blunter indenter (20-700). It can be said that for blunter indenters, less contact pressure is required for fracture.

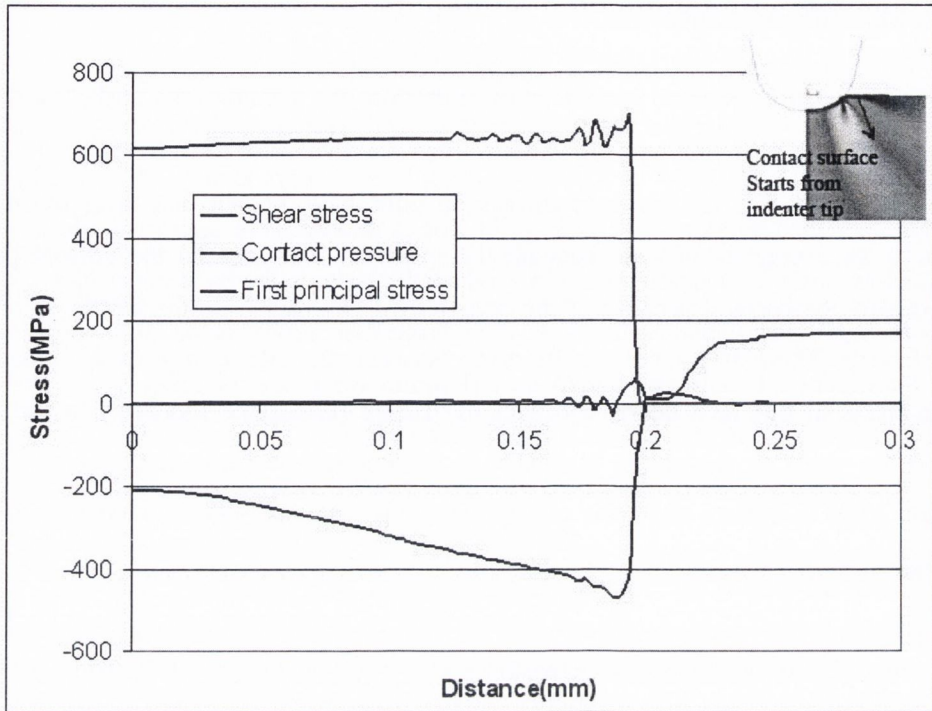


Figure 5-10. Variation of maximum tensile, shear stress and contact pressure on the contact surface for 20°-300 μ m indenter at fracture force.

Figure 5-11 and Figure 5-12 describe the distribution of shear and tensile stress beneath the blade. It is almost the same as the 20°-700 μ m indenter because there is only one type of singularity involved.

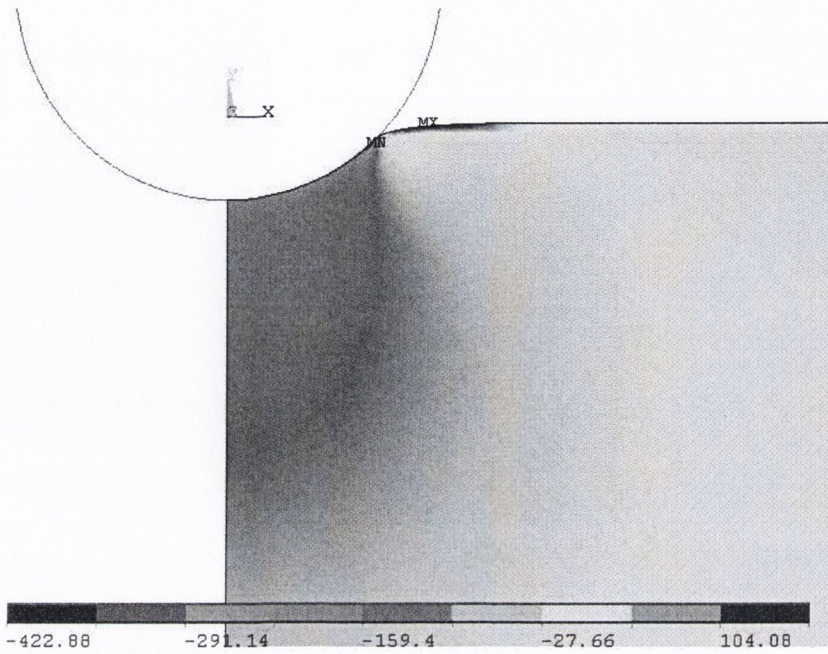


Figure 5-11. Maximum tensile stress under the 20°-300μm indenter at fracture force

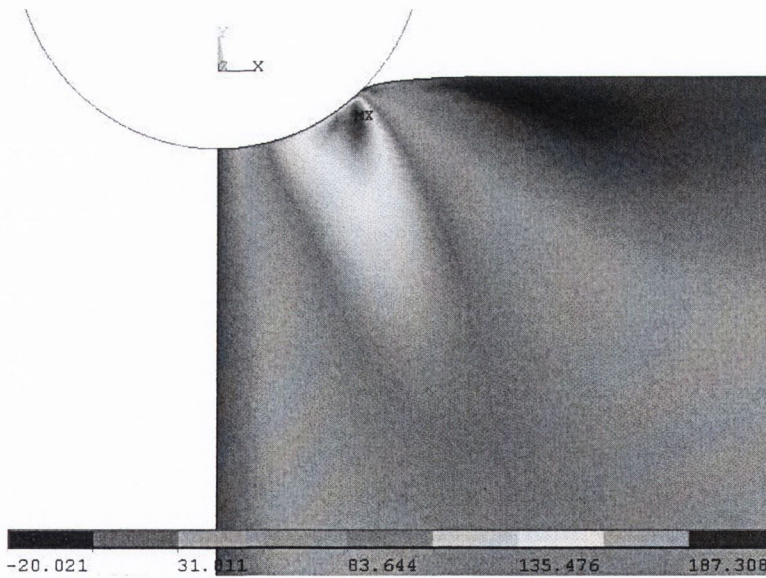


Figure 5-12. Shear stress distribution under the 20°-300μm indenter

5.6. Estimating α and L

Now the two unknown parameters are estimated using the stress distributions on the fracture line and equation 5-1 by means of the stress-distance curve on the critical line and using the fracture criterion described above. Stress-distance curves are shown in Figure 5-13 for these two indenters at fracture force. By using the trial and error method, the value of α was estimated to be 0.3 when two curves meet each other at $\tau_v=73\text{MPa}$. Since the two curves have to meet at the critical point, then the distance on the x-axis equals $L/2$ which is 0.16mm, therefore $L=0.32\text{mm}$ which is in the range of the critical distances calculated in previous chapter. This value of critical distance will therefore be employed to predict the fracture force for other indenters. Indenters with different angles of 20° , 40° and 70° and different radii of 50 , 300 and $700\mu\text{m}$ were chosen to investigate the effects of the angle and radius on the fracture force. It has been seen that for large radii of $300\mu\text{m}$ and $700\mu\text{m}$ the angle does not have any effect on fracture force because the amount of indentation before fracture is small, therefore the only part of the indenter, which is in contact with material just before fracture, is the curved part near the tip. For sharper blades, like the $50\mu\text{m}$ blade, the angle will have an effect on the fracture force.

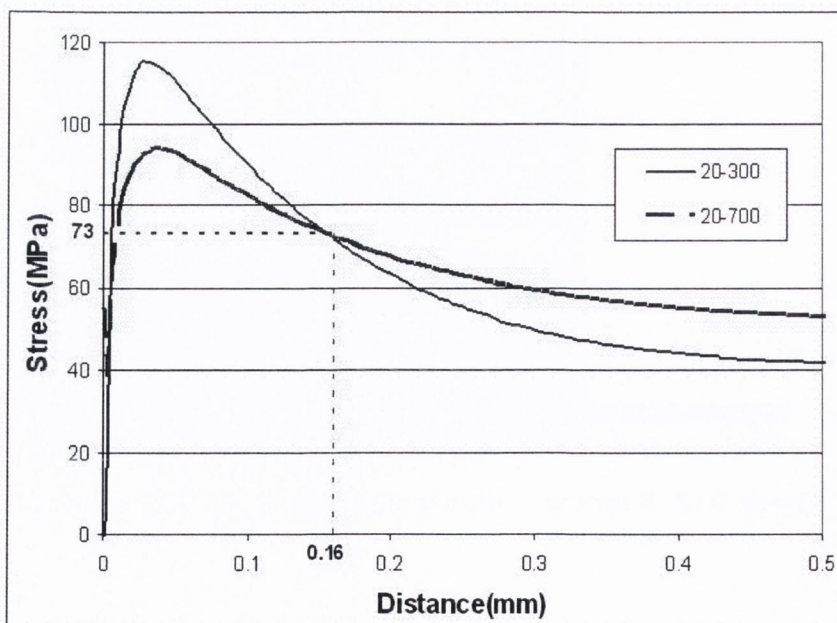


Figure 5-13. Fracture stress ($\sigma + \alpha\tau$) on the fracture line for two different blades when $\alpha=0.3$. The critical distance found to be 0.32mm.

5.7. Sharp Blades

From the singularity point of view, the 50 μm blades are different from the blunter ones (300 and 700 μm). In this case, the geometric singularities are in contact with the material at fracture, therefore there are two high gradient pressures on the contact surface. It is obvious in Figure 5-14 that the geometric singularity changes the pressure and stress distribution as the radius of the blade curve changes from 50 μm to infinite (along the side of the blade). Normal stress around the geometric singularity is tensile while that is compressive close to the boundary one (Figure 5-15). We saw in the previous chapter that in most cases of using sharp blades the crack initiates at a spot close to the boundary singularity.

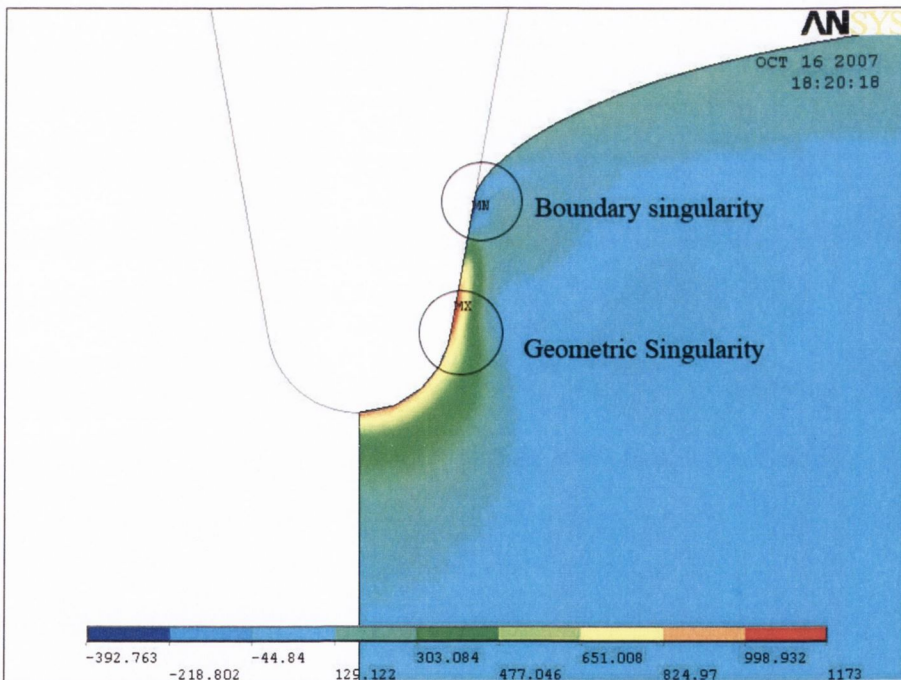


Figure 5-14. Contours of maximum principal stress around the indenter tip for 20°-50 μm blade. It shows the effects of different singularities on the stress distribution.

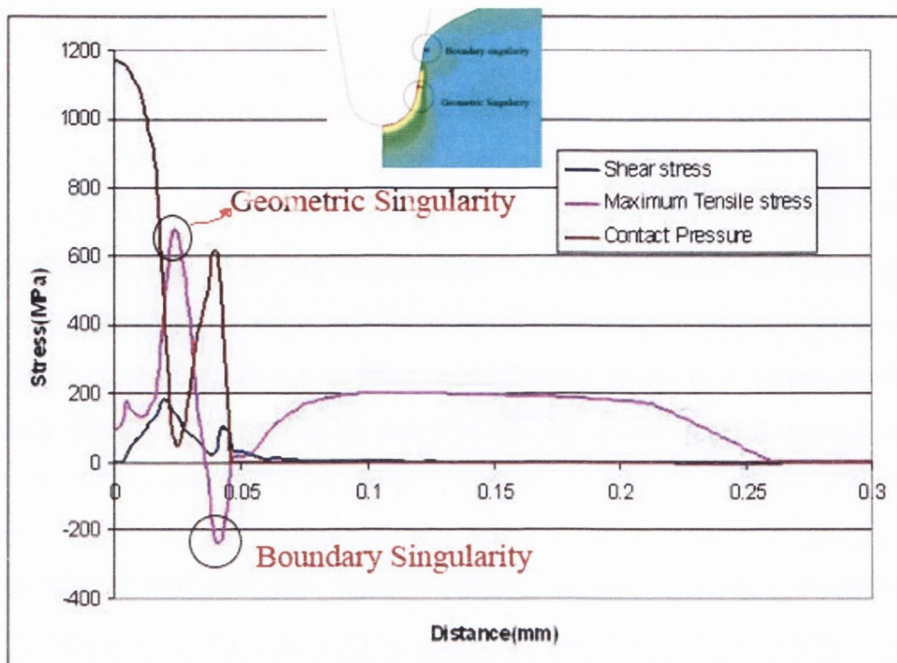


Figure 5-15. Stress variation along the contact line at the fracture force for 20°-50 μ m indenter at fracture force. Stress distribution is affected by two kinds of singularities

The TCD was used to find the crack initiation point. A force of 1024N, which was obtained from the average experimental fracture force, was applied to the model. It is assumed that the fracture line is in the longitudinal orientation, as with the previous tests. The crack initiation point was changed to find the point at which minimum fracture force is required. For each fracture line, the stress at the critical distance was recorded as σ_r . Defining σ_{max} as the maximum stress amongst them; a stress ratio is defined as: σ_r / σ_{max} , this ratio can be used to get the idea of the probability of a crack initiation at each point. Figure 5-16 shows this stress ratio versus different crack initiation points. The first point (labeled 0) is the indenter tip which bears the maximum contact pressure. The stress ratio is just over 4 at this point, implying that, if the equivalent stress increases linearly, the force required to initiate the fracture at this point is 4 times more than the minimum required force. In other words, if we assume that bone is homogenous material, it is almost impossible that the crack starts from the indenter tip. The second point shows the geometric singularity; even though the predicted fracture force for this point is much less than the indenter tip there is still a significant difference between that and the minimum fracture force. The minimum

fracture force was predicted for the boundary singularity. For the last point it is assumed that the crack starts from the tensile area out of the contact surface. The TCD predict a high required force for this point. The graph shows that the points around the boundary singularity are probable locations for crack initiation in longitudinal indentation.

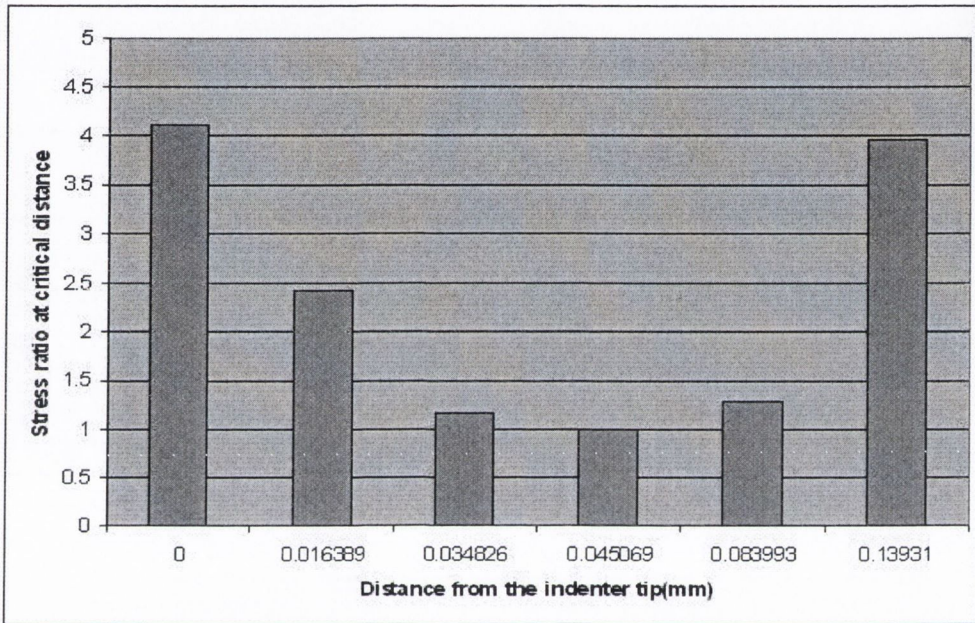


Figure 5-16. The stress ratio for different crack initiation points, defined by distance from the indenter tip, for 20° - $50\mu\text{m}$ indenter. The second and the fourth points are located at the geometric and boundary singularity respectively.

This is another view of critical distances theory. Figure 5-17 shows the contour of the critical stress ahead of a crack. The size of the zone depends on the applied force. The higher the force, the larger the critical zone. The critical distance theory says that, the fracture happens if the zone size grows until the diameter in the certain direction (critical plane direction) reaches the critical distance. In the case of sharp cracks, it is assumed that the crack propagates at the tip of the crack. In some problems, like the indentation of bone, we know that the crack direction, which defines the direction of the critical plane but the crack initiation, is unknown. In this case, we can assume different critical line with different start point. In fact, all the critical lines are parallel. By

increasing the load, the critical zone is growing, until the diameter in one of the critical lines reaches the critical distance. This critical line can define the crack initiation.

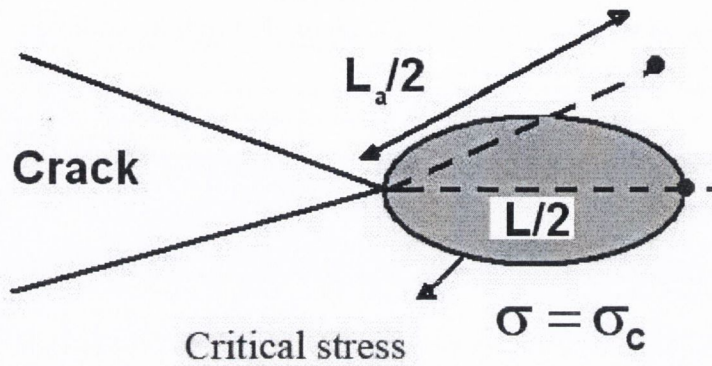


Figure 5-17. Contour of critical stress at the crack tip with two different critical plane directions. The critical stress contour is growing with increasing the applied stress. The crack propagates if the critical stress contour reaches the critical distance in a certain direction

5.8. Prediction of the Fracture Force

Indentation fracture load was predicted using the estimated critical distance and α values as derived above. Predictions have been done for different blades with various angles and radii. Figure 5-18 shows the stress-distance curve of longitudinal indentation for different indenters. For sharper blades, there are both types of singularities which cause a complex stress field close to the indenter tip. It can be seen in the graph that for small distances from the indenter the stress changes unevenly. In fact, the tensile stress around the geometric singular point affects the stress on the fracture line drawn from the boundary singular point, therefore fracture force decreases significantly due to the presence of the geometric singularity, especially when the angle is smaller.

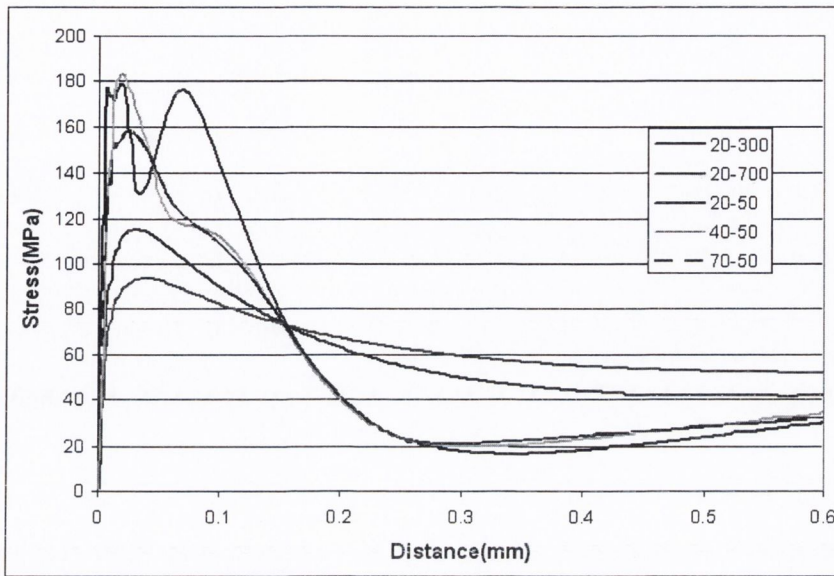


Figure 5-18. Predicted fracture force for different indenters in longitudinal indentation was found by assuming that the stress-distance curves at fracture force for each indenters passes through the critical point, as shown here.

Table 1 shows the predicted fracture force using the TCD for different indenters. It shows strong predictions of the experimental data for different angles and radii: these results will be discussed in detail below.

Table 5-2: Predicted longitudinal fracture load using the TCD for different indenters (prediction error percentage). There is no experimental data for 60°-50 μ m blade to compare with the prediction.

Radius \ Angle	50(μ m)	300(μ m)	700(μ m)
20°	921(-10%)	2100(11%)	2700(4.7%)
40°	1033(-15%)	2100(2.5%)	2700(12.2%)
60°	1230	2100(3.9%)	2700(4.7%)

5.9. Effects of Geometry on Fracture Force

Longitudinal fracture forces for indenters with an angle of 20° with different radii are shown in Figure 5-19. It demonstrates that the predictions using TCD agree

with experiments for all radii studied. Experimental results show that the larger the radius, the higher the indentation fracture force. The fracture force is reduced gradually when the radius of the indenter decreases from $700\mu\text{m}$ to $300\mu\text{m}$ and more steeply when the radius is reduced to $50\mu\text{m}$. In terms of singularities, it can be explained why the fracture force is smaller for the smaller radii. In fact, as it is mentioned earlier for large radii, the sides of the indenter are not in contact with the bone (for angles less than a certain value) before fracture. This means that the boundary singularity is the only singularity in the problem. By decreasing the radius, such as the deformation before fracture is larger than the radius, geometric singularities will appear before fracture. The stress field around the geometric singular points is tensile. This tensile stress affects compression stress in the vicinity of boundary singularity and causes a reduction in the compression stress acting on the critical line. The lower the compression stress the lower the shear stress required for fracture. By increasing the angle at the small radius, the distance between the boundary and geometric singularities increases. This reduces the effect of tensile stress at the geometric singularity on the compression around the boundary of contact. This means that by increasing the angle, the fracture force will increase slightly, as will be discussed below.

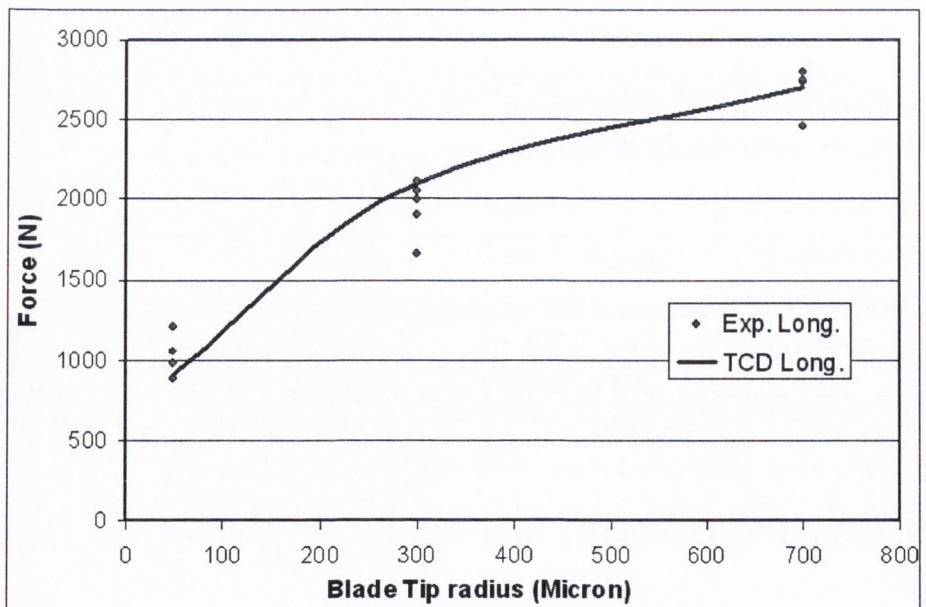


Figure 5-19. Experimental results and TCD predictions of longitudinal indentation force for blades with 20° angle and various radii

For a given angle, there is a certain value that for larger radius, the angle has no effect on fracture force. We call this radius the critical radius for the specific angle used, and which also depends on the blade and specimen properties, as well as indentation conditions. The critical radius is estimated to be about 200 μm in the present case when the angle is 20°. To obtain a better estimation more experimental data is required. The critical radius can be a good parameter to verify the model and can also be used to define whether an indenter is sharp or blunt.

Table 1 (which was shown earlier) demonstrates that the wedge angle does not affect fracture force for indenters with radius larger than 300 μm . however the angle for sharper indenters has a large effect on fracture force. Indentation fracture force of 50 μm indenter increases from 921N to 1230N when the angle changes from 20° to 60°. The experimental results show that the effect of the angle for small radius is statistically significant ($p=0.049$ when comparing 20°-50 μm and 40°-50 μm). In these cases, variation in fracture force is the result of the geometric singularity.

For a given radius, the critical angle is the minimum angle which affects the fracture indentation force. The larger the radius, the larger the critical angle. The defined critical angle and critical radius can be used to identify the sharpness of the blade. For indenter angles larger than the critical angle, it is obvious that the larger the angle, the larger the horizontal component of applied force.

The critical angle can be estimated for blunt indenters. For example, for a 300 μm indenter, the amount of indentation before failure has to be more than the vertical distance between the geometric singularity and indenter tip (I_f). If R and θ_c are radius and the critical angle of an indenter then at the critical angle we will have:

$$R(1 - \sin(\theta_c / 2)) = I_f$$

The amount of indentation for 20°-300 μ m blade was found to be about 0.1mm, then: $\theta_c = 83.6^\circ$ which is much higher than 70° . This critical angle for indenters with radius of 0.7mm was estimated about 120° .

Figure 5-20 shows the effect of the indenter wedge angle on fracture force for three different radii.

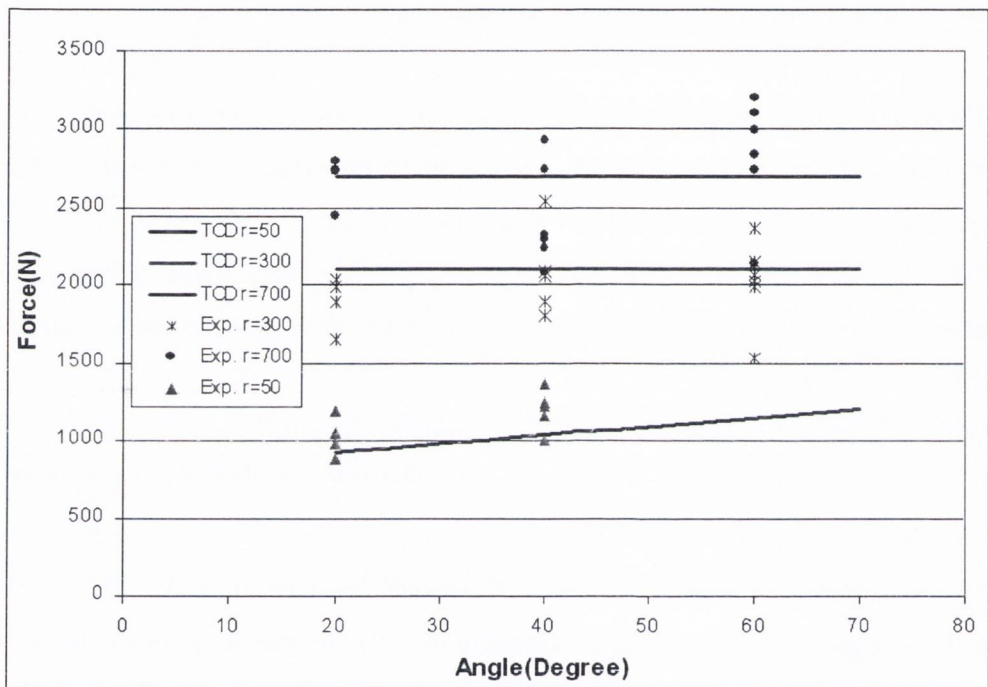


Figure 5-20. Effect of indenter angle on fracture force for longitudinal indentation. TCD prediction and experimental results.

5.10. Transverse Indentation

Predictions have also been made for the transverse indentation using the TCD. Fracture in this direction is different from that in longitudinal and tangential. In transverse indentation a crack starts and grows perpendicular to the indentation direction which is in the tangential plane. In other words, experiments show that the main crack grows in the weakest orientation independent of the indentation direction. As a result, part of the bone is chipped off (Figure 5-21). The fracture line, therefore,

starts from somewhere on the contact surface along the tangential plane, as is shown in figure 5-22. In this case, shear and compressive stresses are acting on the fracture line. The shear stress required for failure is higher than the ultimate shear strength of bone due to the compressive stress acting on the fracture line. There is more indentation before fracture in the transverse direction than in the longitudinal. While in general we could expect that L could have different values in different directions, in practice we found in this case that L has the same value.

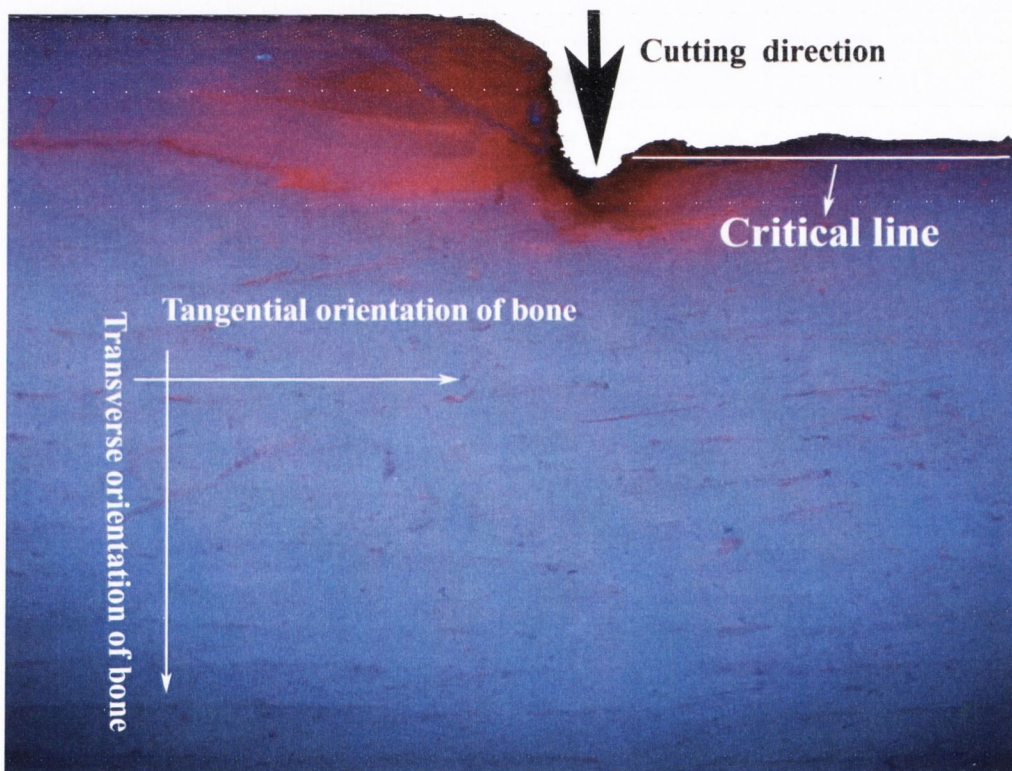


Figure 5-21. Critical line for transverse indentation. The photo shows a sample just after the maximum cutting force. Part of the bone has removed due to the crack growth in the tangential plane.

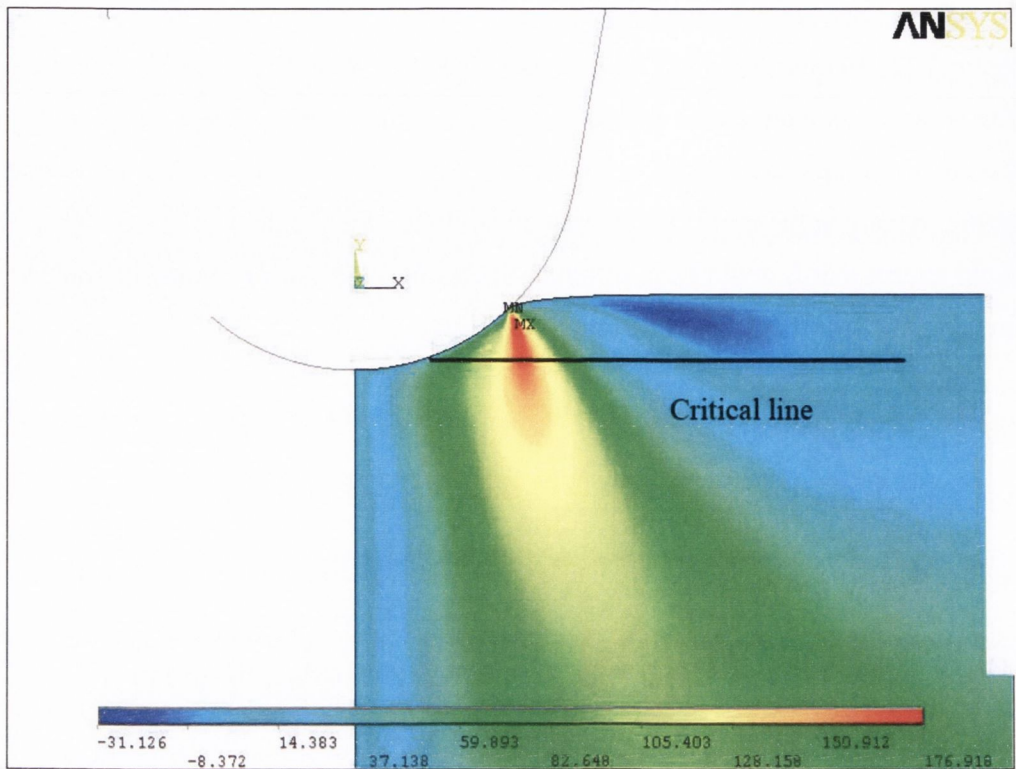


Figure 5-22. Fracture line in the transverse indentation. The main crack grows in the tangential direction which is the weakest structural direction of bone

Figure 5-23 shows the variation of force versus displacement during indentation for the 20° - $50\mu\text{m}$ blade. It demonstrates that indentation force increases approximately linearly with the displacement of indenter. During this process microcracks are formed, as will be discussed in detail in the next chapter. The force rises until the required conditions for fracture occur, when the main crack grows in a tangential direction, as it was shown in Figure 5-21. It is at time that a piece of material is removed, therefore the force decreases sharply. If the process is continued, the force increases again and reaches a maximum, when another part of material is chipped off. The second peak force is less than the first fracture force. This process continues with further cutting, but in this section we are going to predict only the first maximum point in the force-displacement curve.

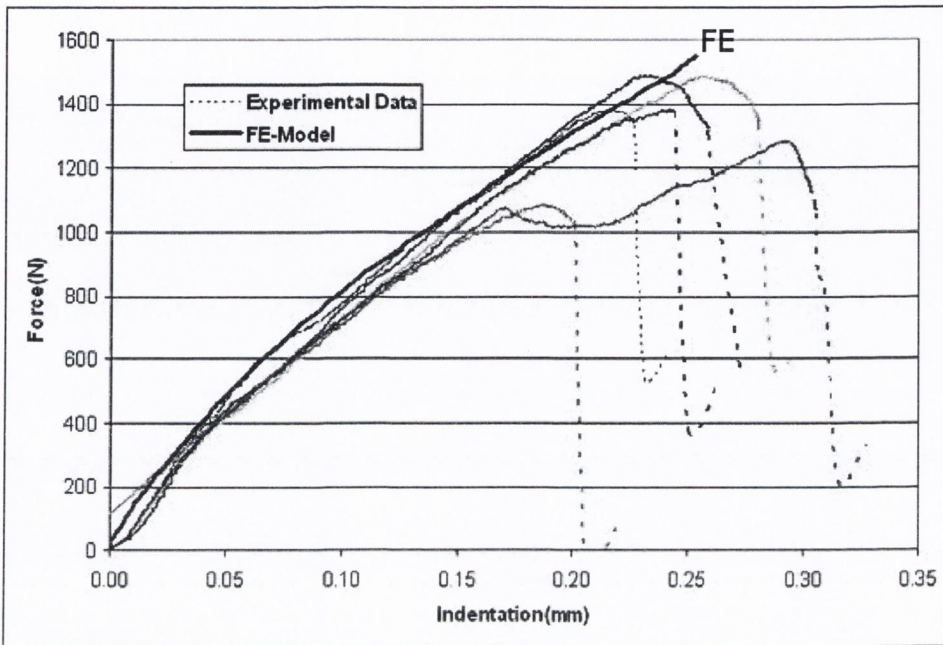


Figure 5-23. Finite element model verification with the experimental data for 20-50 blade in transverse direction

Figure 5-23 also compares the experimental results with the FE simulation. It is clear that the FE model can predict the force displacement well. The FE predicts a roughly linear relationship between the force and indentation before the fracture, however it demonstrates a small decrease in compliance of bone with increasing force. The objective is to find the point on this curve when the fracture happens.

Figure 5-21 was taken after indentation. It does not explain the relative situation of the blade and indenter at the time of fracture. Answering this question is important to find the crack initiation spot. The process was recorded for all blades. The camera was placed to record the images in the front face of the specimen. Figure 5-24 was taken from the video when the fracture occurs. In this figure the position of the crack line with respect to the indenter is obvious. It shows that for very sharp blades the crack initiates -if it is not exactly at the blade tip- from somewhere around the indenter tip which is different from the case of longitudinal indentation. The contact

boundary on the other side of the blade which did not fracture shows sink-in (i.e. downwards displacement) of bone under indentation.

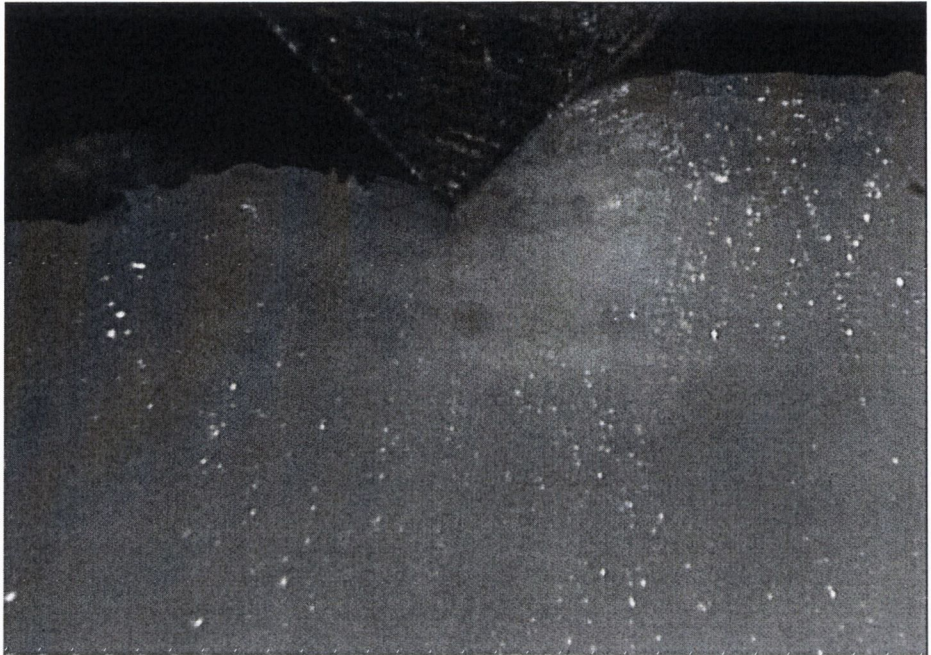


Figure 5-24. Fracture plane in transverse direction for sharp blade; photo taken just after fracture of the first piece of bone (from the left hand side).

To model the bone material, the Young's modulus was assumed to be the same as the experimental results obtained experimentally (10 GPa). The yield stress and post-yield tangent modulus, therefore, were calculated to be, 100 MPa and 1000 MPa to give the best fit for load displacement. These material properties can predict the force-displacement curves as it was seen in Figure 5-23 for 20°-50 μ m indenter.

Looking at stress distribution on the contact surface it shows a change in stress status at contact boundary (Figure 5-25). The most compressive principal stress (S_3) has the same pattern as contact pressure. It increases gradually along the contact area and drops at the contact boundary. Contact pressure is highly dependant on the geometry of indenter as well as the material properties of bone. The stress on the contact surface is highly compressive and turns to a tensile stress outside this area. Shear stress is zero on the contact surface as the result of the frictionless contact

conditions. First and second principal stresses follow the same pattern as the third principal stress with different extremum points. It was assumed that the critical line is in the direction perpendicular to the indentation while the initiation location has not been defined yet. To find this location it was used the same approach as described above for longitudinal indentation: we looked at the equivalent stress on different lines with different beginning points (Figure 5-26). These points were picked between the indenter tip and contact boundary. The line which predicts the minimum fracture load is the critical line.

Figure 5-27 shows the fracture force ratio for different lines. It is defined by the ratio between the maximum stress at the critical distance and the stress at the critical distance for each line. It demonstrates that the 3rd principal stress peak point is the most probable point for crack propagation, however there is not much difference between that point and the indenter tip but it has to be noted that at the tip of indenter- especially for blunt indenters- the equivalent stress is negative at the critical distance (0.16mm).

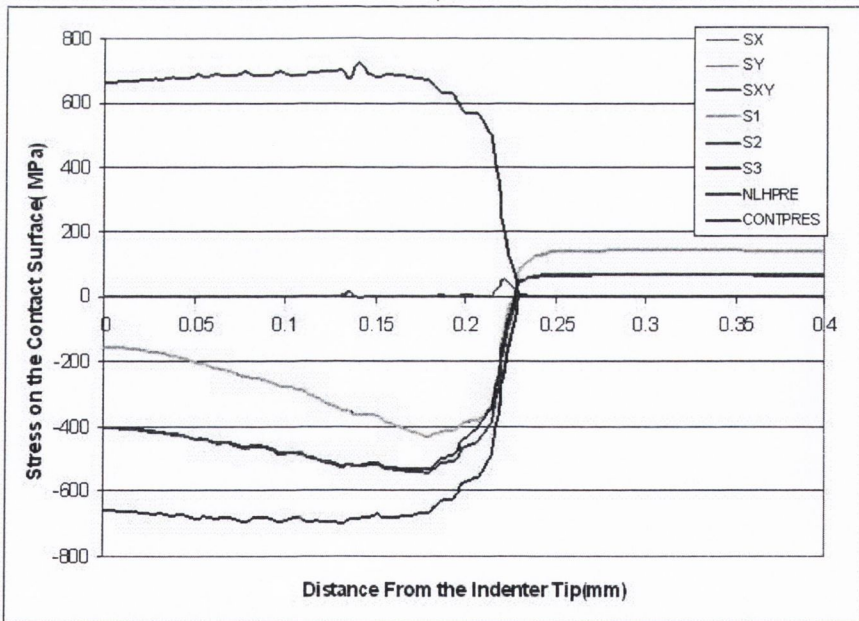


Figure 5-25. Stress on the contact surface of transversal indentation using 20°-300µm indenter

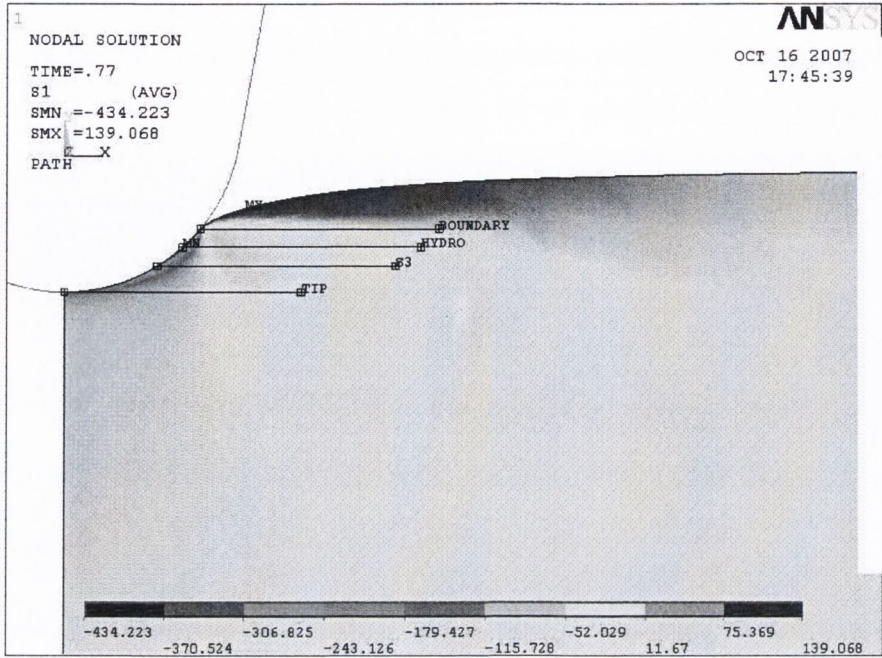


Figure 5-26. Possible critical lines for different crack initiation points (Transversal Indentation) the lines started from different points: the tip of the indenter, the largest compressive stress spot, an optional point and the boundary of contact

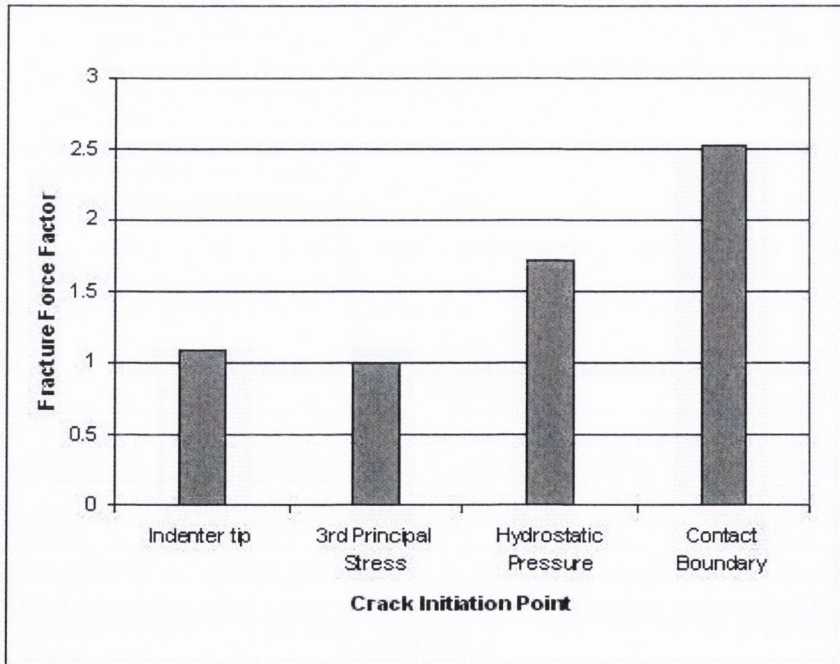


Figure 5-27. Fracture force factor for 20°-300µm indenter in transversal direction

A crack initiation point based on the compressive stress can be defined. Studying a sharper indenter like the 20° - $50\mu\text{m}$ can confirm this. Figure 5-28 shows that in this case the indenter tip is predicted as the location giving the minimum fracture force. It means that this point can be defined as the crack initiation point. Figure 5-29 and Figure 5-30 present the distribution of the principal stresses around the indenter. It can be seen that the first principal stress changes from compression to tension when the contact pressure varies due to the disparity in contact geometry. The stress at the indenter tip is compressive and the third principal stress is minimum. This is in agreement with the predictions for the 20° - $300\mu\text{m}$ indenter and also as it was observed experimentally it is close to the main crack initiation point.

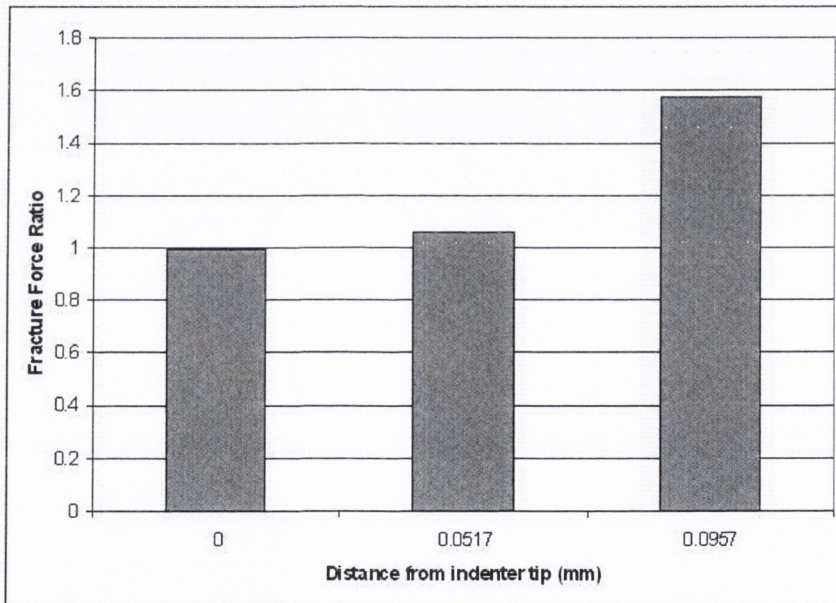


Figure 5-28. Fracture force factor for transversal indentation using 20° - $50\mu\text{m}$ indenter. The three points show the indenter tip, the geometric and the boundary singularities respectively.

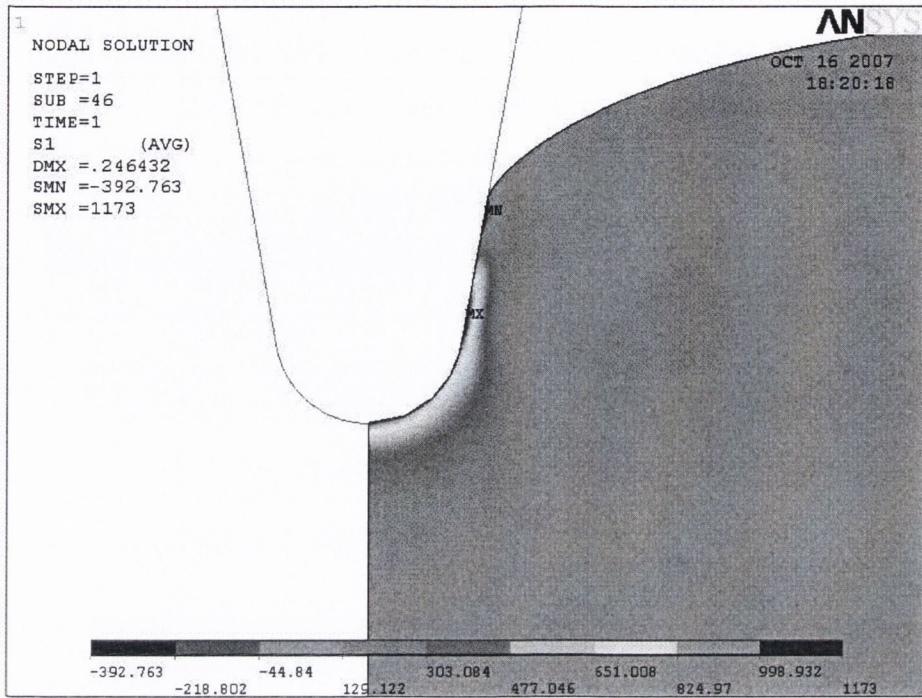


Figure 5-29. First Principal stress distribution of transverse indentation around the 20°-50µm indenter

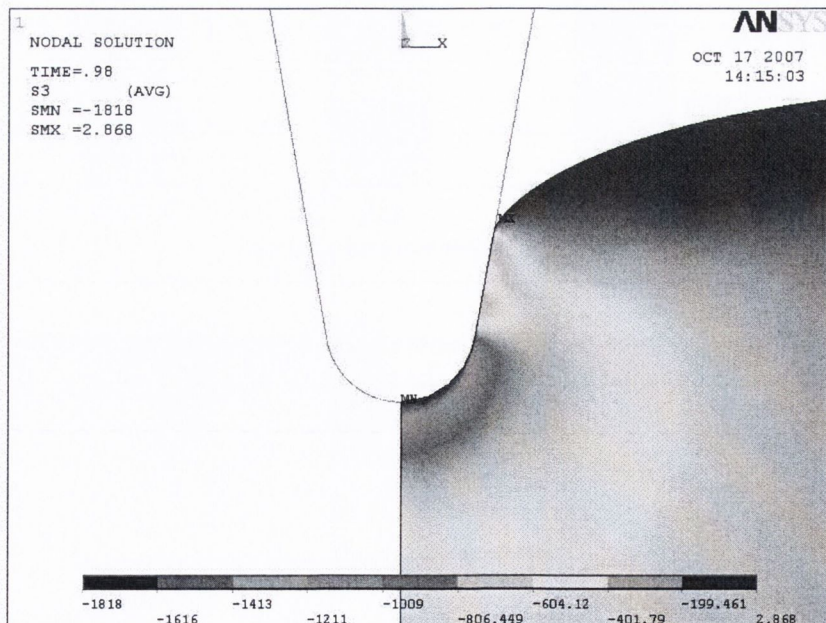


Figure 5-30. 3rd Principal stress around the indenter of transverse direction for 20°-50µm blade

In the case of transverse indentation, the main crack propagates from the location of the largest compressive principal stress. This crack initiation point is used to predict the fracture force. Predictions have been performed for other experiments in this direction. Table 5-3 shows the predicted value and prediction error in each case. It can be seen that for the transverse direction, the critical angle for 300 μm blades is between 40° and 60°. The critical angle for 700 μm indenter is over 100° but for 50 μm blade is zero. It means that the angle will affect the indentation fracture force when the radius is 50 μm .

Table 5-3: Transverse indentation fracture force for different indenters and the difference between average experimental results and FE predictions

Radius \ Angle	50(μm)	300(μm)	700(μm)
20°	1470(5.9%)	2460(-2.2%)	3700(-2.4%)
40°	1910(1.8%)	2460(-1.4%)	3700 (-7%)
60°	1980(-19%)	2860(1.4%)	3700(-13.4%)

Figure 5-31, Figure 5-32 and Figure 5-33 compare experimental results and predictions using the TCD. Each figure is for indenters with the same angle and various radii.

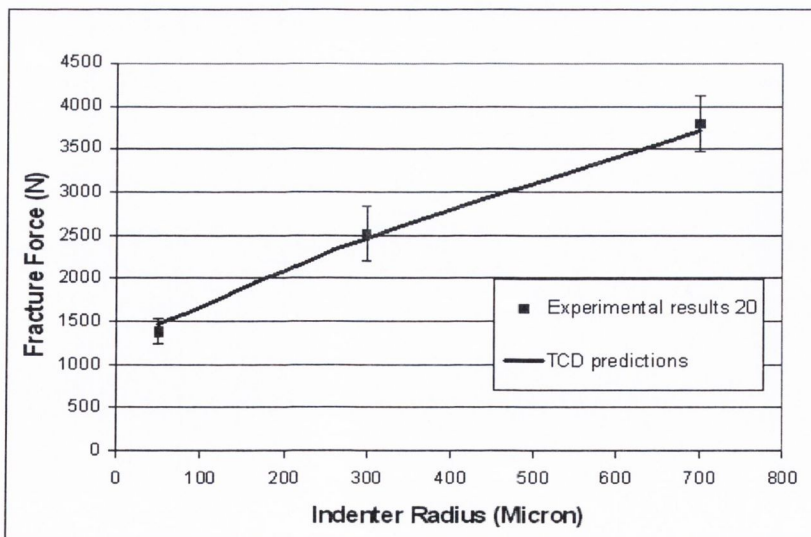


Figure 5-31. Transverse indentation fracture force for 20° indenter. Experimental vs TCD prediction. Error bars show standard deviation: dotted lines show maximum and minimum experimental values

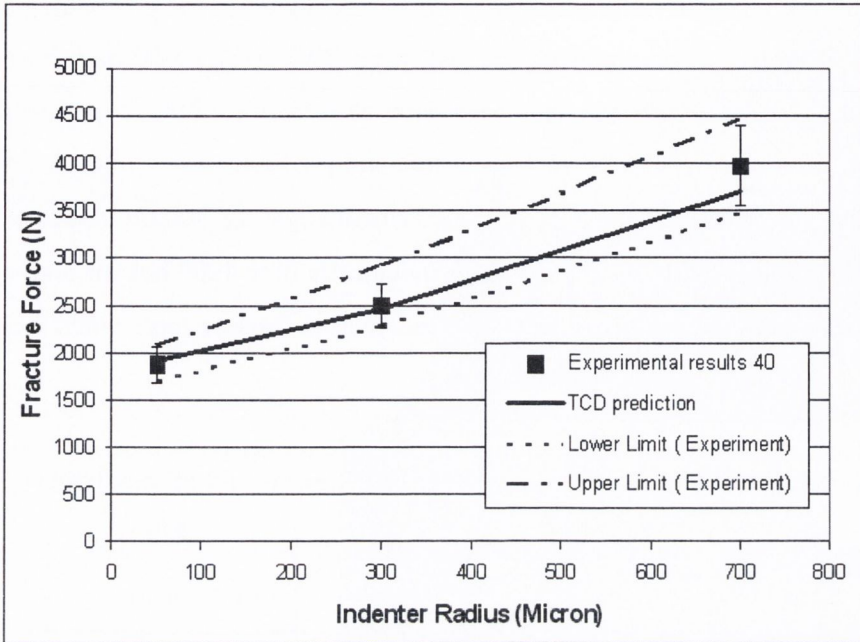


Figure 5-32. Transverse indentation fracture force for 40° indenter. It compares the predictions using the TCD and the experimental results. The indentation fracture force increases with radius. Error bars show standard deviation: dotted lines show maximum and minimum experimental values

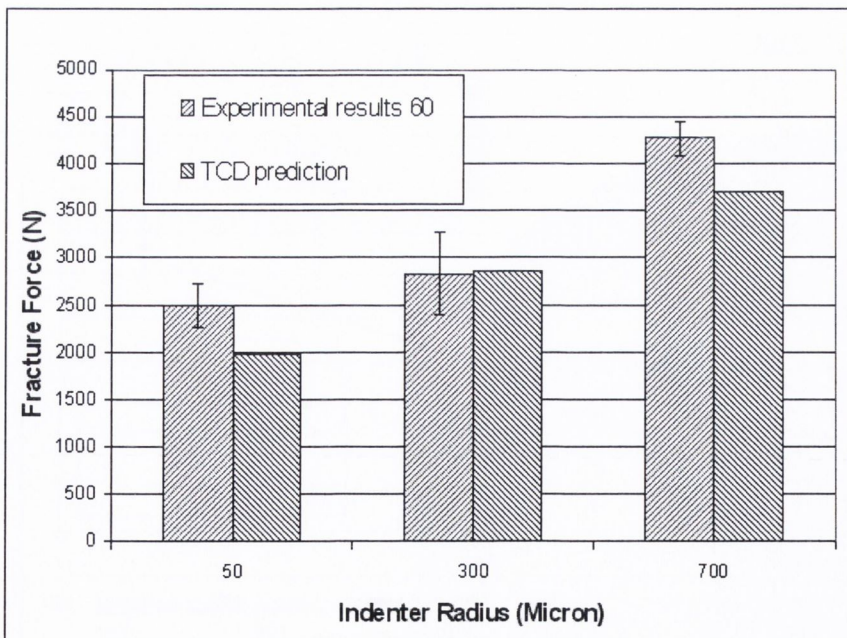


Figure 5-33. Transverse indentation fracture force for 60° indenters and different tip radius. Experimental results vs TCD predictions.

The predictions for 20° and 40° indenters agree with the experimental results. Looking at the fracture force against angle explains the variation of fracture force with angle. Figure 5-34 and Figure 5-35 show the effects of wedge angle on fracture force. This shows that for smaller radius the angle has more effect on fracture force. For example, for 50µm blades when the radius changes from 20° to 40° the fracture force changes markedly from 1388N to 1876N. The predictions and the experiments are somewhat different for the 60-50 indenter, but even here the greatest prediction error is only 20%. The prediction as it was expected, estimates a higher fracture force in transverse than longitudinal indentation for a given indenter.

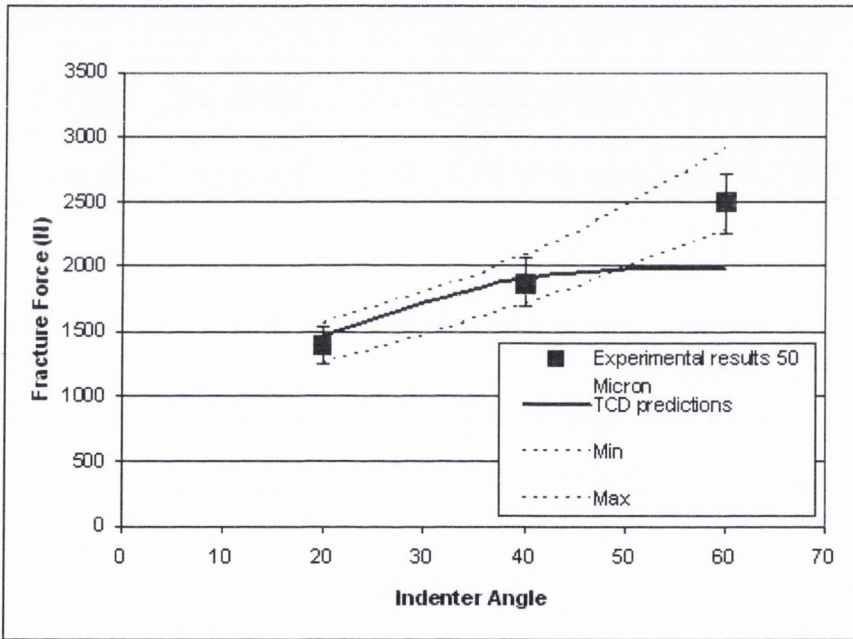


Figure 5-34. Fracture force of transverse indentation for indenters with radius 50 Micron

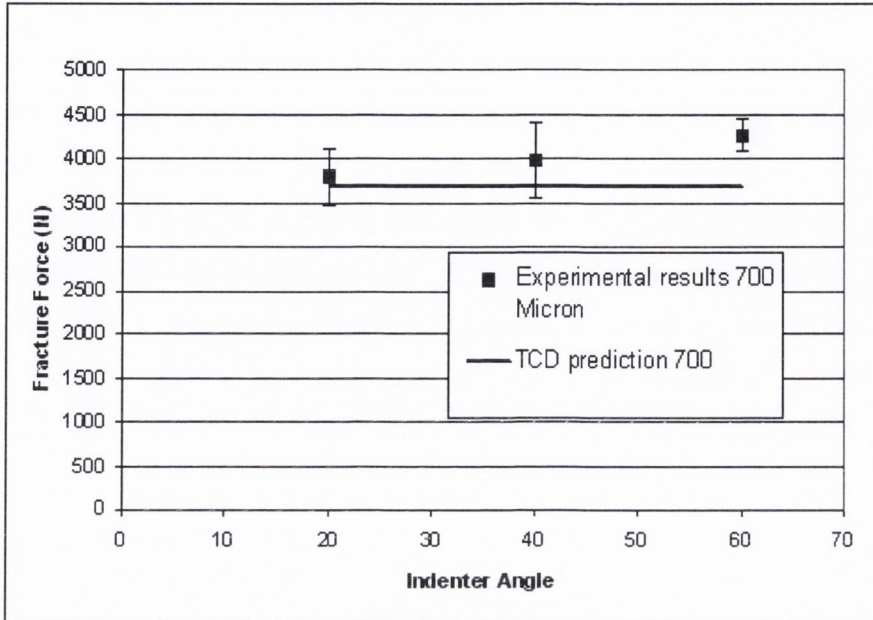


Figure 5-35. Fracture force of transverse indentation for indenters with radius of $700\mu\text{m}$. The TCD predicts no change with increasing the angle. The statistic test rejects any significant difference between the experimental results for various angles.

The crack initiation spot for transverse indentation is different from that for longitudinal. Applying the TCD to different fracture lines that started from various points on the contact surface demonstrates that the required force for fracture is less when the crack initiation point moves from the boundary to the indenter tip. This is especially true when the indenter is sharp. For blunter indenters, this point is somewhere between the contact boundary and the indenter tip at the contact. This agrees with the experimental observation of transverse indentation. In a very sharp blade, it has been observed that the crack initiates at the blade tip in the longitudinal direction. The reason for that could be the high shear stress at the critical line started from the tip especially when the indenter is sharper because of the horizontal stress from the indenter against the material. In this case the fracture line is highly under compression.

5.11. Tangential Indentation Fracture Force

Indentation fracture in the tangential direction is different from that in the longitudinal and transverse directions, however there are similarities between tangential and longitudinal indentation. For example, crack initiation locations geometrically are roughly the same and cracks propagate parallel to the indentation direction. The critical plane for tangential indentation is the weakest available material plane. This plane is the same as the transversal indentation critical plane. The material properties in the tangential and longitudinal directions are different: it is much weaker in tangential direction. Bone microstructure arrangements are different in longitudinal and tangential planes, characterized by a layered arrangement that is arranged normal to the longitudinal plane but parallel to the tangential plane. Thus, a tangential crack would travel along a layer of canals, but a longitudinal crack would have to propagate across these layers. The canal system in bovine bone is mainly formed in the tangential plane and stacking up along the longitudinal direction of bone. Such a canal system causes a decrease of fracture toughness in tangential orientation because these cavities make bones less resistant to crack propagation. The fracture toughness in longitudinal direction has higher value because of the fewer cavities or natural discontinuities encountered by a crack in this orientation[115]. It is expected that the critical distances will be roughly the same in different directions as it was shown in chapter 3. it will be seen that the same value of critical distance gives a good prediction in the case of tangential indentation. The critical stress which is the shear strength of bone is roughly the same in tangential and longitudinal directions. The Young's modulus in the tangential orientation was assumed to be $E=8.5$ GPa taken from experimental results. The yield stress and tangent modulus were found to be $Y=75$ MPa $E_t=700$ MPa for the best load-displacement fit. These material properties are close to those found for the transverse orientation. There is not much data on the post yielding properties of bone in this direction to compare these results with.

Figure 5-36, Figure 5-37, Figure 5-38 Figure 5-39 show applied force versus displacement for different blades when the indentation occurs in the tangential direction, and the results of the FE model verification. The force increases linearly with

indentation and then it becomes nonlinear before fracture which is probably because of the damage in bone, as will be shown in the next chapter. Load and deformation at fracture in tangential cases is much lower than in the other two directions which is because of the bone material in this orientation, as explained above.

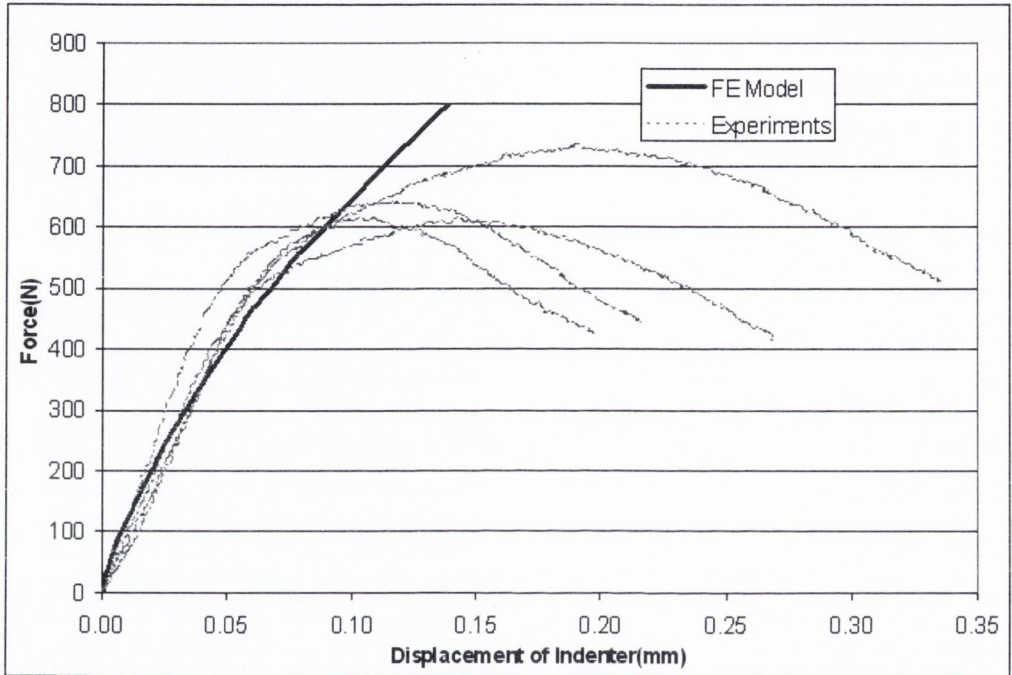


Figure 5-36. Load-displacement for 20°-50μm blade in tangential indentation

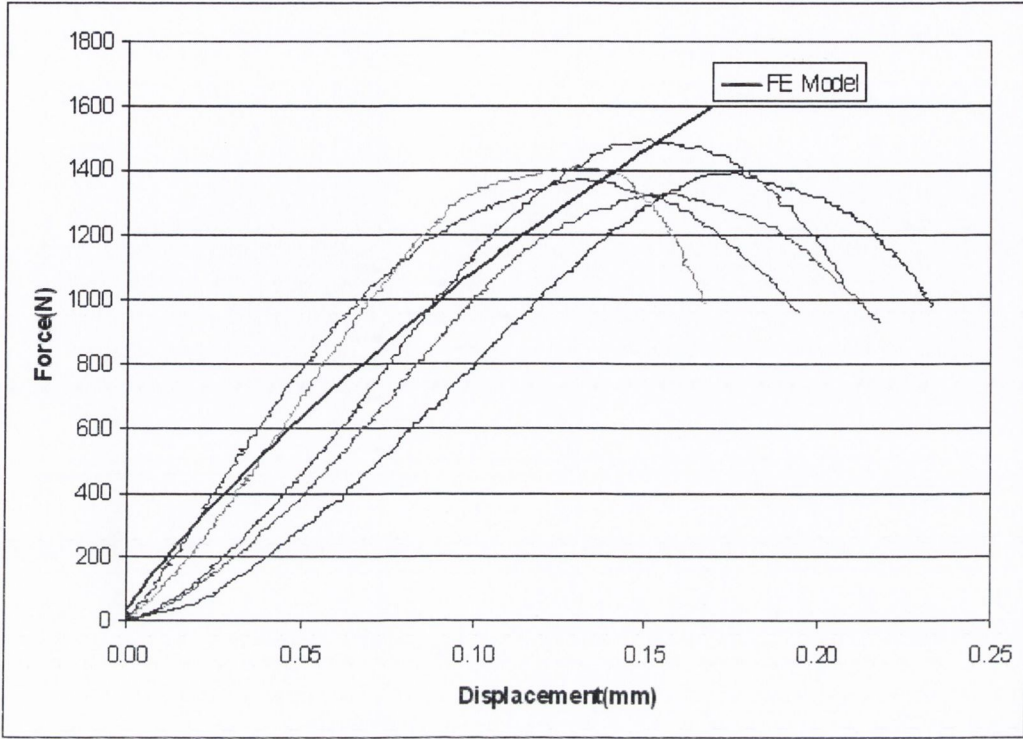


Figure 5-37. Load-displacement for 20°-300µm indenter in tangential indentation

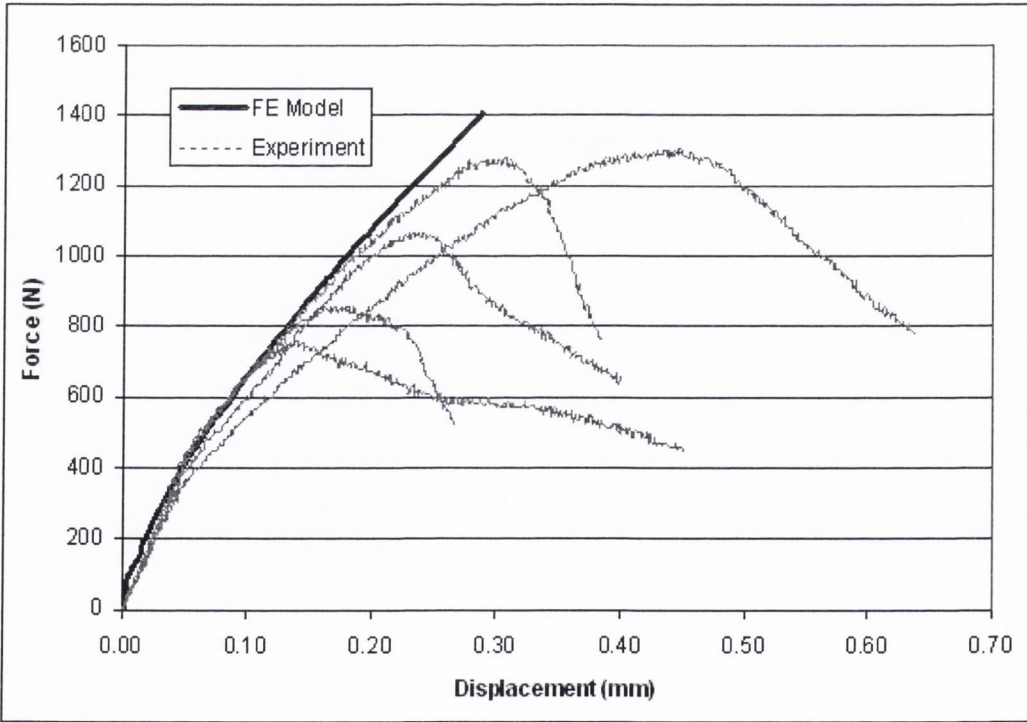


Figure 5-38. Load-displacement for 40°-50µm indenter in tangential indentation

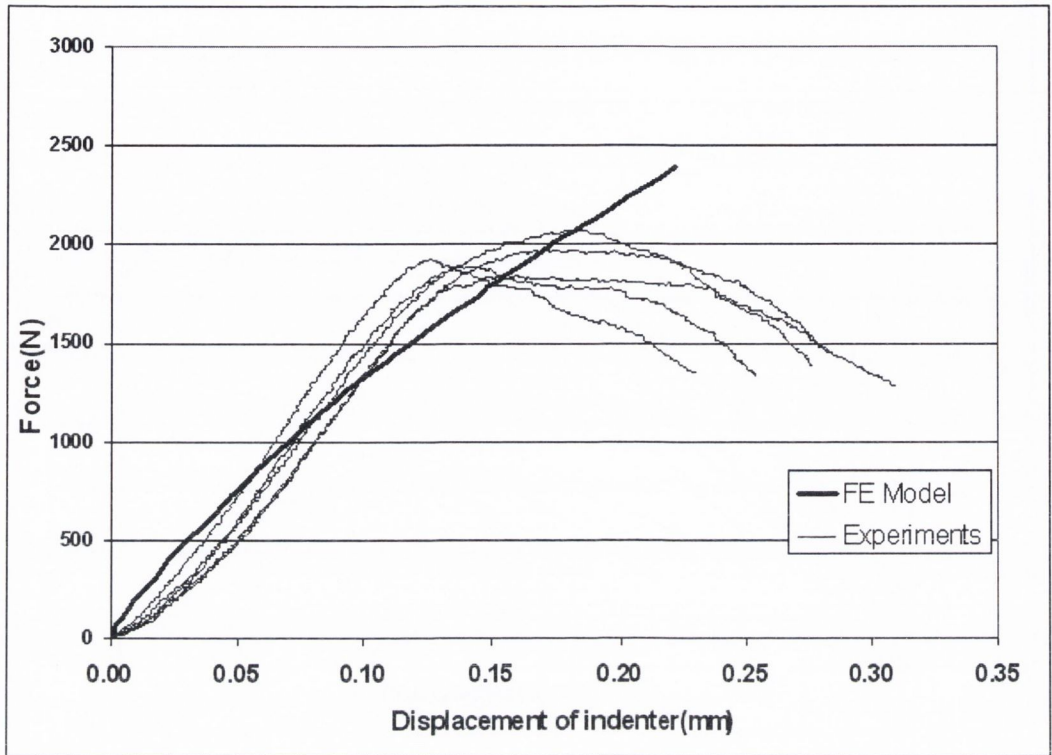


Figure 5-39. Load-displacement for 20° - $700\mu\text{m}$ indenter in tangential indentation

The fracture line is parallel to the indentation direction. This is due to having the weakest properties in this orientation and experimental results also verify this. The same approach was used to predict fracture in the tangential direction as the other two directions, using the same material constants. Figure 5-40, Figure 5-41 and Figure 5-42 show the fracture force for different indenters. These graphs also demonstrate the effects of the indenter radius on the fracture force for certain angles of indenters. The same as other indentation directions, the radius has large effect on the fracture force. For example for 20° indenters, the fracture force becomes 3 times larger when the radius increases from $50\mu\text{m}$ to $700\mu\text{m}$. This effect can be seen for other indenters. The dashed lines in the figures show the minimum and maximum values of experimental results and the error bars show the standard deviation of each group of data. Comparing the experimental data and the prediction using the TCD shows that the theory can predict the fracture force well. The interesting thing is the result were obtained using the same critical distance for the tangential and longitudinal directions in spite of difference in fracture mechanism.

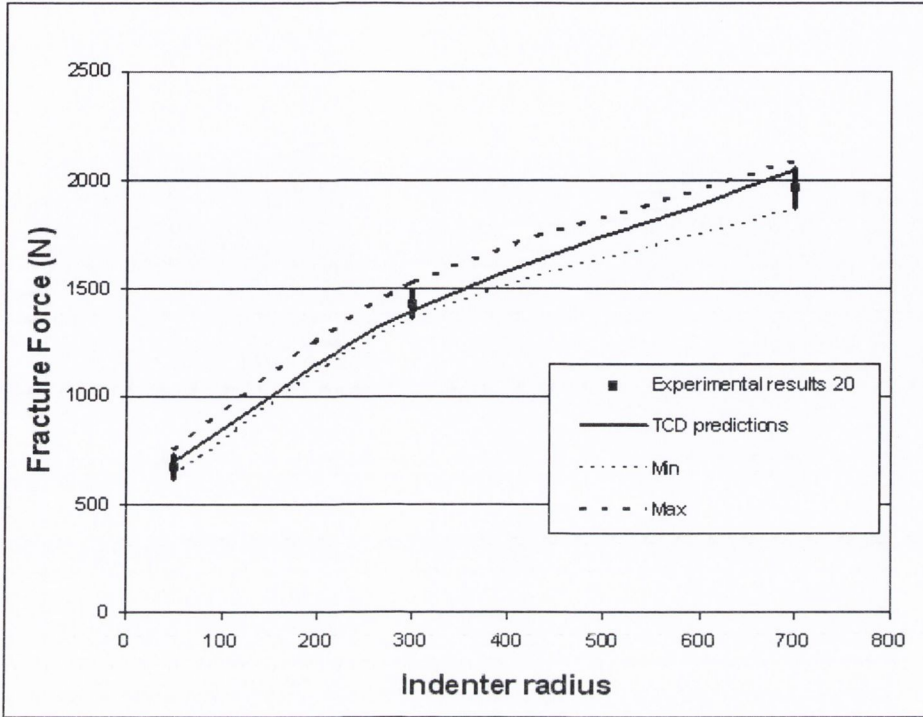


Figure 5-40. Tangential indentation fracture force for blades with angle of 20° and different radii.

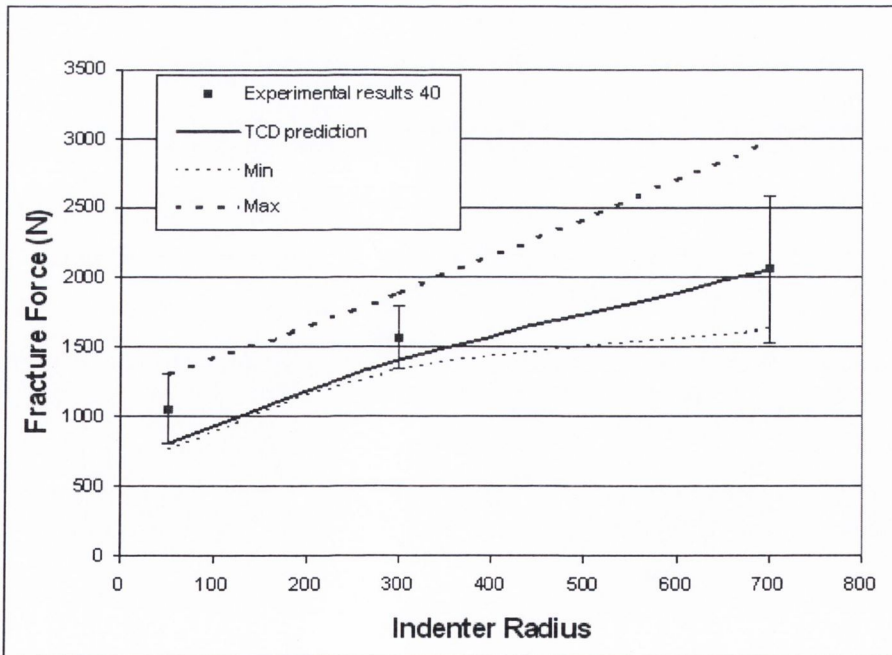


Figure 5-41. Tangential indentation fracture force for blades with angle of 40° and different radii. Error bars show standard deviation: dotted lines show maximum and minimum experimental values

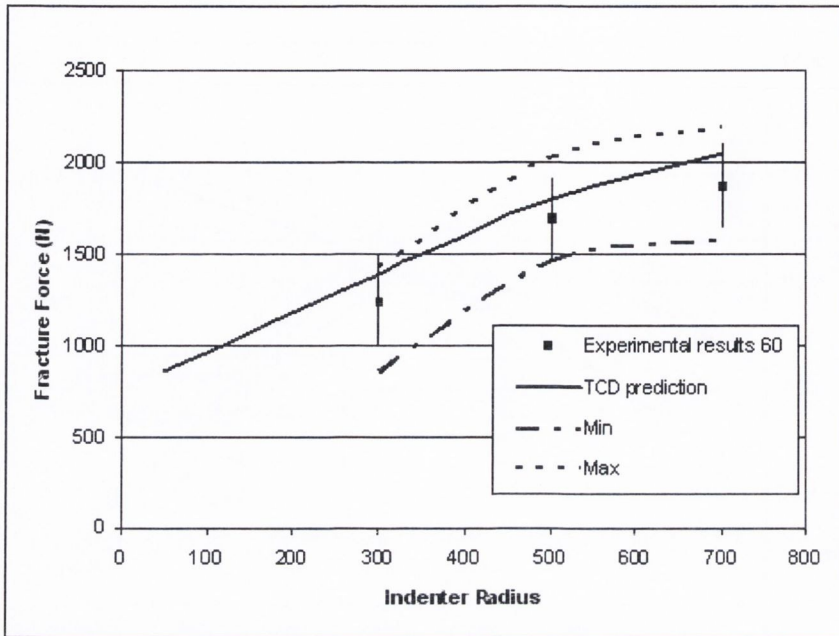


Figure 5-42. Tangential indentation fracture force for blades with angle of 60° and different radii.

Looking at the effect of angle on indentation fracture force (Figure 5-43, Figure 5-44 and Figure 5-45) demonstrates that the angle does not have large effect on the fracture force. As we saw in the transverse and longitudinal direction when the radius is large enough the angle does not play any role on the indentation fracture. Because of the smaller amount of indentation at fracture for the tangential direction compared to other directions the critical angle for a given blade radius is much higher than the one in transverse or longitudinal directions. For 300 and 700 μm indenters changing the angle does not change the fracture force. The experimental results show even a decrease in fracture force with increasing the angle for blunt indenters (it is not statistically significant) which is due to some errors.

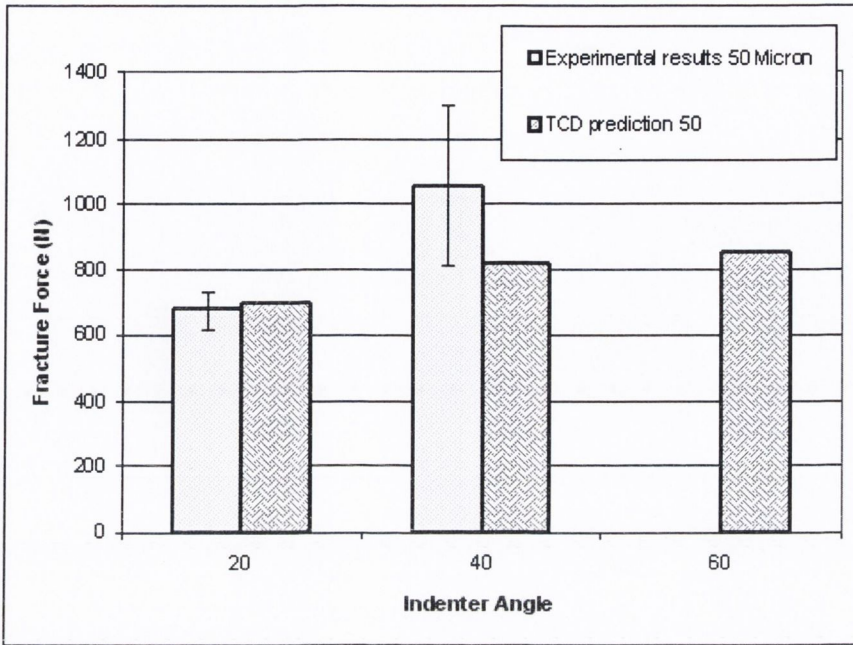


Figure 5-43. Tangential indentation fracture force for blades with radius of 50µm and different angles. The TCD predicts the experimental results for 20° and 40° blades well but there is no experimental result for 60 degrees blade to compare with the predictions.

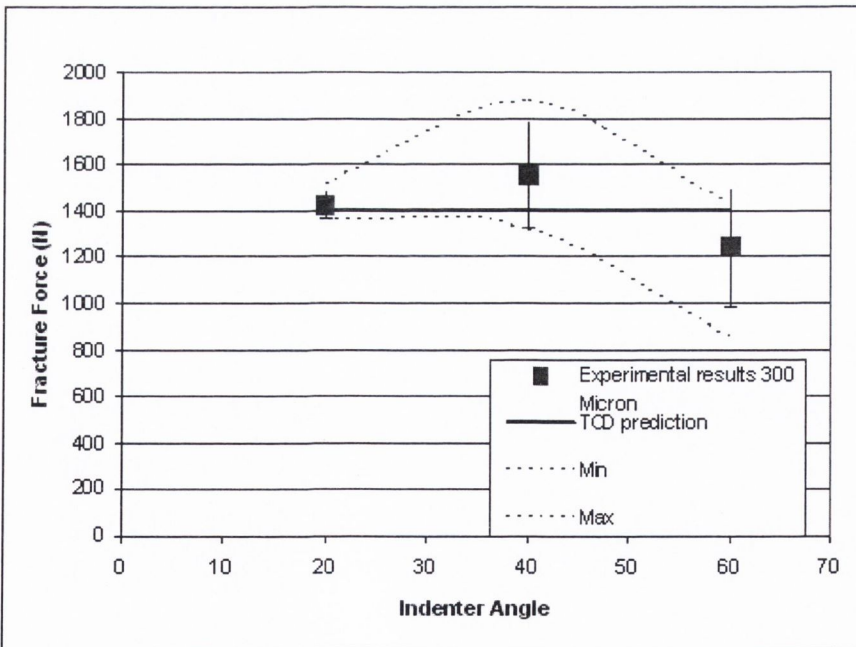


Figure 5-44. Tangential indentation fracture force for blades with radius of 300µm. The TCD predicts no change with increasing the angle. The experimental data agrees with these predictions.

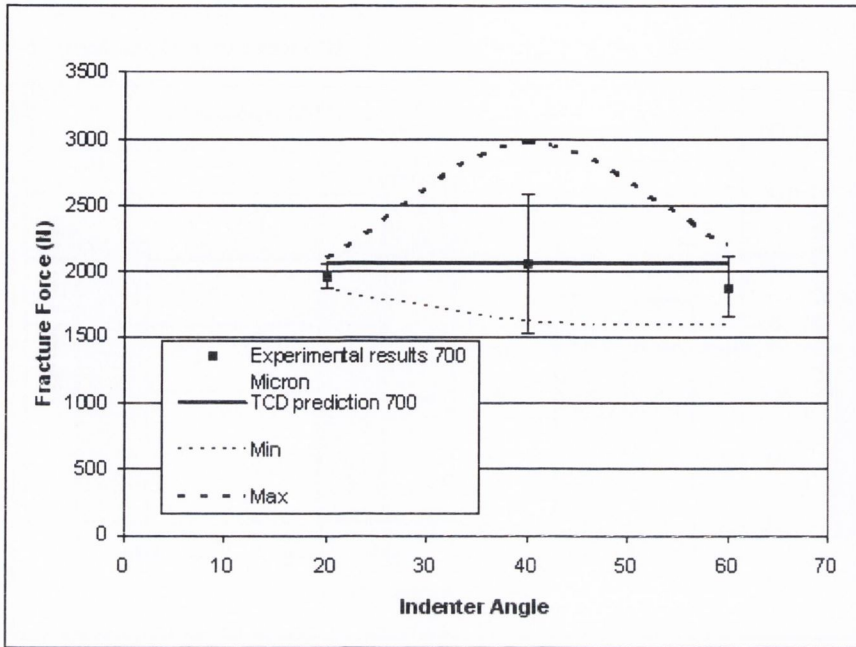


Figure 5-45. Tangential indentation fracture force for blades with radius of 700 μm . The TCD predictions are in good agreement with experimental data, which show that for this indenter, the angle does not have any effect on the indentation fracture force

5.12. Discussion

The TCD was applied to predict the indentation fracture of bone. The prediction is in excellent agreement with experimental data. The maximum error of prediction compared to the average experimental results is less than 20%. The overall results of experiments and predictions show that the tangential and transverse indentation force are the lowest and highest respectively. On average the transverse fracture force is twice as large as tangential force. It is interesting because the material properties of bone are almost the same in both directions. The difference is due to the crack propagation direction, being either parallel or perpendicular to the indentation direction, respectively. This is also the major toughening mechanism of transverse crack propagation which causes the highest fracture toughness in this direction. Using the TCD method, it can be explained in terms of the maximum shear stress in the fracture plane. The shear stress causes the fracture and the compression stress tends to stop it. Looking at two fracture lines at indentation, one parallel and the other one

perpendicular to the cutting direction, shows that for an applied force, the shear stress is greater and the compression stress is less in the former direction. This causes an earlier fracture in the first line providing that both fracture line have the same properties.

The predictions show that the radius of indenter tip has a large effect on the critical force. For example, in a longitudinal indentation using a 20° blade, the force is 2.5 times greater when the radius changes from $50\mu\text{m}$ to $300\mu\text{m}$. The experimental results show that this difference is significant ($p=0.001$). In other directions, the large effects of the radius on fracture force were. Consequently, the smaller the radius of indenter, the more efficient the blade. Linear interpolation for smaller radius shows that the critical force for smaller radii is predicted to be not much different from that for the 50° blade. The experimental results prove that as there is less than 10% difference between the longitudinal fracture force of 20° - $50\mu\text{m}$ blade and very sharp 20° blade.

The angle of the indenter will affect the fracture force if the radius is less than a certain value. In the longitudinal direction, the critical angle for $300\mu\text{m}$ indenter was calculated at around 83.6° , therefore the theory does not predict any difference between 20-300 and 70-300 blades. The average experimental results are slightly different for those blades but they are not statistically significant ($p=0.397$). For $700\mu\text{m}$ indenters, when the angle changes from 20° - 60° the critical force does not change significantly ($p=0.401$) which was predicted by the TCD. For the transverse direction, both experimental results and the TCD confirmed that the angle has effect on the critical force for $50\mu\text{m}$ indenter. The experimental results show that there is no difference for $300\mu\text{m}$ blades when the angle changes from 20° to 40° , but there is a significant difference between 40° and 60° blades ($p=0.155$). Our model was able to predict this behavior. For blunter indenters ($700\mu\text{m}$), however, the TCD predicted the critical angle much higher than 70° , but there is a significant difference between the 20° and 60° indenters ($p=0.023$). That would be because of the large scatter in data especially for 20-700 indenter ($\sigma=313$). In the tangential indentation, increasing the angle of indenter does not vary the critical force for $300\mu\text{m}$ and $700\mu\text{m}$. It was predicted using the TCD and experimental results. The angle has the more effect for $50\mu\text{m}$ blade, critical force

changes from 678N to 1053N when angle varies from 20° to 40°. The TCD can predict the effects of the angle and radius on the fracture force well. As a result, the smaller the angle, the less the indentation fracture force.

The critical distance calculated from indentation test is in the range we calculated before using data on brittle fracture from tensile, bending and torsion tests. The analysis shows that the same value of critical distance can be employed to predict the fracture in different directions. That agrees with the hypotheses that the critical distance of bone does not vary considerably with orientation. On the other hand, the type of bones are different from the ones that were used in the previous study in chapter 3. The specimens were picked from lateral bovine femur which is plexiform but in the previous section osteonal bones were tested. Using the same critical distance value for osteonal and plexiform bones, confirms that it is almost constant for different types of bone.

Some guesswork was used to predict the indentation fracture force for different cutting directions. The experimental results show no pile up during the indentation, which agrees with the observations of other researchers [36, 118]. A linear hardening model, therefore, was employed to model the bone. Because of lack of pile-up and the linear relationship between the force and penetration, it was assumed that bone under indentation does not flow but compacts[118, 43]. This means that in the sides of the compact zone shear stress and inherent friction play important roles in fracture, therefore the Coulomb-Mohr criterion was used. The applied fracture criterion associated with the TCD, could predict the fracture of bone well. In the case of indentation the fracture criterion was different from the one in chapter 3 when the material is under tensile stress. It is due to the different types of loading and fracture mechanisms. It shows that the assumption under indentation was acceptable.

In chapter 3 it was shown that the T factor works as a correction factor when there is nonlinearity before fracture. The T factor therefore is related to the amount of nonlinearity before failure. Bone experiences more post-yield deformation under compression than tension then a larger T factor is expected under compression. Also under compression, there is significant difference between the deformations in various

orientations. In other words, in the case of indentation the T factor changes with indentation direction. On the other hand, when a nonlinear model is employed the T factor equals 1 due to the fact that the nonlinear model carries the effect of T factor. In this study, for all three orientations (transverse, longitudinal and tangential) the TCD with the same fracture criterion and the same material constants was used. As the bone is weaker in tangential direction than the longitudinal, therefore, it is possible that the T factor in tangential indentation is smaller than the one in longitudinal indentation if an elastic model is employed.

5.13. Conclusion

The TCD can predict the effect of geometry on the indentation fracture force for all three orientations. It shows that the radius of indenter tip has a large effect while the angle will affect the fracture only for small radii. The TCD was also capable to predict the crack initiation spot.

CHAPTER 6. Indentation: Damage Area

In the previous chapter, the indentation fracture force of bone material was predicted using the TCD. Fracture is a result of damage accumulation. During loading microcracks are formed[106, 116, 128-134], creating a zone of micro-damage which grows with increasing load. A main micro-crack forms in this zone and grows until the critical length is reached and the bone consequently fractures. In this chapter, the focus is on investigation on how to predict the size of the damage zone. It will be demonstrated that the size of the damage zone can be estimated using the maximum and minimum principal stresses. The predicted data will be compared to the experimental results.

Different techniques have been used to stain microcracks[135-137]. Fluorescent chelating agents were used by Mr. Ger Reilly to label damage zones during the experimental part of this project. This method had been previously used to label bone damage that occurs during the fatigue compression testing of bone, in which the growth of microcracks occurs slowly and where there is a process of fretting along the crack face[137].

There is a lot of scatter in the experimental data regarding the amount of damage before fracture. The results show that the largest damage zone is formed before fracture

in transverse indentation, and the smallest in the tangential direction. The amount of damage increases with increase of the radius of the indenter tip.

6.1. Methods

In the experiments, a fluorescent chelating agent, in a sequential labelling protocol [136, 137], was used to label the damage. The advantage of this method is that the agent chemically binds to the damage zones in the bone. It can be applied during testing with the potential to be used for labelling of pre-existing damage or sequential growth in the damage sites during increases in load at different load intervals. The specimens were examined under UV light and the total damage zone was measured, i.e. the total area of stained bone, as an alternative to microcrack counting. Acoustic Emission (AE) was also used to detect microcracking during indentation.

6.2. *Damage and Acoustic Emission*

Under loading, microcracks develop beneath the indenter, usually starting around the maximum stress points. The load-penetration curve is linear until a certain point. Figure 6-1 is the AE signal for the longitudinal indentation of bone. It can be seen that there are no AE signals in the linear area. There are some AE signals in the non-linear area, presumably due to the formation of microcracks. These microcracks accumulate in the nonlinear part until the fracture [129, 130].

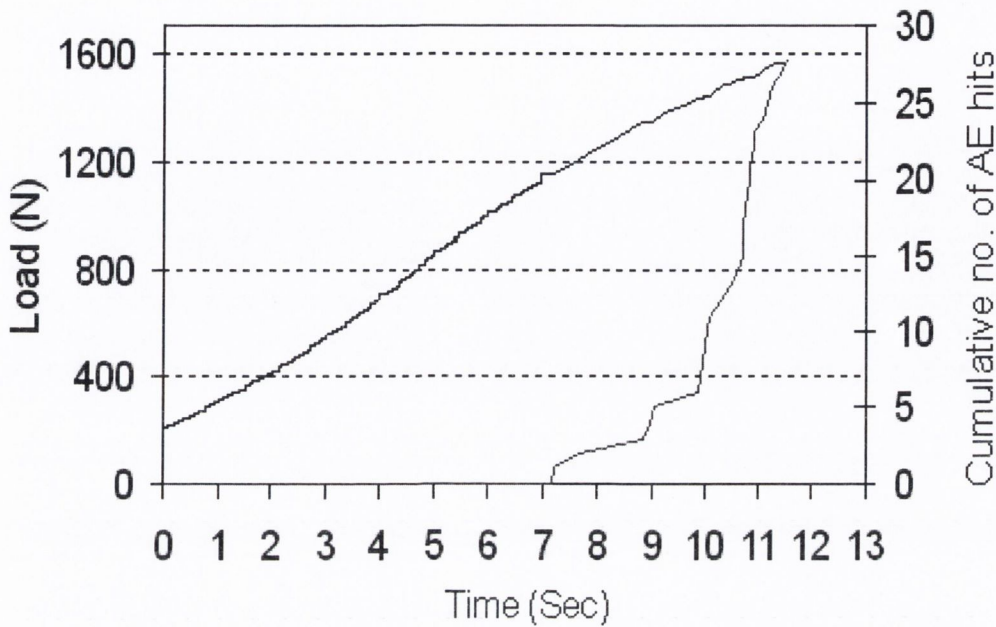


Figure 6-1. Cumulative number of AE hits for bone specimen cut up to maximum fracture load. The onset of micro-cracking is associated with the non-linear phase (A. Safari Masters thesis, Sligo IT).

Under indentation, a tensile zone is formed as well as a compression region. The compression area is located beneath the blade, while the tensile zone is formed outside the contact area as well as underneath the compression zone, as discussed in Chapter 4 and 5. The experiments show that microcracks are formed in both areas. Therefore, there are at least two different mechanisms are involved in the damage process. For sharp indenters, the stress field is singular about the indenter point which leads to irreversible deformation modes. It also happens for the blunter indenter around singular points. These deformation zones were activated by the large components of shear and compression in the singular field and account for the initiation of any consequent micro-fracture. During the indentation, microcracks form, then grow and turn into the major cracks which cause a catastrophic failure. Outside the compression zone, the tensile stress of the material controls the microcracks. A measurement of the damage zone just before fracture, can give an estimate of when the microcracks start.

Microdamage in bone related to the mode of stress or strain[130] and there is no single mode of stress as a universal cause of damage[106]. To estimate the sizes of damage zones, a maximum principal stress criterion was employed. It was assumed that microdamage would form if S_1 (the maximum tensile stress) is greater than a certain value, or if $-S_3$ ($-S_3$ is the maximum compressive stress, S_3 is a negative value in the compression zone) is larger than a certain value as equation 6-1:

$$S_1 \geq S'_{Tuts} \quad or \quad -S_3 \geq -S'_{Cuts} \quad (6-1)$$

6.3. Results

6.3.1. Experimental Results

Looking at the damage area one can see that there are two separate damage zones under indentation apart from the cutting direction. The first zone is formed beneath the indenter and the second one is located close to surface of bone. These two zones can be clearly seen in Figure 6-2 and Figure 6-3. Comparing the two zones illustrates that the first zone is much larger than the second one. In fact the large portion of the damage value above is due to the compression section.

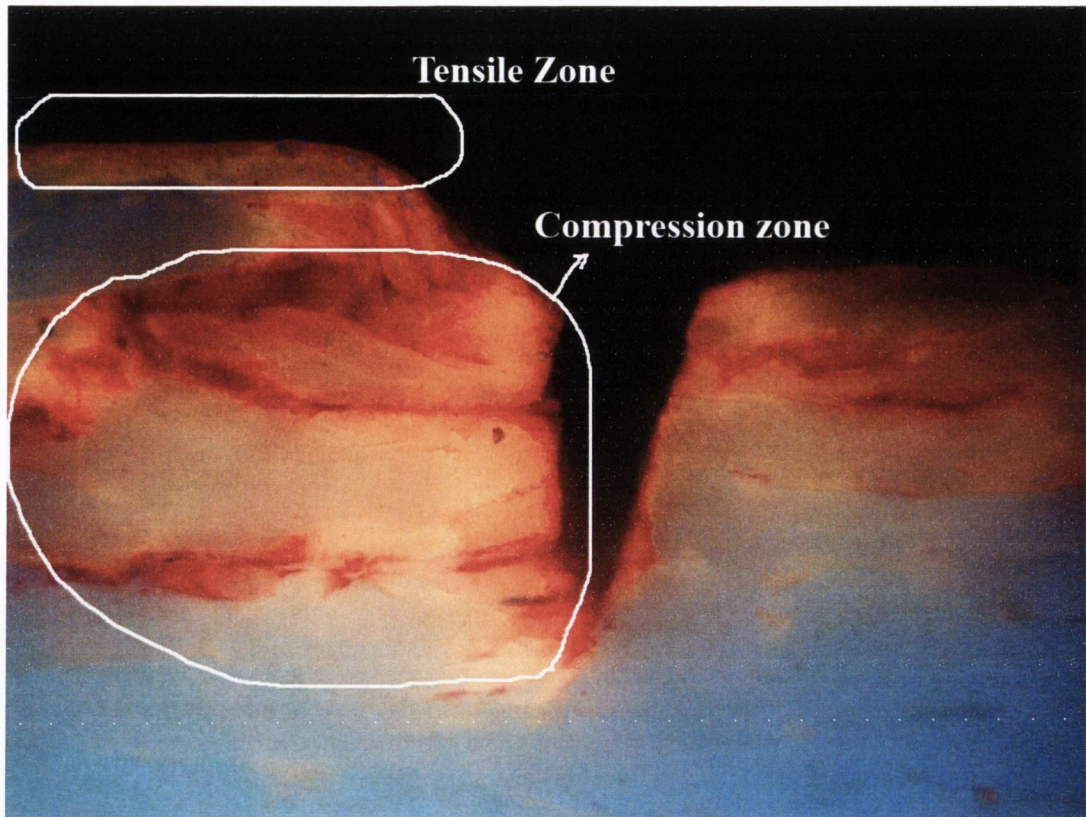


Figure 6-2. Damage zone during the transverse cutting using a sharp blade. Two different damage zones, tensile and compression, are formed .

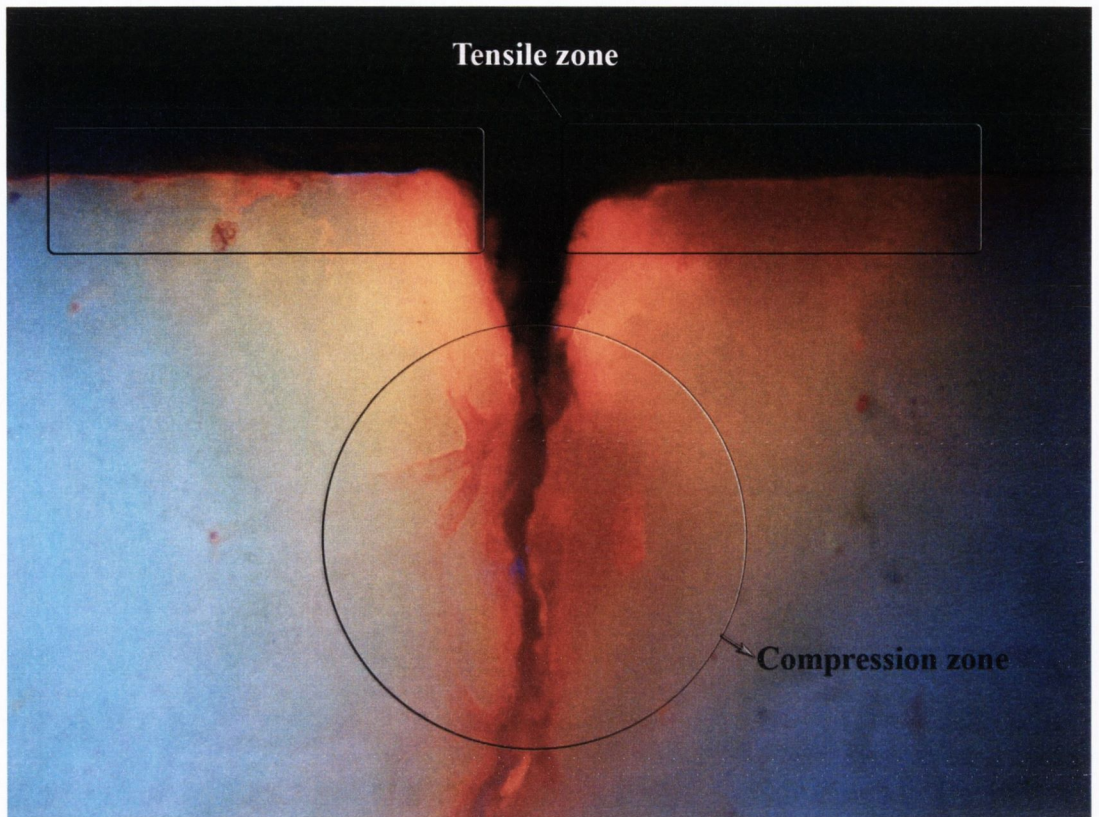


Figure 6-3. Tensile and compression damage zones formed due to longitudinal cutting

In Figure 6-4, is shown the effects of radius size on the damage area for different cutting directions when the blade angle is 20° . From the graph is obvious that the damage area increases when the blade has a larger radius. There is also a large scatter of data for indentation in the transverse direction and the experimental which gives unexpected results which will be discussed below.

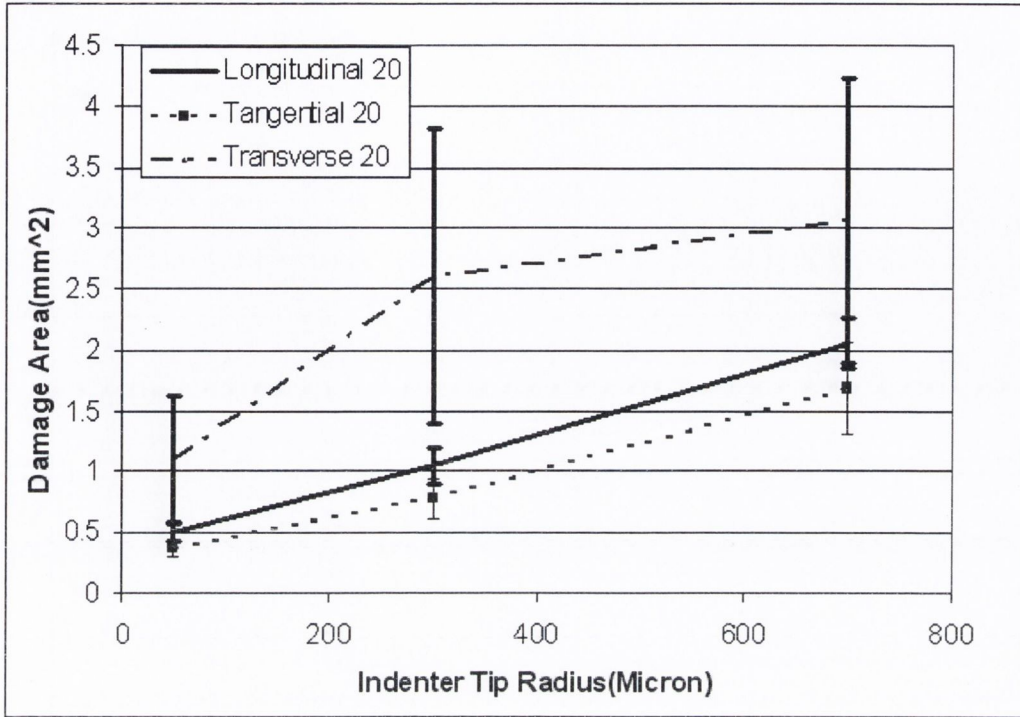


Figure 6-4. Damage area for blade with 20° angle and different radii. (Three different cutting directions)

Figure 6-5 compares the damage area for different cutting directions. The overall results show that the damage area for a given indenter is the largest in transverse direction and lowest in the tangential direction.

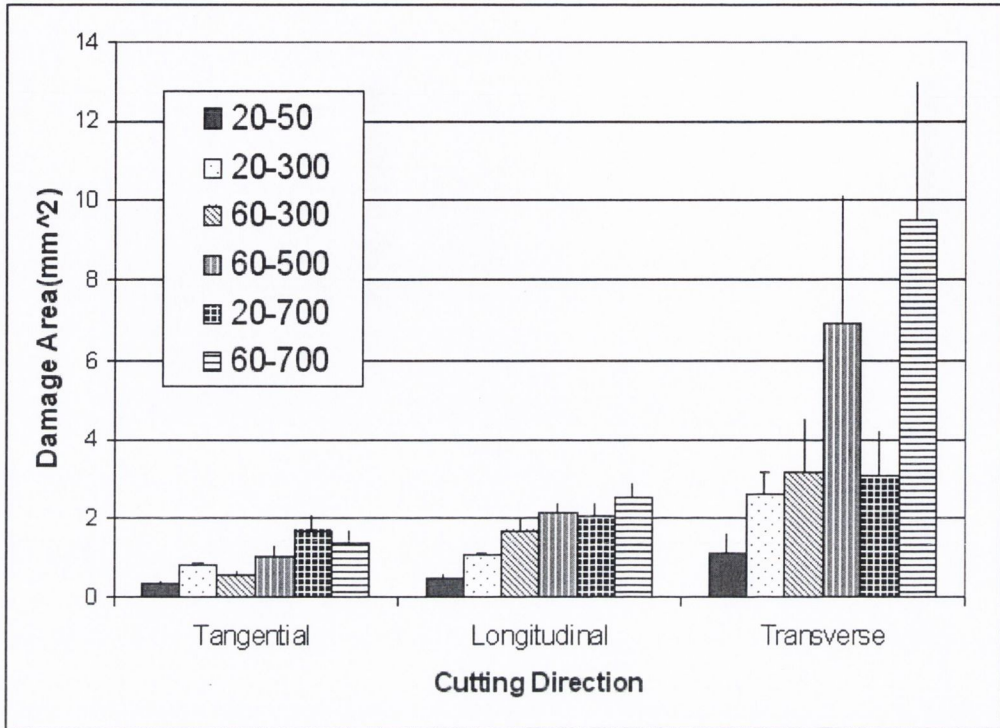


Figure 6-5. Damage area in different cutting directions

In chapter 5, we saw that the TCD predicts that the angle has no effect on the fracture force of large indenter tip radii. It was shown that the experimental results agreed with the prediction. It was because the penetration before fracture is not large enough to bring the sides of the indenter into contact with the bone. For the same reason it can be expected that the damage area for large indenter tip radii will be independent of the angle. Comparing the effects of angle for blades 700 μm in size shows that there is no significant difference between damage zones when the angle changes from 20°-60° for longitudinal and tangential indentation. The difference for the transverse direction could be just because of the high scatter between data. Scatters in measuring damage in transverse indentation are higher than in other directions. It causes some unexpected results, for example, the damage area for 60°-500 μm was measured to be much larger than the one for 20°-700 μm .

6.3.2. Finite Element Predictions

Figure 6-6 displays maximum and minimum principal stresses (greatest tensile and compressive stresses) around the indenter tip of blade 20° - $300\mu\text{m}$ at fracture load in the longitudinal direction. Under indentation, compression and tensile regions are created in bone. The compression zone is located beneath the indenter whilst the tensile zone is on the surface of the bone just outside the boundary of contact. The tensile zone is very small when compared to the compression zone. These factors are clearly shown in the experimental results, demonstrating the two different mechanisms involved in the two zones of stress. In the first zone, compression controls the damage, while the second zone is formed due to tensile stress. The tensile zone is very small, compared to the whole damage area and is negligible when measuring damage area.

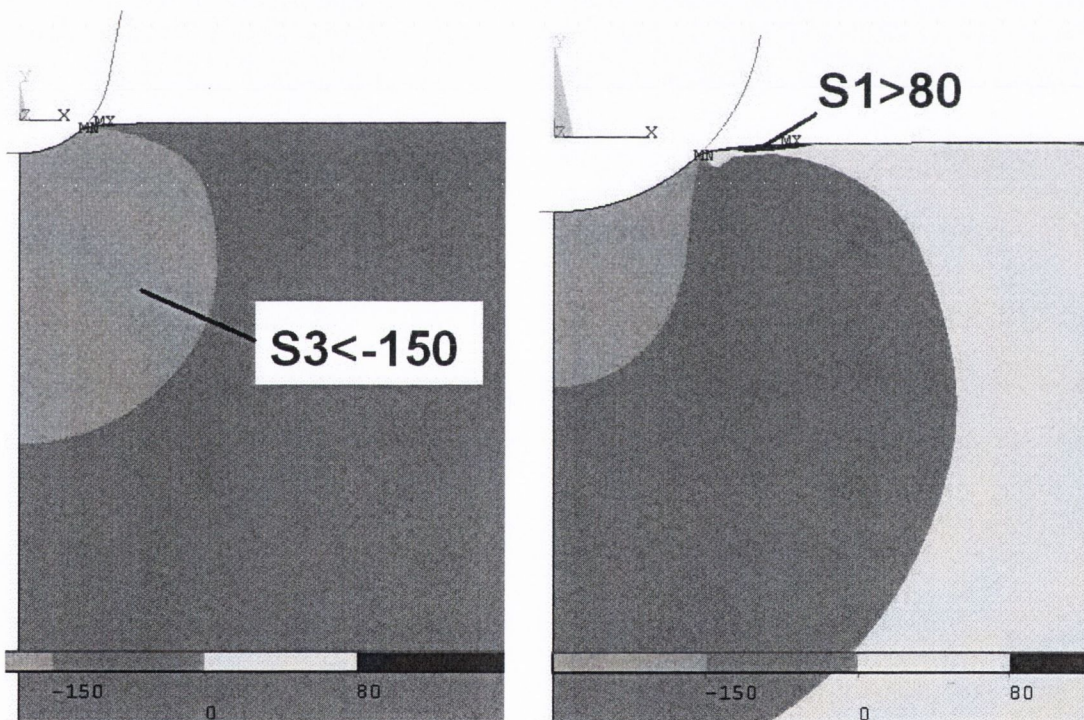


Figure 6-6. Estimating damage area using principal stresses for 20° - $300\mu\text{m}$ indenter. Left: Damage due to compressive stress, Right: Damage due to tensile stress

The high compression and high tensile zones are separate as can be seen in the above figure but separation is not always the case. When the blade is sharper, there is an

area of high tensile and compressive stress around the geometric singularities. This area makes up half of the total tensile damage zone. The damage mechanism in this zone is complicated but the value of damage is small and negligible when measuring the damage size.

By trial and errors the best values for the limits of the damage zones were found to get the best overall prediction of size of damage area. These limits for the longitudinal directions are -150 and 80 MPa for compression and tensile limits. Figure 6-7 compares the results of experimental damage and the finite element model prediction. The graph confirms that choosing a value of 50%-60% of the ultimate stresses as a criterion can predict the damage area. It shows that the damage area is highly dependent on indenter sharpness. The damage is nucleated when the stress level on bone reaches about 50-60% of ultimate stress. Extrapolating the data for the sharp indenter predicts that if a very sharp indenter is used the damage area will be about 40% lower than 50 μ m indenter.

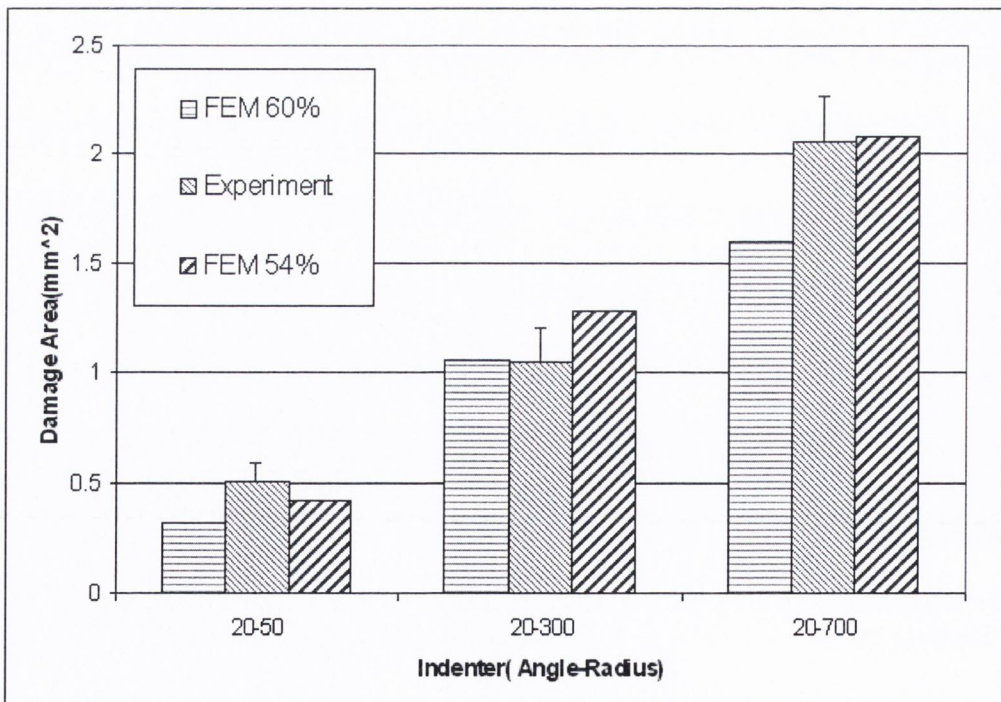


Figure 6-7. Comparing damage area measured using FE model for longitudinal indentation of 20° blades, when critical stresses is 60% and 54% of ultimate stress with experimental results.

Under the indenter, the depth of damage in to the bone increases with increasing blade radius. The damage zone diameter was measured to be 0.42mm, 0.95mm and 1.226mm for blades with angle of 20° and radii $50\mu\text{m}$, $300\mu\text{m}$, $700\mu\text{m}$ respectively. When fracture starts from a notch or crack under tension, the damage zone at fracture is the same size as the critical distance. In the case of indentation, however the damage depth varies with radius and it changes between L and $4L$.

The damage area is much larger for transverse indentation. Employing the principal stress criterion and assuming -100MPa and 40MPa for critical stresses in compression and tension the damage zone can be predicted quite accurately. The critical stresses here are about 60% of the ultimate compression and tensile stresses in the transverse direction. Figure 6-8 compares the experiment results with FE predictions. It can be seen that experiment data scatters a lot in the case of transverse indentation.

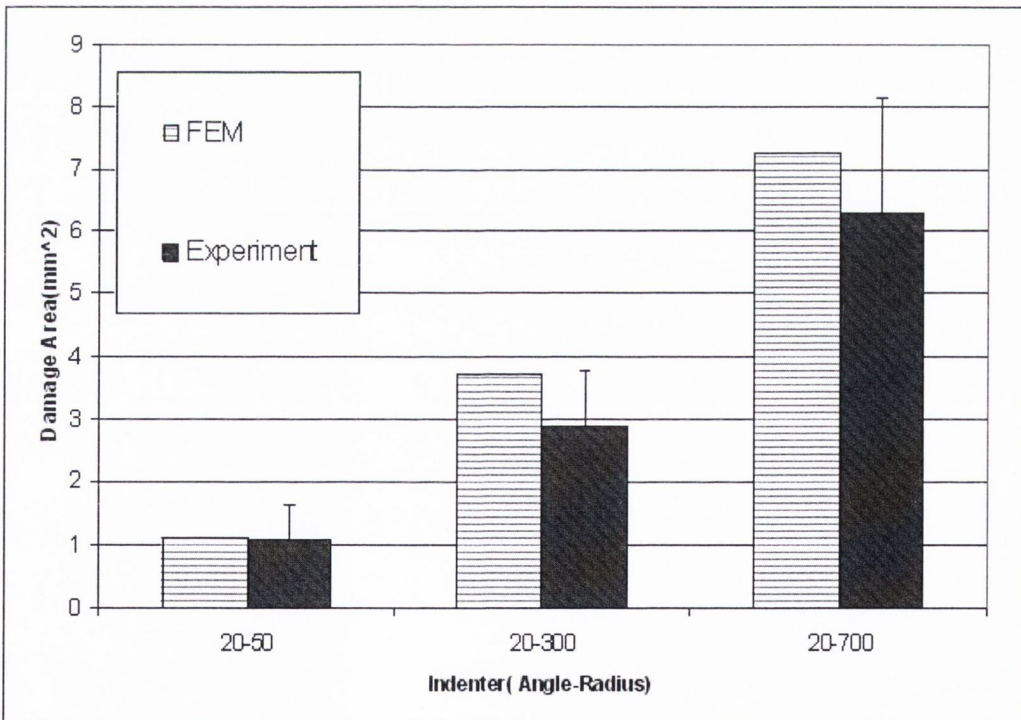


Figure 6-8. Size of damage zone measured experimentally at transverse indentation fracture. It also shows the predictions using the FE model. The damage area in the FE model measured when the stress reaches 60% of ultimate stress.

Analyzing damage in the tangential direction illustrates that $S_3 < 85\text{MPa}$ can predict the best fit for the damage area. This value is approximately the compressive ultimate stress of bone in the tangential direction. With this assumption, the damage zone of the 20° - $50\mu\text{m}$ indenter was estimated to be about 0.36mm^2 . The damage zone size for the 20° - $300\mu\text{m}$ and the 20° - $700\mu\text{m}$ were estimated to be about 0.9 and 1.61mm^2 respectively (Figure 6-9).

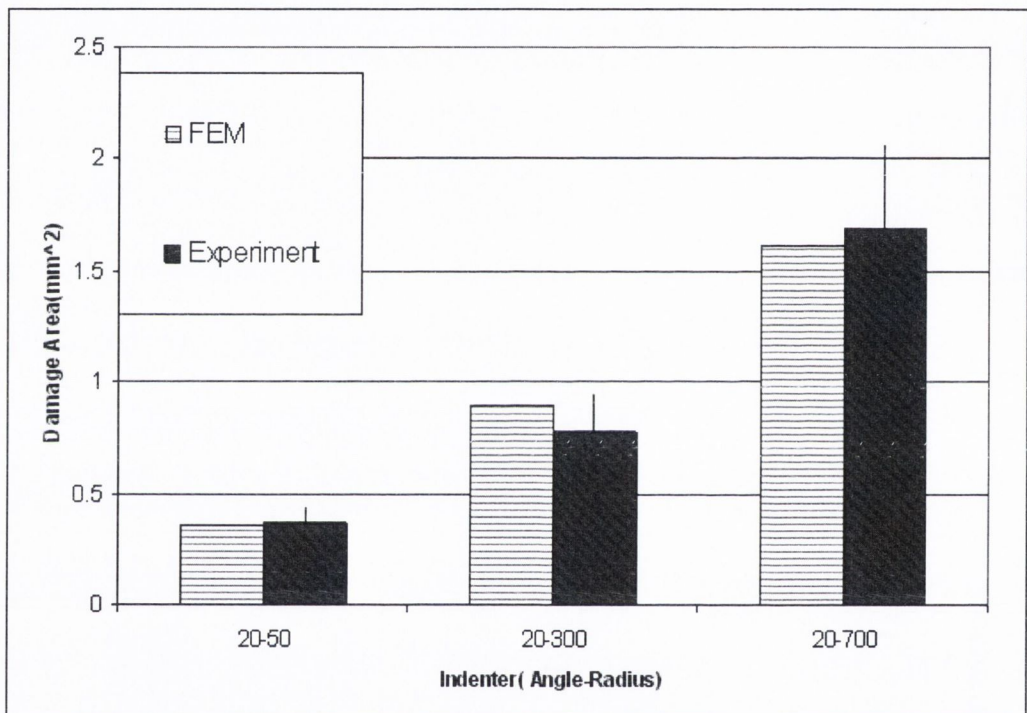


Figure 6-9. Size of damage zone at fracture in tangential indentation. it compares the FE prediction using 90% of ultimate stress.

6.4. Discussion

During the indentation process, diffused damage accumulates in bone[129, 130]. Diffuse damage in bone is formed by large number of short sub microscopic cracks[130, 131, 133] and is a result of breakdowns in the canalicular network[138]. The size of this damage zone before fracture was measured experimentally. It has been shown that the Von Mises stress can predict the microdamage[106]. Due to different

damage zones formed in tensile and compressive area during the indentation, a simple normal stress criterion was employed in this study to estimate the size of the damage zone. Indentation damage can be caused by tensile or compression stresses, however, the compression damage zone is much larger than the tensile one. The origin of indentation damage is not known. During the indentation, the tensile stress is formed at a distance underneath the blade and also at a distance from boundary of contact. These zones of tensile stress turn to compressive stress as the blade indents. The micro damage may form during this process. There is not much information about what happens during the indentation in terms of damage zone as we only look at the damage area after fracture. The other possibility for damage formation is the tensile residual stress on the bone after unloading. In both cases the microdamage occurs under tensile[134]. Choosing 50-60% of the compression ultimate stress as the criterion of failure for the longitudinal and transverse directions can predict the size of the damage zone. In the tangential direction, about 90% of ultimate stress gives the best estimation of damage zone formation. Tangential fracture is more brittle than either transverse or longitudinal fracture, implying that less damage occurs before final failure.

The diameter of the damage zone however depends on indentation direction and wedge geometry but it is in the same order of critical distance. It has been shown that under tension the damage area at crack propagation is related to the critical distance value.

The amount of damage created in the bone during cutting is an important parameter in surgery, because the surgeon would like to create as little damage as possible in the bone. Large amounts of damage could cause necrosis of the bone, creating a layer of dead bone around the cut, which will be resorbed and replaced by new bone. It is useful to be able to predict the amount of damage as a function of indenter parameters such as sharpness (i.e. radius).

Other criteria were used to estimate the damage zone including, for example, the combination of shear and tensile stress as discussed in chapter 5. This complex criterion however, could not predict the size and shape of the resulting damage zone. A simpler criterion, using the principal stresses, predicted the damage size quite well. It showed that the mechanism of damage is different from the final fracture mechanism. The

diffusion damage occurred under high levels of compression but the shear stress in this zone was not large enough to form microcracks. High shear stress acting on the fracture plane causes microcracks to form and ultimately causing fracture.

CHAPTER 7. Discussion

The Theory of Critical Distances (TCD) was employed to study the effect of stress concentration in bone. TCD methods can predict similar results in spite of different approaches. The main differences between methods, is in their applications. FFM and ICM need a crack to be introduced. These methods are not suitable in problems using compression as the introduced crack tends to be closed. For example, indentation fracture of bone occurs under a high level of compressive stress, therefore the crack faces are forced into contact with each other. The TCD has been applied to other materials before [139, 6, 12, 72]but this is the first time in which it is been applied to bone.

It was shown that the TCD is valid for bone as it fails by brittle fracture with limited inelastic deformation[140]. The results demonstrated that the TCD can be applied to this material and predict the effect of stress concentrations under tension. Furthermore, the strength of long bones containing transcortical holes was predicted well when the bone is under torsion or bending. The failure plane for torsion is the plane of 45° [94, 141-143] which is the maximum tensile stress plane. In tension and bending the main crack grows perpendicular to the maximum tensile stress direction [93, 82, 84]. The critical distance of bone was found to be almost constant, varying in the range of 0.3-

0.4mm. This is in agreement with other results in “critical flaw length”[84, 82]. The T factor (ratio between critical stress and the ultimate stress) was calculated to be 1.33.

In some other materials the critical distance value is in the order of the size of microstructural features for example grain size [4]. Cortical bone contains different structures which exist in different levels of scales [144]. Table 7-1 shows the range of levels and their size. It can be seen that the osteon size and the distance between haversian canals is in the order of hundred microns. The obtained critical distance value is about 300-400 μm . It shows that the osteons play an important role in toughening of bone. This is in agreement with other researcher’s observations [145-147]. In large enough samples of bone, the value of critical distance, L, relates to the micro-level, however, effects of the nano structures of bone are carried on T.

Table 7-1: Cortical bone structural organization along with approximate physical scales

Level	Cortical Structure	Size Range
0	Solid Material	> 3000 μm
1	Secondary Osteons Primary Osteons Plexiform	100 to 300 μm
2	Lamellae Lacunae Cement Lines	3 to 20 μm
3	Collagen-Mineral Composite	0.06 to 0.6 μm

In the case of transverse fracture toughness (i.e. when the crack grows in the transverse plane) the critical distance is in the order of the distance between osteons or haversian canals. Therefore these osteons might control the toughening of bone in macro-scale. This agrees with deflection as a major mechanism in toughening of bone when the crack advances in the transverse direction. This deflection is due to the osteons’ property[104].

Figure 7-1 shows the micro-scale discontinuities in bone. The distance between Haversian and Volkmann’s canal are discontinuities in the same order as critical distance. These discontinuities may relate to the critical distance of osteonal bone which

has already been seen for transverse direction. If a crack grows in longitudinal directions, the length of osteons or distance between Volkmann's canals may control the critical distance. In this case it is expected that the longitudinal critical distance changes in a wider range compared to transverse. In the tangential direction, also the vascular channels may define the critical distance. In this case the distance between them is roughly the same as the distance between osteons. There should not be much difference between transverse and tangential critical distance. Haversian canals and vascular canals make a boundary like a grain in bone. The size of these grains is in the order of hundreds of microns and defines the critical distance. It was shown before that the osteons and Volkmann's canal tend to play a crack arresting or diverting roll[78].

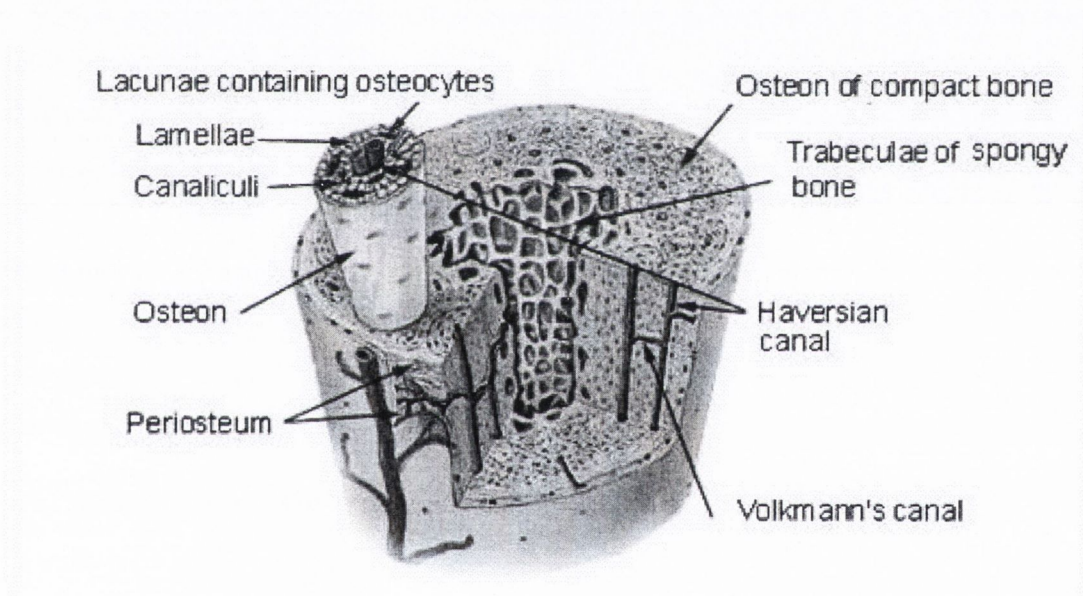


Figure 7-1. Microstructure of compact bone

Critical distance is also in the same order as the size of natural voids in bone. The size of natural microcracks are about $400\mu\text{m}$ parallel to the bone longitudinal direction and $100\mu\text{m}$ perpendicular to that [128, 148, 149]. This again shows that the critical distance might be larger in longitudinal direction compare to the transverse.

In chapter 5, it was found that the same value of critical distance can be employed to predict the indentation fracture of plexiform bone. This value of critical distance was 0.32mm which is in the range of 0.3-0.4mm calculated earlier in chapter 3. The fracture plane in the case of transverse indentation is along the tangential plane. The same value of critical distances was chosen in tangential and longitudinal direction. Plexiform bone arises from mineral buds which grow first perpendicular and then parallel to the outer bone surface. This growing pattern produces the brick like structure characteristic of plexiform bone. Each "brick" in plexiform bone is about 120-500 microns (μm) across. Therefore, in the case of the plexiform bone the critical distance is related to the size of the bricks.

From definition of $T (= \sigma_c / \sigma_{\text{uts}})$ it is obvious that defects with stress concentrations less than T do not have any effect on the strength of material. In fact the critical stress of bone is obtained by ultimate stress multiplying by a factor T . It means that a stress concentration factors less than $T=1.33$ does not reduce the strength of bone. The experiments on bone under torsion and bending confirm this [94, 93]. It has to be noticed that, this does not mean that all defects with the stress concentration greater than T will change the strength, but it depends on how localized the stress distribution is. The T factor demonstrates that there is a crack length (or defect size) below which the crack (defect) has no effect on the strength. The value of T for bone is between that for ceramics [12, 150] and polymers [151, 139, 11], therefore, bone can withstand larger cracks than in ceramics and smaller cracks than in polymers.

$T (= \sigma_c / \sigma_{\text{uts}})$ is a factor which may be related to the microstructure of material. The microstructure of bone has been designed such that its stress concentration is less than that of a homogenous material [152]. In other words, the strength of bone against the stress concentration is more than an elastic material with the same structure. The ratio between the critical stress and ultimate stress T , therefore, can represent the effect of the microstructure on the stress concentration. The larger the T , the stronger the material in presence of the stress concentrators.

The stress concentrations in bone at fracture are less than that predicted by the elastic model [94]. There are two main reasons for this: first, there are small voids in the microstructure of bone which cause stress concentration so introducing a new hole does not have such a marked effect. Secondly, the stress concentration depends on Young's modulus and it changes if there are any non-linearities in the material. As it has been accepted that there is non-linear deformation before fracture [140], this can be another reason for its reduction. An elastic material model which is employed to apply the TCD does not cover any of these irregularities, consequently it overestimate the stress concentration. In this case it can be said that T is a correction factor to reduce the stress of the elastic model. In other words, T as a factor which depends on microstructure of material can define the relation between the theoretical stress concentration actual stress concentrations. Brook [94] obtained the actual stress concentration of bone for 2.5mm hole under torsion using the absorbed energy by drilled and un-drilled bone about 1.65. The theoretical value of stress concentration for a homogenous isotropic material is 4.

In addition, T is a factor that can be applied to the elastic model to correct the effects of the non-linearity on the stress concentration. Applying the TCD to a non-linear model of bone - with the critical stress equal to UTS- can predict the fracture strength well. This means that a non-linear model contains the factor T . Therefore it can be said that, the non-linear model can be employed to apply the TCD, but in this case the critical stress is the same as the ultimate stress, i.e. $T=1$. If a linear model is employed, the factor of T has to be applied to obtain the critical distance. This is in agreement with the indentation problem. For indentation, bone was modelled as a non-linear material therefore there was no need to apply the T factor to the model.

The TCD can predict the effects of short crack as well as the long cracks. The PM predicted the toughness of bone for short cracks (R-curve) which was in good agreement with experimental work [37, 103] done by other workers. This is important as it shows that the TCD can be used to study the effects of voids in bone. This is important especially when the osteoporosis is studied. As the nano-indentation can explain the toughness of bone and the TCD can predict these results, therefore the critical distance can be calculated using a nano-indentation test as well.

Under indentation, bone fracture occurs in a plane which is under high levels of compression. The shear stress acting on the fracture plane is also high. The shear stress tends to cause fracture but high compression field causes resistance against it. The internal friction causes this resistance. This is in agreement with observations of compressive fatigue as Mode II cracking was displayed [133]. This mechanism can be explained using the Coulomb-Mohr failure criterion as it can explain the fracture of porous materials [125], especially rocks and other geological materials [124]. In the Coulomb-Mohr approach the shear fracture is assumed to occur on a given plane when a critical combination of shear and normal stress occurs. The mathematical function giving this critical combination is usually assumed to be a linear relationship.

The critical stress criterion (which in this case is defined using Coulomb-Mohr) depends on the failure mechanism of the material. The damage mechanism depends on the mode of loading [133]. This work suggests that the Coulomb-Mohr can be used to define the critical stress criterion to predict the failure of bone under compression or shear. It is expected that this method also works for porous and granular materials. Also, in porous materials in which Coulomb-Mohr can predict the failure, the Drucker-Prager yield model can predict the deformation and strain distribution better. It might be even better to model compression yielding of bone using Drucker-Prager however, there is not much data to show if this model works for bone or not.

The TCD could predict the effects of indentation direction well in spite of different failure mechanisms. In transverse indentation, deflection is the important toughening mechanism. In this case, the main crack is deflected and grows, perpendicular to the indentation direction, in the tangential plane. Bone is more brittle when the crack develops in the tangential direction [115]. Amongst tangential, longitudinal and transverse indentation, the fracture force for a given wedge is the largest for transverse and smallest for tangential indentation. This is in agreement with former works which showed that the fracture energy of compact bone was greater when cutting across the longitudinal axis than along the longitudinal axis [50, 61].

The fracture force is also related to the geometry of the indenter [54, 55, 50, 56]. The effect of wedge geometry on fracture force was predicted using the TCD. The prediction agreed with the experimental results performed by Mr. Reilly in the parallel project. The maximum errors of prediction were less than 20% compared to the experiments. This is an excellent prediction as there is always a lot of scatter in bone mechanical properties.

For the blunt wedges (large tip radius), the radius has a large effect on the fracture force in all indenting directions, longitudinal, transverse and tangential. The larger the radius the larger the fracture force. This is because of the increasing contact area with increasing tip radius. Increasing the radius from 50 μm to 700 μm , changes the longitudinal fracture force from about 1000N to around 3000N. Statistical analysis demonstrates that the increase in fracture force with increasing radius is significant. It is quite interesting, that there is not a major difference between the fracture load of a sharp blade and a blade with 50 μm radius. For blunt indenters the angle does not have large effect on the fracture force. The critical angle was defined for each radius as the minimum angle of wedge that affects the fracture force. This critical angle depends on indentation direction and increases with the radius of blade tip.

For indenters with small radii, the fracture force increases when increasing the angle. The experiments show that the larger the radius the less the effect of the angle on the fracture force. In fact, for the larger size of radius of indenter, the edges of the indenter that carry the effects of the angle are not in contact with bone before fracture. In this case, just the radius has the effect on the fracture force. The same result can be seen for the damage area for blunt indenters. For small radii, there is enough deformation before the fracture such that the edges of indenter have an effect on the fracture force. This agrees with the work done on orthogonal cutting of bone [54, 53, 56]. These workers reported an increase in cutting force with decreasing rake angle. The rake angle declines with increase of the wedge angle.

Looking at the damage zone at fracture shows that there is more damage during transverse indentation than longitudinal. The damage area in tangential indentation is less than that for longitudinal indentation. In the case of transverse and longitudinal indentation, the damage zone was predicted using a stress of 50-60% of ultimate stress while 80% of ultimate stress must be employed to predict the tangential damage zone. This shows that brittle failure occurs in tangential indentation and more ductile failure (yielding and micro cracking) in the other directions.

Though there is not much difference between the fracture force of very sharp blade and 50 μm one, nevertheless the damage area for 50 μm indenter is almost twice as large as that for a sharp blade. Therefore in designing of surgical blades it has to be noted that the damage formed during cutting can be reduced by using a very small radius.

The indentation fracture plane, were in tangential and longitudinal direction of bone. Interestingly the same value of critical distance ($L=320\mu\text{m}$) could predict the indentation fracture force. The critical distance value is of the same order as the brick size of plexiform bone. It shows that the brick structure affects the fracture of bone. Also there is not much difference between critical distance under compression and tensile loading. This is important because when using other methods based on LEFM defining fracture toughness in compression is difficult while the TCD can be applied to compression fracture as easily as tensile fracture.

It was seen from experimental results that the crack grows in the weakest possible direction. From three different planes, the tangential is the weakest and transverse is the strongest plane against fracture. Regarding the crack growth direction, the transverse direction is the strongest because cracks have to develop perpendicular to the osteons. Comparing the microstructure on longitudinal and tangential crack growth planes can explain why tangential is weaker. Bone microstructure arrangements are different in longitudinal and tangential planes, characterized by the layered canal system that is arranged normal to the longitudinal plane but parallel to the tangential plane. Therefore a tangential crack would travel along a layer of canals, but a longitudinal crack would have to propagate across these layers. Therefore the canal system in bovine bone is

mainly formed in the tangential plane and stacking up along the longitudinal direction of bone. Such a canal system causes a decrease of fracture toughness in tangential orientation because these cavities make bones less resistant to crack propagation. The fracture toughness in longitudinal direction has higher value because of the fewer cavities or natural discontinuities encountered by a crack in this orientation[115].

It was seen that the TCD is applicable to predict the fracture of bone in different directions in spite of different failure mechanisms. The difference between mechanisms of fracture in different directions affects the assumptions for applying LEFM to bone. Therefore the LEFM is not valid in all directions. Linear elastic fracture mechanics can be assumed to be valid for bone as long as crack propagation is limited to the longitudinal direction [3]. The advantage of the TCD is its capacity to predict the failure in different directions.

If the direction of crack propagation is known then TCD can be used to predict the initiation point of the crack. This approach was applied to the indentation problem to find the crack initiation point. It was found the TCD gives good prediction for crack initiation in all directions.

It was seen that damage starts at about 60%-80% of compressive ultimate stress. It demonstrates that initiation of microcracks is relatively easy. It is also in agreement with the results presented in chapter 3 for toughness of bone as it is increasing with the crack length. The microcracks, therefore, form at a smaller level of stress than some of the microcracks grow. Due to the high level of shear stress acting on the critical plane, the microcracks on this plane propagate and cause fracture.

CHAPTER 8. Conclusions

1. Theory of Critical Distances was applied to bone for the first time. The strength of bone is affected by cracks, notches and holes and the TCD is capable of predicting their effects. The TCD is a new approach which has here been used for the first time to study the stress concentration in bone.
2. The critical stress of bone is greater than the ultimate tensile stress. The ratio between the critical stress and ultimate stress (T) depends on the amount of nonlinearity before failure. The value for T for ceramics is about 1 as there is not much nonlinearity. It goes up to 4 and 10 for polymers and metals respectively. This is because of high inelastic deformation before failure. In bone the T value was found to be about 1.33 which is between the value for ceramics and polymers. In the case of indentation fracture the T factor was not required because a nonlinear model was employed.
3. The critical distance (L) is in the order of the size of the microstructure of bone. L was estimated to be about 0.3-0.4mm. This is in the order of the size of osteons and the distance between them. It demonstrates that the osteons have an effect on the fracture toughness of bone.
4. The critical distance value depends on orientation. In longitudinal crack growth the Volkmann's canal are discontinuities which might control the toughness. In

the transverse direction the distance between osteons is related to the critical distance which is in order of 250-400 μ m. In the tangential direction, the length of the Volkmann's canal might be effective on critical distance. This length is of the same order as the distance between osteons. Therefore it is expected that there is not much difference between the critical distance in transverse and tangential directions. In plexiform bone the critical distance value is in the order of the brick size.

5. The TCD could predict the fracture of bone during indentation, which involves high compressive stresses, accompanied by shear stresses. The Coulomb-Mohr criterion could explain these failures.
6. The crack initiation point was predicted using the TCD, with the assumption that the crack grew in the weakest available direction. The prediction agreed with the experiment results in longitudinal, transverse and tangential indentation.
7. The geometry of indenters affects the fracture force. The tip radius of the wedge has a large effect on the indentation fracture force. For a given wedge with certain tip radius, the angle will affect the fracture force only if it is larger than a certain angle.
8. The "weakest possible direction" theory to predict the direction of crack growth worked well for bone. Amongst the tangential, longitudinal and transverse directions, tangential is the weakest and transverse is the strongest direction.
9. The critical distance approach can be used to study the fracture of bone in all directions. This is another advantage of the TCD compared to LEFM.
10. The same approach is expected to work for porous materials such as rocks under compression and shear.
11. The mechanism of forming diffuse damage is different from the one for forming the main crack. In the main crack formation the shear stress plays an important role, but it was found that a principal stress criterion could better predict the initiation of microdamage.

Future works

This work was the first study of application of the Theory of Critical Distances to cortical bone. In this work it was shown that the TCD can be applied to bone however there are many questions have not been answered here. The following questions are potential for future work.

- ◆ How do the critical distance parameters change in different orientation of bone?
- ◆ Are the critical distance parameters of bone sensitive to strain rate or temperature?
- ◆ What is the physical significance of the critical distance parameters in different directions?
- ◆ How do the critical distance parameters of bone change with aging?
- ◆ Can the TCD predict the effect of aging and osteoporosis on bone?

References

- [1] Riggs BL, et al., "The worldwide problem of osteoporosis: Insights afforded by epidemiology," *Bone*, vol. 17, pp. S505-S511, 1995.
- [2] Cooper C, et al., "Hip fractures in the elderly: a world-wide projection," *Osteoporos Int*, vol. 2, pp. 285-9, 1992.
- [3] Bonfield W, "Advances in the fracture mechanics of cortical bone," *Journal of Biomechanics*, vol. 20, pp. 1071-1081, 1987.
- [4] Taylor D, *The theory of critical distances*, 2007, Elsevier science
- [5] Whitney JM, et al., "Stress fracture criteria for laminated composites containing stress-concentrations," *Journal of Composite Materials*, vol. 8, pp. 253-265, 1974.
- [6] Taylor D, et al., "Prediction of fatigue failure location on a component using a critical distance method," *International Journal of Fatigue*, vol. 22, pp. 735-742, 2000.
- [7] Taylor D, "A mechanistic approach to critical-distance methods in notch fatigue," *Fatigue & Fracture of Engineering Materials and Structures*, vol. 24, pp. 215-224, 2001.
- [8] Taylor D, et al., "The fatigue strength of compact bone in torsion," *Journal of Biomechanics*, vol. 36, pp. 1103-1109, 2003.
- [9] Susmel L, et al., "Two methods for predicting the multiaxial fatigue limits of sharp notches," *Fatigue & Fracture of Engineering Materials and Structures*, vol. 26, pp. 821-833, 2003.
- [10] Susmel L, et al., "Fatigue design in the presence of stress concentrations," *International Journal of Strain Analysis*, vol. 38, pp. 443-452, 2003.
- [11] Taylor D, et al., "The effect of stress concentrations on the fracture strength of polymethylmethacrylate," *Materials Science and Engineering A*, vol. 382, pp. 288-294, 2004.
- [12] Taylor D, "Predicting the fracture strength of ceramic materials using the theory of critical distances," *Engineering Fracture Mechanics*, vol. 71, pp. 2407-2416, 2004.
- [13] Taylor D, et al., "The fracture mechanics of finite crack extension," *Engineering Fracture Mechanics*, vol. 72, pp. 1021-1038, 2005.
- [14] Taylor D, "Analysis of fatigue failures in components using the theory of critical distances," *Engineering Failure Analysis*, vol. 12, pp. 906-914, 2005.
- [15] Cornetti P, et al., "Finite fracture mechanics: A coupled stress and energy failure criterion," *Engineering Fracture Mechanics*, vol. 73, pp. 2021-2033, 2006.
- [16] Susmel L, et al., "A simplified approach to apply the theory of critical distances to notched components under torsional fatigue loading," *International Journal of Fatigue*, vol. 28, pp. 417-430, 2006.
- [17] Bellett D, et al., "The effect of crack shape on the fatigue limit of three-dimensional stress concentrations," *International Journal of Fatigue*, vol. 28, pp. 114-123, 2006.
- [18] Taylor D, "The theory of critical distances in detail: The history, background and precise definition of the TCD," in *The Theory of Critical Distances*. Oxford: Elsevier Science Ltd, 2007, pp. 33-49.
- [19] Susmel L, et al., "The theory of critical distances to predict static strength of notched brittle components subjected to mixed-mode loading," *Engineering Fracture Mechanics*, vol. 75, pp. 534-550, 2008.

- [20] Carpinteri A, et al., "A finite fracture mechanics approach to structures with sharp V-notches," *Engineering Fracture Mechanics*, vol. 75, pp. 1736-1752, 2008.
- [21] Feng G, et al., "An analytical expression for the stress field around an elastoplastic indentation/contact," *Acta Materialia*, vol. 55, pp. 2929-2938, 2007.
- [22] Puttick KE, "The mechanics of indentation fracture in poly(methyl methacrylate)," *Journal of Physics D: Applied Physics*, vol. 4, pp. 595-604, 1978.
- [23] Puttick KE, et al., "Stress fields round indentations in poly(methyl methacrylate)," *Journal of Physics D: Applied Physics*, vol. 4, pp. 617, 1997.
- [24] Care G, et al., "Elastic-plastic indentation stress fields using the finite-element method," *Journal of Materials Science*, vol. 32, pp. 5653-5659, 1997.
- [25] Fischer-Cripps A, "Elastic-plastic behaviour in materials loaded with a spherical indenter," *Journal of Materials Science*, vol. 32, pp. 727-736, 1997.
- [26] Lawn BR, et al., "A computer simulation study of Hertzian cone crack growth," *International Journal of Fracture*, vol. 10, pp. 1-16, 1974.
- [27] Lawn BR, et al., "Review indentation fracture: principles and applications," *Journal of Material Science*, vol. 10, pp. 1049-1081, 1975.
- [28] Lawn BR, *Fracture of brittle solids*, 1975, Press Syndicate of the University of Cambridge
- [29] Wang F, et al., "Numerical simulation for three dimensional elastic-plastic contact with hardening behavior," *Journal of Tribology-Transactions of the Asme*, vol. 127, pp. 494-502, 2005.
- [30] Cook NGW, et al., "Observations of crack growth in hard rock loaded by an indenter," *International Journal of Rock Mechanics and Mining Science & Geomechanics Abstracts*, vol. 21, pp. 97-107, 1984.
- [31] Doyle J, et al., "Indentation of wood by wedges," *Wood Science and Technology*, vol. 19, pp. 47-55, 1985.
- [32] Pharr GM, "Measurement of mechanical properties by ultra-low load indentation," *Materials Science and Engineering: A*, vol. 253, pp. 151-159, 1998.
- [33] Bolshakov A, et al., "Influences of pileup on the measurement of mechanical properties by load and depth sensing indentation techniques," *Journal of Materials Research*, vol. 13, pp. 1049-1058, 1998.
- [34] Chiaia B, "Fracture mechanisms induced in a brittle material by a hard cutting indenter," *International Journal of Solids and Structures*, vol. 38, pp. 7747-7768, 2001.
- [35] Hengsberger S, et al., "Nanoindentation discriminates the elastic properties of individual human bone lamellae under dry and physiological conditions," *Bone*, vol. 30, pp. 178-184, 2002.
- [36] Fan Z, et al., "Three-dimensional finite element analysis of the effects of anisotropy on bone mechanical properties measured by nanoindentation," *Journal of Materials Research*, vol. 19, pp. 114-123, 2004.
- [37] Mullins LP, et al., "Measurement of the microstructural fracture toughness of cortical bone using indentation fracture," *J Biomech*, 2007.
- [38] Zysset PK, et al., "Elastic modulus and hardness of cortical and trabecular bone lamellae measured by nanoindentation in the human femur," *Journal of Biomechanics*, vol. 32, pp. 1005-1012, 1999.
- [39] Rho J-Y, et al., "Effects of drying on the mechanical properties of bovine femur measured by nanoindentation," *Journal of Materials Science: Materials in Medicine*, vol. 10, pp. 485-488, 1999.

- [40] Rho J-Y, et al., "Elastic properties of microstructural components of human bone tissue as measured by nanoindentation," *Journal of Biomedical Materials Research*, vol. 45, pp. 48-54, 1999.
- [41] Wang XJ, et al., "Elastic modulus and hardness of cortical and trabecular bovine bone measured by nanoindentation," *Transactions of Nonferrous Metals Society of China*, vol. 16, pp. s744-s748, 2006.
- [42] Tang B, et al., "Viscoelastic effects during depth-sensing indentation of cortical bone tissues," *Philosophical Magazine*, vol. 86, pp. 5653-5666, 2006.
- [43] Wesley M Johnson MS, et al., "Microindentation in bone: Hardness variation with five independent variables," *Journal of Materials Science: Materials in Medicine*, vol. 18, pp. 591-597, 2007.
- [44] Hassan R, et al., "Fracture toughness of human enamel," *J Dent Res*, vol. 60, pp. 820-827, 1981.
- [45] White SN, et al., "Controlled failure mechanisms toughen the dentino-enamel junction zone," *The Journal of Prosthetic Dentistry*, vol. 94, pp. 330-335, 2005.
- [46] Agrawal KR, et al., "The mechanics of the first bite," *Proceedings of the Royal Society B: Biological Sciences*, vol. 270, pp. 1277-1282, 2003.
- [47] Lucas PW, et al., "FOOD TEXTURE AND ITS EFFECT ON INGESTION, MASTICATION AND SWALLOWING," *Journal of Texture Studies*, vol. 35, pp. 159-170, 2004.
- [48] Vincent JFV, "Application of fracture mechanics to the texture of food," *Engineering Failure Analysis*, vol. 11, pp. 695-704, 2004.
- [49] Vincent JFV, et al., "The Use of Critical Stress Intensity Factor to Quantify Hardness and Crunchiness Objectively," *Journal of Texture Studies* vol. 33, pp. 149-159, 2002.
- [50] King MJ, "Knife and impact cutting of lamb bone," *Meat Science*, vol. 52, pp. 29-38, 1999.
- [51] Tatsuya M, et al., "An Application of Indentation Contact Mechanics to the Tactile Sensor," *Nippon Kikai Gakkai Robotikusu, Mekatoronikusu Koenkai Koen Ronbunshu*, 2006.
- [52] Krause WR, et al., "Temperature elevations in orthopaedic cutting operations," *Journal of Biomechanics*, vol. 15, pp. 267-269, 1982.
- [53] Jacobs CH, et al., "A study of the bone machining process--Orthogonal cutting," *Journal of Biomechanics*, vol. 7, pp. 131-132, 1974.
- [54] Krause WR, "Orthogonal bone cutting: saw design and operating characteristics," *Journal of Biomechanical Engineering*, vol. 109, pp. 267-271, 1987.
- [55] Giraud JY, et al., "Bone cutting," *Clinical physics and physiological measurement : an official journal of the Hospital Physicists' Association, Deutsche Gesellschaft für Medizinische Physik and the European Federation of Organisations for Medical Physics*, vol. 12, pp. 1-19, 1991.
- [56] Plaskos C, et al., "Modelling and Optimization of Bone-Cutting Forces in Orthopaedic Surgery," in *Medical Image Computing and Computer-Assisted Intervention - MICCAI 2003*, 2003, pp. 254-261.
- [57] Matthews LS, et al., "Temperatures measured in human cortical bone when drilling," *Journal of Bone Joint Surg* vol. 54-A, pp. 297-308, 1972.
- [58] Natali C, et al., "Orthopaedic bone drills—can they be improved?," *Journal of Bone Joint Surg* vol. 78-B, pp. 357-362, 1996.

- [59] Hillery MT, et al., "Temperature effects in the drilling of human and bovine bone," *Journal of Materials Processing Technology*, vol. 92-93, pp. 302-308, 1999.
- [60] Davidson SRH, et al., "Drilling in Bone: Modeling Heat Generation and Temperature Distribution," *Journal of Biomechanical Engineering*, vol. 125, pp. 305-314, 2003.
- [61] Wiggins KL, et al., "Drilling of bone," *Journal of Biomechanics*, vol. 9, pp. 553-554, 1976.
- [62] de Borst R, et al., "Discrete vs smeared crack models for concrete fracture: bridging the gap," *International Journal for Numerical and Analytical Methods in Geomechanics*, vol. 28, pp. 583-607, 2004.
- [63] Neuber H, " " *Forsch. Ing.-Wes.*, vol. 7 pp. 271-281, 1936.
- [64] Neuber H, "Theory of Notch Stresses.," *Springer*, 1985.
- [65] Peterson RE, Notch-sensitivity 1959, New York, McGraw Hill
- [66] El Haddad MH, et al., "Fatigue crack propagation of short cracks," *Journal of Engineering Materials and Technology*, vol. 101, pp. 42-46, 1979.
- [67] Lukas P, et al., "Fatigue limit of notched bodies," *Materials Science and Engineering*, vol. 34 pp. 61-66, 1978.
- [68] Waddoups ME, et al., "Macroscopic fracture mechanics of advanced composite materials," *Journal of Composite Materials*, vol. 5, pp. 446-454, 1971.
- [69] Seweryn A, et al., "Verification of brittle fracture criteria for elements with V-shaped notches," *Engineering Fracture Mechanics*, vol. 69, pp. 1487-1510, 2002.
- [70] Tanaka K, "Engineering formulae for fatigue strength reduction due to crack-like notches," *International Journal of Fracture*, vol. 22, pp. R39-R45, 1983.
- [71] Taylor D, "Geometrical effects in fatigue: a unifying theoretical model," *International Journal of Fatigue*, vol. 21, pp. 413-420, 1999.
- [72] Taylor D, "The theory of critical distances applied to the prediction of brittle fracture in metallic materials," *Structural Integrity and Durability*, vol. 1, pp. 145-154, 2006.
- [73] Creager M, et al., "Elastic field equations for blunt cracks with reference to stress corrosion cracking," *International Journal of Fracture Mechanics*, vol. 3, pp. 247-252, 1967.
- [74] Sih GC, et al., "On Cracks in Rectilinearly Anisotropic Bodies," *International Journal of Fracture Mechanics*, vol. 1 pp. 189-203, 1965, .
- [75] Taylor D, et al., "The validation of some methods of notch fatigue analysis," *Fatigue and Fracture of Engineering Materials and Structures*, vol. 23, pp. 387-394, 2000.
- [76] Awerbuch J, et al., "Notched strength of composite laminates: predictions and experiments: a review," *Journal of Reinforced Plastics and Composites*, vol. 4, pp. 3-159, 1985.
- [77] Kinloch AJ, et al., "Crack propagation in rubber-toughened epoxy," *International Conference on Yield, Deformation and Fracture, Cambridge Plastics and Rubber Institute, London*, pp. 29.1-29.6, 1982
- [78] Hazenberg JG, et al., "Mechanisms of short crack growth at constant stress in bone," *Biomaterials*, vol. 27, pp. 2114-2122, 2006.
- [79] Lucksanasombool P, et al., "Fracture toughness of bovine bone: influence of orientation and storage media," *Biomaterials*, vol. 22, pp. 3127-3132, 2001.
- [80] Behiri JC, et al., "Orientation dependence of the fracture mechanics of cortical bone," *Journal of Biomechanics*, vol. 22, pp. 863-867, 1989.

- [81] Yan J, et al., "Fracture toughness of manatee rib and bovine femur using a chevron-notched beam test," *Journal of Biomechanics*, vol. 39, pp. 1066-74, 2006.
- [82] Robertson DM, et al., "Fracture toughness, critical crack length and plastic zone size in bone," *Journal of Biomechanics*, vol. 11, pp. 359-364, 1978.
- [83] Moyle DD, et al., "Fracture properties of bovine tibial bone," *Journal of Biomechanics*, vol. 19, pp. 919-927, 1986.
- [84] Bonfield W, et al., "Fracture toughness of compact bone," *Journal of Biomechanics*, vol. 9, pp. 131-132, 1976.
- [85] Norman TL, et al., "Fracture toughness of human bone under tension," *Journal of Biomechanics*, vol. 28, pp. 309-320, 1995.
- [86] Behiri JC, et al., "Fracture mechanics of bone: The effects of density, specimen thickness and crack velocity on longitudinal fracture," *Journal of Biomechanics*, vol. 17, pp. 25-34, 1984.
- [87] Behiri JC, et al., "Crack velocity dependence of longitudinal fracture in bone," *Journal of Materials Science*, vol. V15, pp. 1841-1849, 1980.
- [88] Bonfield W, et al., "Deformation and fracture of bone," *Journal of Applied Physics*, vol. 37, pp. 869-875, 1966.
- [89] Yan J, et al., "Effect of temperature on the fracture toughness of compact bone," *Journal of Biomechanics*, vol. In Press, Corrected Proof, 2006.
- [90] Piekarski K, "Fracture of Bone," *Journal of Applied Physics*, vol. 41, pp. 215-223, 1970.
- [91] Silva FC, et al., "Compartmento a Fractura de osso compacto da tibia de boi, ," *Materiais 87-3-Encontro nacional da sociedade Portuguesa de Materiais*, pp. 345-357, 1987.
- [92] Melvin JW, et al., "Crack propagation in Bone," *Biomaterial Symposium AMD 2(Edited by Fung, Y.C. and Brighton, J.A.). American society of mechanical engineers, NEW YORK*, 1973.
- [93] McBroom RJ, et al., "Strength reductions from metastatic cortical defects in long bones," *Journal of Orthopaedic Research*, vol. 6, pp. 369-378, 1988.
- [94] Brooks DB, et al., "The Biomechanics of Torsional Fractures: The Stress Concentration Effect of a Drill Hole " *Journal of Bone and Joint Surgery Am* vol. 52A, pp. 507-514, 1970.
- [95] Edgerton BC, et al., "Torsional strength reduction due to cortical defects in bone," *Journal of Orthopaedic Research*, vol. 8, pp. 851-855, 1990.
- [96] Hipp JA, et al., "Structural consequences of transcortical holes in long bones loaded in torsion," *Journal of Biomechanics*, vol. 23, pp. 1261-8, 1990.
- [97] Van Buskrik W.C. CSC, Ward R.N., "Ultrasonic measurement of orthotropic elastic constants of bovine femoral bone," *J. Biomechanical Engineering*, vol. 103, pp. 67-72, 1981.
- [98] Peterlik H, et al., "From brittle to ductile fracture of bone," *Nat Mater*, vol. 5, pp. 52-55, 2006.
- [99] Malik CL, et al., "Equine cortical bone exhibits rising R-curve fracture mechanics," *Journal of Biomechanics*, vol. 36, pp. 191-198, 2003.
- [100] Nalla RK, et al., "On the origin of the toughness of mineralized tissue: microcracking or crack bridging?," *Bone*, vol. 34, pp. 790-798, 2004.
- [101] Liu D, et al., "Anisotropic mechanical properties of lamellar bone using miniature cantilever bending specimens," *Journal of Biomechanics*, vol. 32, pp. 647-654, 1999.

- [102] Kruzic JJ, et al., "Propagation of surface fatigue cracks in human cortical bone," *Journal of Biomechanics*, vol. 39, pp. 968-972, 2006.
- [103] Nalla RK, et al., "Effect of aging on the toughness of human cortical bone: evaluation by R-curves," *Bone*, vol. 35, pp. 1240-1246, 2004.
- [104] Nalla RK, et al., "Mechanistic fracture criteria for the failure of human cortical bone," *Nature Materials*, vol. 2, pp. 164-168, 2003.
- [105] Vashishth D, et al., "Crack growth resistance in cortical bone: concept of microcrack toughening," *Journal of Biomechanics*, vol. 30, pp. 763-769, 1997.
- [106] Zioupos P, et al., "Experimentally determined microcracking around a circular hole in a flat plate of bone: comparison with predicted stresses," *Philosophical Transactions: Biological Sciences*, vol. 347, pp. 383-396, 1995.
- [107] Ritchie RO, "Mechanisms of fatigue crack propagation in metals, ceramics and composites: Role of crack tip shielding," *Materials Science and Engineering*, vol. 103, pp. 15-28, 1988.
- [108] Pang SS, et al., "A force-indentation model for brittle rocks," *Rock Mechanics and Rock Engineering*, vol. 22, pp. 127-148, 1989.
- [109] Chamay A, "Mechanical and morphological aspects of experimental overload and fatigue in bone," *Journal of Biomechanics*, vol. 3, pp. 263-264, 1970.
- [110] Currey JD, *Bones: structure and mechanics*, 1932, Princeton University Press
- [111] Reilly DT, et al., "The elastic modulus for bone," *Journal of Biomechanics*, vol. 7, pp. 271-272, 1974.
- [112] Reilly DT, et al., "The elastic and ultimate properties of compact bone tissue," *Journal of Biomechanics*, vol. 8, pp. 393-396, 1975.
- [113] Cezayirlioglu H, et al., "Anisotropic yield behavior of bone under combined axial force and torque," *Journal of Biomechanics*, vol. 18, pp. 61-69, 1985.
- [114] Edgerton BC, et al., "Cortical defects in bone: a new torsional model and a critical analysis of the stress riser and open section effects under torsional load load " in Report submitted in consideration for the conventry award Rochester, Minnesota: Biomechanics Laboratory, Mayo clinic, 1987.
- [115] Wang X, et al., "Fracture toughness of bone using a compact sandwich specimen: Effects of sampling sites and crack orientations," *Journal of Biomedical Materials Research*, vol. 33, pp. 13-21, 1996.
- [116] Norman TL, et al., "Effect of groove on bone fracture toughness."
- [117] Peterlik H, et al., "Orientation dependent fracture toughness of lamellar bone," *International Journal of Fracture*, vol. 139, pp. 395-405, 2006.
- [118] Wesley M Johnson MS, et al., "Charactrization of Microindentation in Bone Via Scaning Electron Microscopy," *Summer Bioengineering Conference*, vol. FL,USA, 2003.
- [119] Le-Ngoc L, et al., "A cellular finite element model for the cutting of softwood across the grain," *International Journal of Mechanical Sciences*, vol. 42, pp. 2283-2301, 2000.
- [120] Susmel L, "Modified Wohler curve method, theory of critical distances and Eurocode 3: A novel engineering procedure to predict the lifetime of steel welded joints subjected to both uniaxial and multiaxial fatigue loading," *International Journal of Fatigue*, vol. In Press, Corrected Proof, pp. 435.
- [121] Taylor D, "Multiaxial loading: Fracture and fatigue under complex stress states," in *The Theory of Critical Distances*. Oxford: Elsevier Science Ltd, 2007, pp. 213-233.

- [122] Araujo JA, et al., "On the use of the Theory of Critical Distances and the Modified Wohler Curve Method to estimate fretting fatigue strength of cylindrical contacts," *International Journal of Fatigue*, vol. 29, pp. 95-107, 2007.
- [123] Susmel L, et al., "Non-propagating cracks and high-cycle fatigue failures in sharply notched specimens under in-phase Mode I and II loading," *Engineering Failure Analysis*, vol. 14, pp. 861-876, 2007.
- [124] Ramamurthy T, "Shear strength response of some geological materials in triaxial compression," *International Journal of Rock Mechanics and Mining Sciences*, vol. 38, pp. 683-697, 2001.
- [125] Palchik V, "Application of Mohr-Coulomb failure theory to very porous sandy shales," *International Journal of Rock Mechanics and Mining Sciences*, vol. 43, pp. 1153-1162, 2006.
- [126] Follansbee PS, et al., "Quasi-static normal indentation of an elasto-plastic half-space by a rigid sphere--I : Analysis," *International Journal of Solids and Structures*, vol. 20, pp. 81-91, 1984.
- [127] Reilly DT, et al., "The Mechanical Properties of Cortical Bone," *J Bone Joint Surg Am*, vol. 56, pp. 1001-1022, 1974.
- [128] Taylor D, et al., "Living with cracks: Damage and repair in human bone," *Nat Mater*, vol. 6, pp. 263-268, 2007.
- [129] Zioupos P, et al., "An examination of the micromechanics of failure of bone and antler by acoustic emission tests and Laser Scanning Confocal Microscopy," *Medical Engineering & Physics*, vol. 16, pp. 203-212, 1994.
- [130] Zioupos P, et al., "The extent of microcracking and the morphology of microcracks in damaged bone," *Journal of Materials Science*, vol. 29, pp. 978-986, 1994.
- [131] Vashishth D, et al., "In vivo diffuse damage in human vertebral trabecular bone," *Bone*, vol. 26, pp. 147-152, 2000.
- [132] Vashishth D, et al., "Experimental validation of a microcracking-based toughening mechanism for cortical bone," *Journal of Biomechanics*, vol. 36, pp. 121-124, 2003.
- [133] George WT, et al., "Damage mechanisms and failure modes of cortical bone under components of physiological loading," *Journal of Orthopaedic Research*, vol. 23, pp. 1047-1053, 2005.
- [134] Diab T, et al., "Effects of damage morphology on cortical bone fragility," *Bone*, vol. 37, pp. 96-102, 2005.
- [135] Burr DB, et al., "Alterations to the en bloc basic fuchsin staining protocol for the demonstration of microdamage produced in vivo," *Bone*, vol. 17, pp. 431-433, 1995.
- [136] Lee TC, et al., "Sequential labelling of microdamage in bone using chelating agents," *Journal of Orthopaedic Research*, vol. 18, pp. 322-325, 2000.
- [137] O'Brien FJ, et al., "An improved labelling technique for monitoring microcrack growth in compact bone," *Journal of Biomechanics*, vol. 35, pp. 523-526, 2002.
- [138] Parsamian GP, et al., "Diffuse damage accumulation in the fracture process zone of human cortical bone specimens and its influence on fracture toughness," *Journal of Materials Science: Materials in Medicine*, vol. 12, pp. 779-783, 2001.
- [139] Hoey D, et al., "Fatigue in porous PMMA: The effect of stress concentrations," *International Journal of Fatigue*, vol. In Press, Corrected Proof, pp. 99.
- [140] McBroom RJ, et al., "strength reductions from metastatic cortical defects in long bones," *J orthopaedic research*, vol. 6, pp. 369-378, 1988.

- [141] Edgerton BC, et al., "Torsional strength reduction due to cortical defects in bone," *J Orthopaedic Research*, vol. 8, pp. 851-855, 1990.
- [142] Peterson DL, et al., "Fracture of long bone: rate effects under singular and combined loading states," *Journal of Orthopaedic Research*, vol. 1, pp. 244-250, 1984.
- [143] Habernek H, et al., "Cerclage for torsional fractures of the tibia," *Journal of Bone and Joint Surgery Br*, vol. 71-B, pp. 311-313, 1989.
- [144] Rho J-Y, et al., "Mechanical properties and the hierarchical structure of bone," *Medical Engineering & Physics*, vol. 20, pp. 92-102, 1998.
- [145] O'Brien FJ, et al., "The behaviour of microcracks in compact bone," *European Journal of Morphology*, vol. 42, pp. 71 - 79, 2005.
- [146] O'Brien FJ, et al., "The effect of bone microstructure on the initiation and growth of microcracks," *Journal of Orthopaedic Research*, vol. 23, pp. 475-480, 2005.
- [147] Martin RB, et al., "In vitro fatigue behavior of the equine third metacarpus: Remodeling and microcrack damage analysis," *Journal of Orthopaedic Research*, vol. 14, pp. 794-801, 1996.
- [148] Lee TC, et al., "Fluorescence-aided detection of microdamage in compact bone," *Journal of Anatomy*, vol. 193, pp. 179-184, 1998.
- [149] Lee TC, et al., "Detecting microdamage in bone," *Journal of Anatomy*, vol. 203, pp. 161-172, 2003.
- [150] Taylor D, "Ceramics: Brittle fracture in engineering ceramics, building materials, geological materials and nanomaterials," in *The Theory of Critical Distances*. Oxford: Elsevier Science Ltd, 2007, pp. 63-91.
- [151] Taylor D, "Polymers: Brittle fracture in polymeric materials," in *The Theory of Critical Distances*. Oxford: Elsevier Science Ltd, 2007, pp. 93-118.
- [152] Currey JD, "Stress Concentrations in Bone," *Quarterly Journal of Microscopical Science*, vol. s3-103, pp. 111-133, 1962.

Appendices

Appendix I: Stress Intensity Factor for Orthotropic Materials

Calculating the Stress Intensity Factor (SIF) using Ansys is limited to linear elastic problems with a homogeneous, isotropic material near the crack region. Therefore, for the orthotropic material (like bone) an analytical method was used to calculate this parameter.

Sih (1965) developed an expression for these sorts of materials. This expression was used to look at a 2D crack. The x-y plane was picked as the plane of analysis with the crack along the x-axis. For a linear anisotropic Hookian material the stress and strain are related as follows:

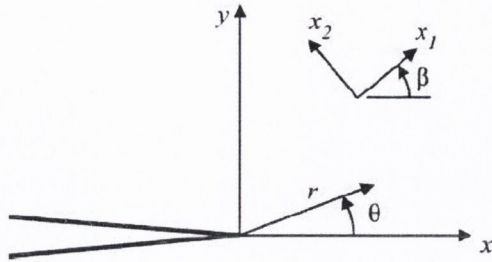
$$\{\varepsilon\} = [E]\{\sigma\}$$

$$\begin{Bmatrix} \varepsilon_x \\ \varepsilon_y \\ \varepsilon_z \\ \gamma_{xy} \\ \gamma_{yz} \\ \gamma_{zx} \end{Bmatrix} = \begin{bmatrix} 1/E_1 & -\nu_{21}/E_2 & -\nu_{31}/E_3 & 0 & 0 & 0 \\ -\nu_{12}/E_1 & 1/E_2 & -\nu_{32}/E_3 & 0 & 0 & 0 \\ -\nu_{13}/E_1 & -\nu_{23}/E_2 & 1/E_3 & 0 & 0 & 0 \\ 0 & 0 & 0 & 1/G_{12} & 0 & 0 \\ 0 & 0 & 0 & 0 & 1/G_{23} & 0 \\ 0 & 0 & 0 & 0 & 0 & 1/G_{31} \end{bmatrix} \begin{Bmatrix} \sigma_x \\ \sigma_y \\ \sigma_z \\ \tau_{xy} \\ \tau_{yz} \\ \tau_{zx} \end{Bmatrix}$$

If the in-plane material axes are rotated with respect to the Cartesian axes then :

$$\{\varepsilon\} = [T]^T [E][T]\{\sigma\} = [S]\{\sigma\}$$

Where T is the rotation matrix, which is expressed in the following in the simple case of rotation around x axes. β is the angle between the x Cartesian axis and the x material axis.



$$[T] = \begin{bmatrix} \cos^2 \beta & \sin^2 \beta & 0 & \cos \beta \cdot \sin \beta & 0 & 0 \\ \sin^2 \beta & \cos^2 \beta & 0 & -\cos \beta \cdot \sin \beta & 0 & 0 \\ 0 & 0 & 1 & 0 & 0 & 0 \\ -2 \cos \beta \cdot \sin \beta & 2 \cos \beta \cdot \sin \beta & 0 & \cos^2 \beta - \sin^2 \beta & 0 & 0 \\ 0 & 0 & 0 & 0 & \cos \beta & -\sin \beta \\ 0 & 0 & 0 & 0 & \sin \beta & \cos \beta \end{bmatrix}$$

In the case of plane stress and plane strain the equation becomes simpler. For the plane stress state, we have:

$$\begin{Bmatrix} \epsilon_x \\ \epsilon_y \\ \gamma_{xy} \end{Bmatrix} = \begin{bmatrix} S_{11} & S_{12} & S_{14} \\ & S_{22} & S_{24} \\ Sym & & S_{44} \end{bmatrix} \begin{Bmatrix} \sigma_x \\ \sigma_y \\ \tau_{xy} \end{Bmatrix}$$

And in the plane strain state:

$$\begin{Bmatrix} \varepsilon_x \\ \varepsilon_y \\ \gamma_{xy} \end{Bmatrix} = \begin{bmatrix} S_{11} - \frac{S_{12}S_{13}}{S_{33}} & S_{12} \left(1 - \frac{S_{23}}{S_{33}} \right) & S_{14} - \frac{S_{12}S_{34}}{S_{33}} \\ & S_{22} \left(1 - \frac{S_{23}}{S_{33}} \right) & S_{24} - \frac{S_{22}S_{34}}{S_{33}} \\ \text{Sym} & & S_{44} - \frac{S_{22}S_{34}}{S_{33}} \end{bmatrix} \begin{Bmatrix} \sigma_x \\ \sigma_y \\ \tau_{xy} \end{Bmatrix} =$$

$$\begin{bmatrix} S'_{11} & S'_{12} & S'_{14} \\ & S'_{22} & S'_{24} \\ \text{Sym} & & S'_{44} \end{bmatrix} \begin{Bmatrix} \sigma_x \\ \sigma_y \\ \tau_{xy} \end{Bmatrix}$$

The only difference between the plane stress and plane strain conditions is the matrix of coefficients.

From Sih et al. the in-plane stress near a crack tip, can be expressed in polar coordinates:

$$\sigma_x = \frac{K_I}{\sqrt{2\pi r}} \operatorname{Re} \left[\frac{\mu_1 \mu_2}{\mu_1 - \mu_2} \left(\frac{\mu_2}{d_2} - \frac{\mu_1}{d_1} \right) + \frac{K_{II}}{K_I} \frac{1}{\mu_1 - \mu_2} \left(\frac{\mu_2^2}{d_2} - \frac{\mu_1^2}{d_1} \right) \right]$$

$$\sigma_y = \frac{K_I}{\sqrt{2\pi r}} \operatorname{Re} \left[\frac{1}{\mu_1 - \mu_2} \left(\frac{\mu_1}{d_2} - \frac{\mu_2}{d_1} \right) + \frac{K_{II}}{K_I} \frac{1}{\mu_1 - \mu_2} \left(\frac{1}{d_2} - \frac{1}{d_1} \right) \right]$$

$$\tau_{xy} = \frac{K_I}{\sqrt{2\pi r}} \operatorname{Re} \left[\frac{\mu_1 \mu_2}{\mu_1 - \mu_2} \left(\frac{1}{d_1} - \frac{1}{d_2} \right) + \frac{K_{II}}{K_I} \frac{1}{\mu_1 - \mu_2} \left(\frac{\mu_1}{d_1} - \frac{\mu_2}{d_2} \right) \right]$$

$$u = K_I \sqrt{\frac{2r}{\pi}} \operatorname{Re} \left[\frac{1}{\mu_1 - \mu_2} \left(\mu_1 p_2 d_2 - \mu_2 p_1 d_1 + \frac{K_{II}}{K_I} [p_2 d_2 - p_1 d_1] \right) \right]$$

$$v = K_I \sqrt{\frac{2r}{\pi}} \operatorname{Re} \left[\frac{1}{\mu_1 - \mu_2} \left(\mu_1 q_2 d_2 - \mu_2 q_1 d_1 + \frac{K_{II}}{K_I} [q_2 d_2 - q_1 d_1] \right) \right]$$

With:

$$d_i = \sqrt{\cos \theta + \mu_i \sin \theta}$$

$$p_i = S_{11}\mu_i^2 + S_{12} - S_{14}\mu_i$$

$$q_i = S_{12}\mu_i + \frac{S_{22}}{\mu_i} - S_{24}$$

In which μ_1, μ_2 are two roots with positive imaginary parts of the equation :

$$S_{11}\mu^4 - 2S_{14}\mu^3 + (2S_{12} + S_{44})\mu^2 - 2S_{24}\mu + S_{22} = 0$$

In this case, the energy release rate can be obtained by substituting the stress and displacement into Irwin's crack closure integral:

$$G = \lim_{\Delta L \rightarrow 0} \frac{1}{\Delta L} \int_0^{\Delta L} \sigma_{2i}(\Delta L - r, \theta = 0) u_i(r, \theta = \pi) dr$$

By separating modes:

$$G_I = -\frac{1}{2} K_I S_{22} \operatorname{Im} \left[\frac{K_I (\mu_1 + \mu_2) + K_{II}}{\mu_1 \mu_2} \right]$$

$$G_{II} = -\frac{1}{2} K_{II} S_{11} \operatorname{Im} [K_{II} (\mu_1 + \mu_2) + K_I \mu_1 \mu_2]$$

SIF's can be calculated from the above equations.

Example:

Here, the above method was applied to a plate with a hole in the centre. It was assumed that the plate is wide enough compare to the radius of the hole and also it's a plane stress state condition. The comparison is being done in two different material properties, isotropic and orthotropic.

σ_u	K_c	L
28.32	22.4522	0.2

In the case of isotropic material:

$$E=2.38e3$$

$$\nu=0.4$$

$$G_c = K_c^2 / E = 0.211$$

In the case of orthotropic:

$$E_{xx}=11000 \quad E_{yy}=20400 \quad E_{zz}=11000$$

$$G_{xy}=4100 \quad G_{xz}=4100 \quad G_{yz}=4100$$

$$\nu_{xy}=0.31 \quad \nu_{xz}=0.49 \quad \nu_{yz}=0.31$$

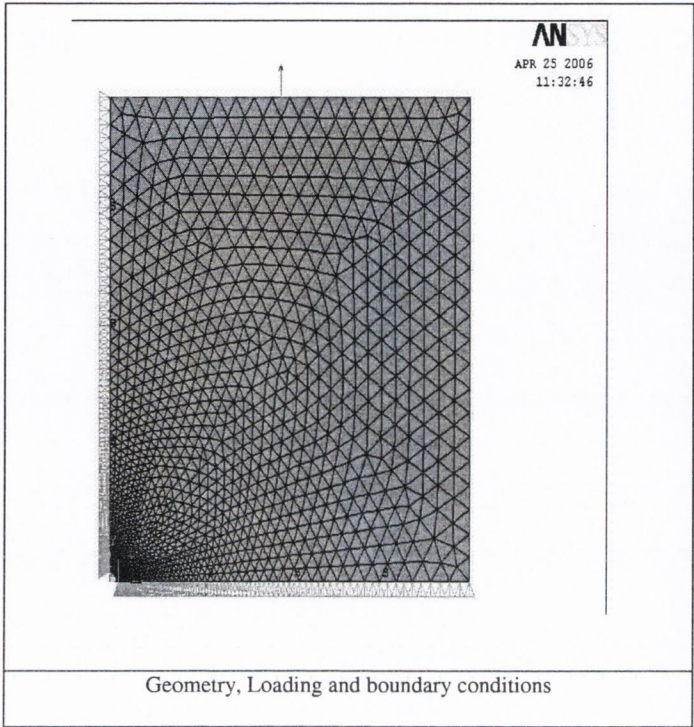
$$[S] = \begin{bmatrix} 9.091E-5 & -2.8182E-5 & 0 \\ & 4.902E-5 & 0 \\ \text{Sym} & & 2.439E-04 \end{bmatrix}$$

$$\mu_1 = 1.32507583i \quad \mu_2 = 0.554166829i$$

$$G_I = \frac{1}{2} S_{22} \frac{\mu_1 + \mu_2}{\mu_1 \mu_2} \cdot K_I^2$$

$$\text{Then } G_c = 3.162E-02.$$

Because of symmetry in our problem $K_{II}=0$.



Appendix II: More Details about the FE Modeling

Elements

Plane82, was used to mesh the model. This is an 8-node element which provides more accurate results for mixed (quadrilateral-triangular) automatic meshes and can tolerate irregular shapes without as much loss of accuracy. This element has compatible displacement shapes and is well suited to model curved boundaries.

Material

Bone was modeled as a bi-linear, isotropic material. The Von Mises yield criterion was coupled with an isotropic work hardening assumption. The material behavior is described by a bilinear stress-strain curve starting at the origin with positive stress and strain values. The initial slope of the curve is taken as the elastic modulus of the material. At the specified yield stress, the curve continues along the second slope defined by the tangent modulus. The tangent modulus cannot be less than zero nor greater than the elastic modulus.

Contact Modeling

Contact problems which are highly nonlinear and require significant computer resources to solve, present two significant difficulties. First, generally the regions of contact are unknown until the problem is run. Depending on the loads, material, boundary conditions, and other factors, surfaces can come into and go out of contact with each other in a largely unpredictable and abrupt manner. Second, most contact problems need to account for friction. There are several friction laws and models to choose from, and all are nonlinear. Frictional response can be chaotic, making solution convergence difficult. The model of contact in our problem is simple. The amount of mesh required around the contact area is a major issue. The indenter is modeled as a rigid material because we are not interested in stress distribution and deformation of indenter, and because steel is much stiffer than bone. The Contact172 and Target169 elements were employed at contact due to their compatibility with the Plane82. The standard behavior was selected.

Path Operation

To apply the critical distance to the model, the stress on a fracture line is required. Therefore, a path is defined as the fracture line. Generally the FE models which are associated with the TCD assume elastic material behaviour. There is not a large deformation at the critical force for elastic materials. In this case the path can be defined in the original model. However, in the case of indentation this is a high deformation at the critical load. Therefore a non-linear material model is used, and the fracture line where the deformation is high must be defined in the deformed model. After solving the model, the nodal coordinates were upgraded using Upcoord command in the Preprocessor menu. Then the new coordinates which were computed using $X' = X + u$ are used to define the path.

Appendix III: Indentation Using 20°-300µm blade

This is an example of the Macros as written in ANSYS. This is to model the indentation of 20°-300µm.

```
!***** Dimensions are in mm( Length), N (Force), MPa (Pressure)
E=18000
YE=0.01      ! Ratio between Yield stress and Young's Modulus
ETE=1/100    ! Ratio between Tangent Modulus and Young's Modulus
```

```
ra=0.5
wt=8
a=8          ! Dimension of specimen mm
h=2          ! Height of blade
x=-0.00001  ! To close the gap between blade and bone
bladeangle=20      ! Wedge angle of blade in degrees
angle=90+bladeangle/2
rock=0.3       !Blade tip radius in micron
toler=0.1
*afun,deg
inter=x+(1-1/sin(bladeangle/2))*rock
!***** Making Key-point
```

```
/prep7
r1=0.05
r2=0.6
k,1,r1,0,0
k,2,0,0,0
k,3,0,-r1,0
k,4,r2,0,0
k,5,0,-r2,0
k,6,0,-a,0
k,7,a/2,-a,0
k,8,a/2,-a/2,0
k,9,a/2,0,0
```

```
!***** Making lines
```

```
lstr,1,2
lstr,2,3
lstr,3,5
lstr,5,6
lstr,6,7
lstr,7,8
lstr,8,9
lstr,9,4
lstr,4,1
larc,3,1,2,r1
larc,5,4,2,r2
numcmp,all
```

```

!***** Areas
al,1,2,10
al,10,3,11,9
al,8,11,4,5,6,7
!***** Material type
MP,ex,1,E
MP,nuxy,1,.31
MP,dens,1,8490
TB,BISO,1
TB,DATA,1,E*YE
TB,DATA,2,E*ETE

Mp,ex,2,210000
Mp,nuxy,2,0.3

Mp,ex,3,204000
Mp,nuxy,3,0.3
!***** Elements type
et,1,82
keyopt,1,3,2      ! Plane strain
keyopt,1,6,1

et,2,169          ! Target

et,3,172          ! Contact
keyopt,3,2,3
keyopt,3,3,0
keyopt,3,5,1
keyopt,3,9,0
keyopt,3,10,1
keyopt,3,12,0     ! Standard behavior
r,2,rock
!***** Meshing specimen
div1=20
div2=40
div3=20
div4=40

Type, 1
Mat, 1
Lesize,1,,div1,1
Lesize,2,,div1,1
Lesize,11,,div2
Lesize,3,,div2,10
Lesize,9,,div2,1/10
Lesize,10,,div2
Lesize,4,,div4,10
Lesize,8,,div3,1/10

```

```

Lesize,6,,div3
Lesize,7,,div3
Lesize,5,,div3

Mshape,0,2D
Mshkey,0
Amesh,1

Mshkey,1
Amesh,2

Mshkey,0
Amesh,3
!***** Number of elements and nodes
*get,noel,elem,0,num,max
*get,nonode,node,0,num,max
!***** Modeling of Blade
k,100,0,h+inter+bladeuy,0
k,101,2*a,h+inter+bladeuy,0
k,102,-2*a,h+inter+bladeuy,0
k,103,0,inter+bladeuy,0

lstr,103,100
lstr,100,101
lstr,100,102
lang,13,103,angle
lang,14,103,angle
lfillt,16,18,rock
ldele,15
ldele,17
ldele,12,14,1
kdele,100,102,1
lstr,10,11
numcmp,all
!***** Contact
h1=0.004
Mat,2
Type,2
esize,h1
lreverse,13
lreverse,15
lsel,s,line,,13,15
!lcomb,all,,0
lccat,all
lmesh,16
alls
*get,PilotID,node,,num,max
PilotID=PilotID+1

```

```

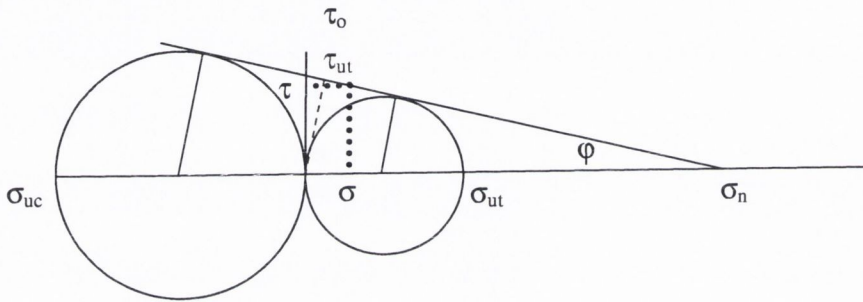
kbtw,10,11,50
nkpt,PilotID,50
tshap, pilo
e,PilotID

nset,s,loc,x,0,0.7
nset,r,loc,y,0
mat,3
type,3
!real,2
esize,h1
esurf
alls
/prep7
cncheck    ! check the contact
!***** Boundary conditions
d,PilotID,ux,0.0
d,PilotID,rotz,0.0
nset,s,loc,y,-a
d,all,uy,0
allsel
nset,s,loc,x,a/2
nset,r,loc,y,-a,-a+1
d,all,ux
allsel
nset,s,loc,x,0
dsym,symm,x
allsel
fini
!*****solution control
/solution
rescontrol,,all,1
pred,off
nlgeom,on
time,1
D,pilotid,uy,-0.3    ! Applied Displacement to the model
NSUBST,100,200,5
outres,all,all
solve              ! Solve the model
fini

```

Appendix IV: Coulomb-Mohr Failure Criterion

The Coulomb-Mohr failure criterion has been widely used to explain the failure of brittle materials. It was especially used to predict the failure of porous materials like rocks under compression.



The above figure shows a Mohr Circle diagram to visualize the Coulomb-Mohr failure. In our notation, the tensile principal stresses are >0 and compressive principal stresses are negative. τ is the shear stress axis and σ is the normal stress axis and the line elevated at angle φ represents the failure threshold for Coulomb-Mohr failure. Failure occurs where the Mohr circle tangents to the line. The value, τ_o , represents any cohesion in the material. $\mu = \tan \varphi$ is defined as coefficient of friction.

$$\mu = \tan \varphi = \frac{\tau_o}{\sigma_n}$$

Assuming values of shear and normal stress at failure on the fracture plane as τ and σ then:

$$\frac{\tau}{\tau_o} + \frac{\sigma}{\sigma_n} = 1$$

$$\frac{\tau}{\tau_o} + \frac{\sigma}{\tau_o / \mu} = 1$$

$$\tau + \mu\sigma = \tau_o$$

Therefore there is a linear relationship between the shear and normal stress at failure. This relationship has to be true in absence of normal stress ($\sigma=0$). Using the Mohr circle with this assumption gives:

$$\frac{\tau_{ut}}{\tau_o} = \cos \varphi = \frac{1}{\sqrt{1 + \tan^2 \varphi}} = \frac{1}{\sqrt{1 + \mu^2}}$$

$$\tau_o = \sqrt{1 + \mu^2} \tau_{ut}$$

In which, τ_{ut} , is the shear strength of material.